STAGNATION POINT MERGED LAYER FLOW WITH AND WITHOUT ABLATION

by
JATINDER SINGH

DEPARTMENT OF AERONAUTICAL ENGINEERING
INDIAN INSTITUTE OF TECHNOLOGY, KANPUR
DECEMBER 1987

STAGNATION POINT MERGED LAYER FLOW WITH AND WITHOUT ABLATION

A Thesis Submitted
in Partial Fulfilment of the Requirements
for the Degree of

MASTER OF TECHNOLOGY

by
JATINDER SINGH

to the
DEPARTMENT OF AERONAUTICAL ENGINEERING
INDIAN INSTITUTE OF TECHNOLOGY, KANPUR
DECEMBER 1987

To

My Guide

Dr.A.C. Jain

CERTIFICATE

This is to certify that this work entitled, "STAGNATION POINT MERGED LAYER FLOW WITH AND WITHOUT ABLATION" has been carried out by Jatinder Singh under my supervision and that this has not been submitted elsewhere for a degree.

December, 1987

(A.C. JAIN)
Professor
Department of Aeronautical Engineeri
Indian Institute of Technology
KANPUR-208016, INDIA

ACKNOWLEDGEMENTS

I express my sincere gratitude to my guide Dr. A.C. Jain for his assiduous guidance, constant encouragement and erudite suggestions throughout this endeavour. I am deeply indebted to him for his keen interest and concientious efforts.

Thanks also to Mr. U.S. Misra for his excellent typing and Mr. A.K. Ganguly for tracing and drawings.

Jatinder Singh
- JATINDER SINGH
Author

CONTENTS

NOMENCLATURE

ABBREVATIONS

AFE	=	Aero-assisted Flight Experiment Vehicle
ASR	=	Accelerated Successive Replacement
DSMT	=	Direct Simulation Monte-Carlo Technique
HML	=	Hypersonic Merged Layer
HVSL	=	Hypersonic Viscous Shock Layer
ML	=	Merged Layer
NS	=	Navier-Stokes
ODE	=	Ordinary Differential Equations
VSL	=	Viscous Shock Layer

Symbols

a	=	Speed of sound
C_p	=	Constant pressure specific heat
C_v	=	Constant volume specific heat
C_H	=	Heat transfer coefficient
C_F	=	Skin friction coefficient
e	=	Internal energy; $e = C_v T$
h	=	Specific enthalpy
Kn	=	Knudsen number
M_∞	=	Free stream Mach number
n_{eo}	=	Merged layer thickness at the stagnation point
p	=	Pressure
Pr	=	Prandtl number
q	=	Heat flux

R = Gas constant

Re = Stagnation Reynolds number; $Re = \frac{\rho_\infty U_\infty r_B}{\mu_{o\infty}}$

r = Radius vector

r_B = Body radius

T = Temperature

u = Tangential component of velocity

U_∞ = Free stream velocity

v = Normal component of velocity

z = Degree of freedom

ρ = Density

Θ = Body angle

μ = Viscosity coefficient

σ = Momentum accommodation coefficient

α = Thermal accommodation coefficient

λ = Mean free path of the gas

Λ = Function given by equation (18)

γ = Ratio of specific heats; $\gamma = \frac{C_p}{C_v}$

η = Transformation function (See Eq. (23))

ω = Acceleration factor (See equation (68))

κ = Coefficient of thermal conductivity; $\kappa = \frac{\mu C_p}{Pr}$

Δ = Thickness of the shock wave

δ = Thickness of the viscous layer

For Ablation:

a_i, a_{ij}, a_{ijk} = Coefficients of velocity distribution, See Eq.

F = Maxwellian velocity distribution function, See Eq. (47)

F_s = Velocity distribution function defined by Eq. (46)

F_s' = Velocity distribution function defined by Eq. (50)

G = Term in F_s defined by Eq. (48)

H_1, H_2, H_3 = Dimensionless molecular velocities

m = Weight of one gas molecule

M = Mass transfer parameter; $M = \bar{\rho}\,\bar{v}$

N = Number density of gas molecules, number of molecules/volume

U,V,W = Molecular velocities relative to macroscopic velocities in x, y and z directions respectively

u,v = Macroscopic velocity components tangential and normal to the body surface respectively

v' = Transformed velocity, See Eq. (56)

β = Injection coefficient, See Eq. (49)

Θ = Parameter proportional to the number of diffusely reflected molecules

Subscripts

e = Outer edge of merged layer

eo = Outer edge of merged layer at the stagnation poi

I = Injection value

o = Zeroth order terms

2 = denotes second order term

$o\infty$ = Value of variable at the free stream stagnation conditions

∞	=	Value of the variable at free stream location
w	=	Value of the variable at wall
r,θ	=	denotes derivative of dependent variable w.r.t r and θ
s	=	Value of the variable in fluid

Superscripts

$-$	=	dimensionless quantity
$'$	=	derivative w.r.t. η

ABSTRACT

The steady state Navier-Stokes equations (NS) with slip and temperature jump conditions, with and without ablation effects on the surface are solved for a stagnation point merged layer flow on the spherical nose of a space vehicle. Local similar solutions have been obtained and the resulting ordinary differential equations (ODE) have been solved by method of Successive Accelerated Replacement (ASR).

Particular emphasis is placed to understand the physics of the real gases through the concept of effective gamma (γ). The ambient fluids in different tunnels have different fluid characteristics which have widely different values of γ and Pr. A detailed study of varying γ , Pr, surface temperature and viscosity-temperature relations has been carried out in order to enable the experimentalist to interpret his data appropriately in relation with the available results of ideal fluids (γ = 1.4).

Computations have also been carried out for the merged layer with ablation, represented by the oozing out of the gases from an impervious surface in the presence and absence of surface slip and temperature jump conditions. Slip conditions modified due to injection of gases from the surface have been used. General interesting features of the flow field have been pointed out in the text.

SECTION I

INTRODUCTION

1.1 General Remarks

In the present investigation, an attempt has been made to understand the basic physics of the flow field around a space vehicle under conditions that it encounters during the early stages of its reentry into the earth's atmosphere. Due to the rarefaction of the flow, the shockwave like structure in the outer shockwave like region of the disturbed zone of the space vehicle is thick and merges smoothly with the viscous flow underneath. Also, due to lack of enough number of collisions among the fluid particles in the disturbed zone, the particles reach the surface with sufficient momentum and slip along it. Consequently, the temperature at the base of the viscous layer is also different from the surface temperature. This entire zone of disturbance (including the shockwave like structure) with slip and temperature jump conditions is termed as Merged Layer (ML). The full Navier-Stokes (NS) equations with surface slip and temperature jump conditions are integrated from the surface to the free stream. Shockwave like structure comes out as part of the integration domain.

As the vehicle descends through the atmosphere, a denser region is encountered by the space vehicle and consequently, the shock and viscous layer zones become thinner. In particular, the incipient merged layer, viscous shock layer, vorticity interaction regime and ultimately the boundary layer regime pass over the stagnation region of the flow field (Ref. 3).

Here, we strive to understand the various phenomenon associated with the rarefaction effects of the flow field. Particular attention has been paid in understanding the effect of variation in the wall temperatures, with and without surface slip and temperature jump conditions, on the flow field structure and overall characteristics (C_H and C_F) of the flow field. A very interesting feature is observed. For a very cold wall case ($\frac{T_w}{T_{o\infty}} \leq 0.15$), slip increases the heat transfer and skin-friction coefficients in comparison to the noslip case while for hot wall ($\frac{T_w}{T_{o\infty}} \geq 0.15$) slip decreases the heat transfer and skin friction coefficient. Also, we find that for low Reynolds number, adiabatic wall temperature is greater than the stagnation temperature, while for higher Reynolds number, adiabatic wall temperature and stagnation temperature tend to become equal. A possible explanation of this phenomenon is given in Section - III on "Results and Discussion". A thorough investigation of the various viscosity-temperature (μ- T) relations on the flow field was carried out. It

was found that for prescribed free stream conditions, data for the heat transfer coefficient against the free stream Reynolds number with slip fell on different curves for different μ-T relations. The different curves collapse into a single curve when the same set of data are plotted against the stagnation Reynolds number ($Re = \frac{\rho_\infty U_\infty r_B}{\mu_{o\infty}}$). We call this curve as universal curve in the sense that it is valid for all values of stagnation Reynolds number.

When the space vehicle enters the earth's atmosphere, intense heat is generated in the disturbed zone of the flow field and the molecules dissociate and ionise. Thermodynamic properties which are constant for a perfect fluid no longer remain constant. Also, to analyse the disturbed zone of the flow field, we have to solve species conservation equation in addition to the mass, momentum and energy equations. Chemical kinetics come into picture which makes the analysis all the more difficult, time consuming and tedious. Here, we have tried to incorporate the real gas effects in a simple way by using the concept of effective 'γ' (Ref. 4). The results predict the behaviour of the flow quantities and overall flow characteristics only qualitatively.

This kind of study is extremely useful for wind tunnel data as well. In wind tunnels, different types of gases are being used which have different values of γ and Pr. Nitrogen (diatomic), Argon or Helium (Monatomic) and air are most extensively used in the experiments. In NASA Langley Research Centre, Freon (with $\gamma = 1.28$) is being used to simulate real gas effects in the wind tunnel.

The present study helps to understand the effect of these gases (with different values of gamma) on the flow characteristics in comparison to air ($\gamma = 1.4$). Here, intensive investigations have been carried out and the values of C_H, C_F and flow parameters are plotted against gamma and Prandtl number. Particular attention has been paid to study the effect of gamma on the wall pressure and the overall flow characteristics at different values of stagnation Reynolds number. It is observed that the results for wall pressure are in agreement with the experimental results of Potter and Bailey[17].

The space vehicle surface is made up of composites like carbon-carbon, carbon phenolic or carbon epoxy. During the reentry of the space vehicle, due to intense heat in the disturbed zone of the flow field, a chemical degradation of these materials takes place. The surface gets charred, and the material melts, vaporises or sublimates. The pyrolysis gases which ooze out mix with the main flow and affect the flow parameters and overall flow characteristics. In the process of sublimation the space vehicle surface may receed.

In the present analysis, the effect of receeding of the surface is ignored. Here, an attempt has been made to study the effect of ablation in a very simple way by

simulating the ablation process through the emission of gases from the impervious surface. The high heat capacity of the pyrolysis gas, surface recession and roughness due to charring have been ignored. Under such surface conditions, surface slip and temperature jump conditions are modified due to injection of gases in the Knudsen layer. The modified slip conditions at the surface are used in the integrations of the governing equations. Extensive computations under varied small emission rates of gases have been carried and the results are plotted as a function of mass transfer parameter, M ($M = \frac{\rho v}{\rho_\infty U_\infty}$).

1.2 Review of Literature

Different approaches have been used to analyse the rarefied hypersonic flow past a blunt body. During the reentry of the space vehicle, it has to pass through various flow regimes which have been classified by Probstein et al[3]. The flow past the space vehicle cannot be solved by one method for all the regimes. Consequently different procedures have been adapted to investigate these regimes.

Van Dyke[20] developed second order boundary layer theory to evaluate the viscous hypersonic flow past the nose of a blunt body on the basis of asymptotic expansions of the NS equations. In the process he identified seven second order effects: longitudinal

curvature, transverse curvature, slip, temperature jump, entropy gradient, stagnation enthalpy gradient and displacement. He defined a parameter ε (viscous hypersonic similarity parameter) given by

$$\varepsilon = \frac{\left[(\gamma - 1)\, M_\infty^2\right]^{\omega/2}}{\sqrt{Re_\infty}}$$

where ω is the index in μ-T law. Van Dyke[20] carried out the analysis by expanding the flow variables asymptotically in powers of ε for the inner (viscous flow) and the outer (inviscid flow) regions of the flow field. Matching the two expansions gave a set of equations valid for the entire region behind the shock. Van Dyke[20] calculated the flow upto second order term. Kao[11] developed third order boundary layer approximation. He too used the method of matched asymptotic expansions. He termed the boundary layer and the shock wave as the "inner" layer (viscosity is significant in these regions) and the nearly inviscid region between them as the "outer" region. After expanding the flow variables in the various powers of ε in the inner and outer regions, he collected like powers of ε which yielded a set of equations to third order. These equations were found to be valid in the entire disturbed zone. Viscous effects appear in the third order equations for inviscid flow region. This procedure is generally applied to the incipient merged layer regime. The higher order boundary layer method gives accurate results only upto slightly rarefied regimes. Also, this method is very time

consuming.

Another way of attacking the problem is through viscous shock layer approximation. Davis[2] developed viscous shock layer (VSL) equations to solve the flow past axisymmetric blunt body moving at hypersonic speeds. These equations are truncated NS equations retaining terms upto second order in the inverse square root of the Reynolds number. These equations along with surface slip and shock slip conditions can describe the entire disturbed zone. Implicit finite difference method was used by Davis[2] to solve these equations.

Probstein and Kemp[16] also used viscous layer and incipient merged layer approach to solve the flow past a sphere and a cylinder. The shock layer region is considered to be fully viscous. Rankine-Hugoniot relations give the outer boundary conditions for the VSL approach. Locally similar solutions were used by Probstein et al.[16] to estimate the flow in the stagnation region.

The above approaches, though simple to use, are valid in the range from intermediate to very high Reynolds number. This formulation fails at sufficiently low Reynolds number where the other terms that have been neglected in the NS equations become significant.

Hypersonic Merged Layer (HML) approximation is another method to estimate the hypersonic flow past a blunt body. This is the only method which holds promise and gives good results even at sufficiently low Reynolds number and the surface quantities obtained from this approach and kinetic approach are found to be in good agreement. Levinsky and Yoshihara[12] were the first to use this method on the basis of thin layer approximation with noslip surface conditions. Their results predicted a decrease in impact pressure with decrease in Reynolds number which was not in agreement with the experimental results of Potter and Bailey[17]. Levinsky and Yoshihara[12] attributed this anomaly to the neglect of slip boundary conditions. But later it was shown by Jain and Admurthy[6] that inclusion of slip effects further decreased the impact pressure. Jain et al.[6] improved upon the analysis of Levinsky and Yoshihara[12] using full NS equations with slip and temperature jump effects to describe the flow field. They developed local similar solutions valid in the stagnation zone of the flow past the nose of a space vehicle.

Jain and Prabha[5] compared the results of HVSL, HML and DSMC (Direct Simulation Monte-Carlo Technique) with the experimental results to find the limit of validity of HVSL theory. It was found that HML gave good results upto Kn $\leq$ 0.6 while HVSL gave accurate results only upto Kn $\leq$ 0.06.

Jain[9] developed two term indented series solution of the full NS equations for the merged layer flow on the spherical nose of a body incorporating the downstream effects. Jain and Prabha[8] derived the equations governing the first two indented terms of the series expansion with asymmetry effects. Jain[7] in his series of lectures on reentry aerodynamics tried to generate an understanding of the flow under hypersonic rarefied conditions for adiabatic and cold wall cases.

Till now, various numerical techniques have been used to solve the equations of motion. Levinsky and Yoshihara[12] integrated the equations from each end and matched the solution at a common point between the shock and the boundary layer where the integration procedure was stable. Jain[9] used the method of Accelerated Successive Replacement (ASR) to integrate the equations numerically. In the present investigation, ASR method has been used.

The problem of ablation involves slip boundary conditions at the surface with mass transport effects. Whitehead and Davis[22] used the analysis of Shidlovsky[19] and Patterson[18] to give a set of such equations which allow for the mass transport across a porous surface. Lewis et al.[14] solved the full VSL equations for hyperbloids at zero lift and spherically blunted cones at large angles of attack. They modified the boundary conditions given by Davis[22] for the case of ablation,

assuming porosity at the wall to be zero. Moss[15] showed the effect of mass injection on flow properties within and downstream of the injection region under noslip surface conditions.

SECTION II

MATHEMATICAL FORMULATION OF PROBLEM

2.1 Discussion of Governing Equations

The steady state Navier-Stokes equations in spherical polar coordinate system with axial symmetry for an ideal compressible fluid are given in Yuan[23] and (Ref. 8). These are as follows:

Continuity Equation:

$$(\rho v)_r + \frac{2\rho v}{r} + \frac{1}{r}(\rho u)_\theta + \rho u \frac{\text{Cot } \theta}{r} = 0 \qquad (1)$$

Radial Momentum Equation:

$$p_r + \rho\left(v\, v_r + \frac{u}{r} v_\theta - \frac{u^2}{r}\right)$$

$$= 2\left[\mu v_r - \frac{\mu}{3r}(r\, v_r + 2v + u_\theta + u \text{ Cot } \theta)\right]_r$$

$$+ \frac{1}{r}\left\{\mu\left[r\left(\frac{u}{r}\right)_r + \frac{v_\theta}{r}\right]\right\}_\theta + \frac{2\mu}{r}\left(2v_r - \frac{u \text{ Cot } \theta}{r}\right)$$

$$+ \frac{\mu}{r}\left\{\text{Cot } \theta\left[r\left(\frac{u}{r}\right)_r + \frac{v_\theta}{r}\right] - \frac{2}{r}(v + u \text{ Cot } \theta)\right\} \qquad (2)$$

Transverse Momentum Equation:

$$\frac{p_\theta}{r} + \rho\left(v\,u_r + \frac{u}{r}\,u_\theta + \frac{uv}{r}\right)$$

$$= \frac{2}{r}\left[\frac{\mu}{r}\,(u_\theta + v) - \frac{\mu}{3r}\,(r\,v_r + 2v + u_\theta + u\,\mathrm{Cot}\,\theta)\right]_\theta$$

$$+\left\{\mu\left[r\left(\frac{u}{r}\right)_r + \frac{v_\theta}{r}\right]\right\}_r + \frac{3\mu}{r}\left[r\left(\frac{u}{r}\right)_r + \frac{v_\theta}{r}\right]$$

$$+ \frac{2\mu}{r^2}\,\mathrm{Cot}\,\theta\,(u_\theta - u\,\mathrm{Cot}\,\theta) \qquad (3)$$

Energy Equation:

$$\rho\left(v\,h_r + \frac{u}{r}\,h_\theta\right) = v\,p_r + \frac{u}{r}\,p_\theta$$

$$+ \frac{1}{r\,Pr}\left[(\mu_r\,h_r)_r + \frac{\mu}{r}\,h_\theta + \mu h_r + \mu h_\theta\,\frac{\mathrm{Cot}\,\theta}{r}\right]$$

$$+ \mu\left[2v_r^2 + \frac{2}{r^2}\,(u_\theta + v)^2 + \frac{2}{r^2}\,(v + u\,\mathrm{Cot}\,\theta)^2\right.$$

$$\left. + r\left\{\left(\frac{u}{r}\right)_r + \frac{v_\theta}{r}\right\}^2\right]$$

$$- \frac{2\mu}{3r^2}\left[r\,v_r + u_\theta + 2v + u\,\mathrm{Cot}\,\theta\right]^2 \qquad (4)$$

Equation of State:

$$p = \rho RT \qquad (5)$$

and viscosity temperature relation is defined as

$$\mu = \mu(T) \qquad (6)$$

Here r represents the radial distance and θ represents the vectorial angle; u and v represent the tangential and normal velocity components in increasing r and θ directions (See Fig. A); ρ , p, h are the density, pressure and specific

enthalpy respectively. Suffixes r and Θ denote the derivatives of the dependent variables with respect to 'r' and 'Θ' respectively.

Boundary Conditions

At the edge of the merged layer $r = r_e$

$$\begin{aligned} u &= U_\infty \text{ Sin } \Theta \\ v &= -U_\infty \text{ Cos } \Theta \\ p &= p_\infty \\ \rho &= \rho_\infty \\ T &= T_\infty \end{aligned} \tag{7}$$

(a) At $r = r_B$, i.e. at the surface of the body, slip velocity and temperature boundary conditions are

$$u = \frac{2-\sigma}{\sigma} \left[\lambda \left(\frac{\partial u}{\partial r}\right) \right]_{r_B}, \quad v = 0 \tag{8}$$

$$T = T_w + \frac{2-\alpha}{\alpha} \frac{2\gamma}{\gamma+1} \left[\frac{\lambda}{Pr} \frac{\partial T}{\partial r}) \right]_{r_B} \tag{9}$$

λ_w is the mean free path of the gas at the body surface and

$$\lambda = \sqrt{\frac{\pi\gamma}{2}} \frac{\mu}{\rho a}$$

For adiabatic wall case,

$$\left(\frac{\partial T}{\partial r}\right)_{r_B} = 0 \tag{10}$$

(b) For the noslip case at $r = r_B$

$$u = v = 0 \text{ and } T = T_w \text{ or } \left(\frac{\partial T}{\partial r}\right) = 0$$

2.2 Non-Dimensionalisation Procedure

The variables have been non-dimensionalised as follows:

$$\bar{u} = \frac{u}{U_\infty}, \quad \bar{v} = \frac{v}{U_\infty}, \quad \bar{p} = \frac{p}{\rho_\infty U_\infty^2}, \quad \bar{\rho} = \frac{\rho}{\rho_\infty} \qquad (11)$$

$$\bar{T} = \frac{T}{T_{o\infty}}, \quad \bar{\mu} = \frac{\mu}{\mu_{o\infty}}, \quad \bar{r} = \frac{r}{r_B}, \quad Re = \frac{U_\infty r_B \rho_\infty}{\mu_{o\infty}}$$

where suffix ' ∞' denotes the value of variable at the free stream location and the suffix '$o\infty$' denotes its value at the free stream stagnation conditions; r_B is the nose radius.

The governing equations (1) to (6) in the non-dimensional form become

Continuity Equation:

$$(\bar{\rho}\,\bar{v})_{\bar{r}} + \frac{2\,\bar{\rho}\bar{v}}{\bar{r}} + \frac{(\bar{\rho}\bar{u})_\Theta}{\bar{r}} + \bar{\rho}\bar{u}\,\frac{\cot\Theta}{\bar{r}} = 0 \qquad (12)$$

Radial Momentum Equation:

$$\bar{p}_{\bar{r}} + \bar{\rho}\left(\bar{v}\,\bar{v}_{\bar{r}} + \frac{\bar{u}}{\bar{r}}\,\bar{v}_\Theta - \frac{\bar{u}^2}{\bar{r}}\right)$$

$$= \frac{2}{Re}\left[\bar{\mu}\,\bar{v}_{\bar{r}} - \frac{\bar{\mu}}{3\bar{r}}\left(\bar{r}\,\bar{v}_{\bar{r}} + 2\bar{v} + \bar{u}_\Theta + \bar{u}\cot\Theta\right)\right]_{\bar{r}}$$

$$+ \frac{1}{Re}\,\frac{1}{\bar{r}}\left\{\bar{\mu}\left[\bar{r}\left(\frac{\bar{u}}{\bar{r}}\right)_{\bar{r}} + \frac{\bar{v}_\Theta}{\bar{r}}\right]\right\}_\Theta + \frac{2}{Re}\,\frac{\bar{\mu}}{\bar{r}}\left[2\bar{v}_{\bar{r}} - \frac{\bar{u}_\Theta + \bar{v}}{\bar{r}}\right]$$

$$+ \frac{1}{Re}\,\frac{\bar{\mu}}{\bar{r}}\left\{\cot\Theta\left[\bar{r}\left(\frac{\bar{u}}{\bar{r}}\right)_{\bar{r}} + \frac{\bar{v}_\Theta}{\bar{r}}\right] - \frac{2}{\bar{r}}\left(\bar{v} + \bar{u}\cot\Theta\right)\right\} \qquad (13)$$

Transverse Momentum Equation

$$\frac{1}{\bar{r}}\,\bar{p}_{\theta} + \bar{\rho}\left(\bar{v}\,\bar{u}_{\bar{r}} + \frac{\bar{u}}{\bar{r}}\bar{u}_{\theta} + \frac{\bar{u}\bar{v}}{\bar{r}}\right)$$

$$= \frac{2}{Re}\,\frac{1}{\bar{r}}\left[\frac{\bar{\mu}}{\bar{r}}\left(\bar{u}_{\theta} + \bar{v}\right) - \frac{\bar{\mu}}{3\bar{r}}\left(\bar{r}\,\bar{v}_{\bar{r}} + 2\bar{v} + \bar{u}_{\theta} + \bar{u}\,\mathrm{Cot}\,\theta\right)\right]$$

$$+ \frac{1}{Re}\left[\bar{\mu}\left\{\bar{r}\left(\frac{\bar{u}}{\bar{r}}\right)_{\bar{r}} + \frac{\bar{v}_{\theta}}{\bar{r}}\right\}\right]_{\bar{r}} + \frac{3\,\bar{\mu}}{Re\,\bar{r}}\left[\bar{r}\left(\frac{\bar{u}}{\bar{r}}\right)_{\bar{r}} + \frac{\bar{v}_{\theta}}{\bar{r}}\right]$$

$$+ \frac{2\,\bar{\mu}}{Re\,\bar{r}^{2}}\,\mathrm{Cot}\,\theta\,\left(\bar{u}_{\theta} - \bar{u}\,\mathrm{Cot}\,\theta\right) \qquad (14)$$

Energy Equation

$$\Lambda\,\bar{\rho}\left(\bar{v}\,\bar{T}_{\bar{r}} + \frac{\bar{u}}{\bar{r}}\,\bar{T}_{\theta}\right) = \bar{v}\,\bar{p}_{\bar{r}} + \frac{\bar{u}}{\bar{r}}\,\bar{p}_{\theta}$$

$$+ \frac{1}{Re}\,\frac{1}{Pr}\,\frac{\Lambda}{\bar{r}}\left[\left(\bar{\mu}\,\bar{r}\,\bar{T}_{\bar{r}}\right)_{\bar{r}} + \frac{\bar{\mu}}{\bar{r}}\,\bar{T}_{\theta} + \bar{\mu}\,\bar{T}_{\bar{r}} + \frac{\bar{\mu}\,\bar{T}_{\theta}\,\mathrm{Cot}\,\theta}{\bar{r}}\right]$$

$$+ \frac{1}{Re}\,\bar{\mu}\left[2\,\bar{v}_{\bar{r}}^{2} + \frac{2}{\bar{r}^{2}}\left(\bar{u}_{\theta} + \bar{v}\right)^{2} + \frac{2}{\bar{r}^{2}}\left(\bar{v} + \bar{u}\,\mathrm{Cot}\,\theta\right)^{2}\right.$$

$$\left. + \left\{\bar{r}\left(\frac{\bar{u}}{\bar{r}}\right)_{\bar{r}} + \frac{\bar{v}_{\theta}}{\bar{r}}\right\}^{2}\right]$$

$$- \frac{1}{Re}\,\frac{2}{3}\,\frac{\bar{\mu}}{\bar{r}^{2}}\left[\bar{r}\,\bar{v}_{\bar{r}} + \bar{u}_{\theta} + 2\bar{v} + \bar{u}\,\mathrm{Cot}\,\theta\right]^{2}$$

(15)

Equation of State

$$\bar{p} = \frac{\gamma-1}{\gamma}\,\Lambda\,\bar{\rho}\,\bar{T} \qquad (16)$$

$$\bar{\mu} = \bar{\mu}\left(\bar{T}\right) \qquad (17)$$

where

$$\Lambda = \frac{C_p T_{o\infty}}{U_\infty^2} = \frac{1}{2} + \frac{1}{(\gamma - 1) M_\infty^2} \qquad (18)$$

The boundary conditions in the non-dimensionalised form are as follows:

At $\bar{r} = \bar{r}_e$

$$\bar{u} = \text{Sin } \Theta$$

$$\bar{v} = -\text{Cos } \Theta \qquad (19)$$

$$\bar{\rho} = 1, \ \bar{T} = 1 - \frac{1}{2\Lambda}, \ \bar{p} = \frac{1}{\gamma M_\infty^2}$$

γ is the specific heat ratio and M_∞ is the free stream Mach number.

At $\bar{r} = 1$

$$\bar{u} = \sqrt{\frac{\pi\gamma}{2}} \ \frac{2-\sigma}{\sigma} \ \frac{M_\infty}{Re} \sqrt{\frac{T_\infty}{T_{o\infty}}} \left(\frac{\bar{\mu}}{\bar{\rho}\sqrt{\bar{T}}}\right) \left(\frac{\partial \bar{u}}{\partial \bar{r}} - \bar{u}\right) \qquad (20)$$

$$\bar{v} = 0$$

and the temperature jump condition is

$$\bar{T} = \bar{T}_w + \sqrt{\frac{\pi\gamma}{2}} \ \frac{2-\alpha}{\alpha} \ \frac{2\gamma}{\gamma+1} \ \frac{M_\infty}{Pr \ Re} \sqrt{\frac{T_\infty}{T_{o\infty}}} \left(\frac{\bar{\mu}}{\bar{\rho}\sqrt{\bar{T}}} \ \frac{\partial \bar{T}}{\partial \bar{r}}\right) \qquad (21)$$

where

$$\bar{T}_w = \frac{T_w}{T_{o\infty}}$$

For noslip case

$$\bar{u} = \bar{v} = 0 \text{ and } \bar{T} = \bar{T}_w \text{ or } \frac{\partial \bar{T}}{\partial \bar{r}} = 0 \tag{22}$$

for adiabatic wall case.

The physical domain of integration is now transformed to computational domain by the following transformation

$$\eta = \frac{\bar{r} - 1}{\bar{r}_e - 1} \tag{23}$$

This transformation changes the domain of integration from zero to unity. If $\bar{r}_{eo}$ denotes the extent of the merged layer at the stagnation point of the body, then

$$\bar{r}_e = \bar{r}_{eo}$$

$$\text{If } n_{eo} = \bar{r}_{eo} - 1 \tag{24}$$

$$\bar{r} = 1 + \eta n_{eo}$$

n_{eo} appears as a parameter in the governing equation. It is an additional unknown in the governing equations and is evaluated by a criterion ensuring a smooth merging of the ML flow with the ambient flow. In the present investigation it is found that the velocity profile converges earlier than the temperature profile. We have imposed the condition that the temperature gradient at $\bar{r}_e = \bar{r}_{eo}$ should be negligible.

To transform the governing equations into computational domain, we use the relation

$$\frac{\partial}{\partial \bar{r}} = \frac{\partial}{\partial \eta} \frac{\partial \eta}{\partial \bar{r}} = \frac{1}{n_{eo}} \frac{\partial}{\partial \eta} \tag{25}$$

Consistent with the form of boundary conditions about the axis and the fact that Rankine Hugonite pressure behind the shock wave and Newtonian pressure on the surface vary as $\sin^2\theta$, we assume the following form of series expansion for the various thermodynamic variables[12]

$$\bar{u}(\eta, \theta) = \bar{u}_o(\eta) \sin\theta + \bar{u}_2(\eta) \sin^3\theta + \ldots\ldots$$

$$\bar{v}(\eta, \theta) = \bar{v}_o(\eta) \cos\theta + \bar{v}_2(\eta) \cos\theta \sin^2\theta + \ldots\ldots$$

$$\bar{\rho}(\eta, \theta) = \bar{\rho}_o(\eta) + \bar{\rho}_2(\eta) \sin^2\theta + \ldots\ldots$$

$$\bar{p}(\eta, \theta) = \bar{p}_o(\eta) + \bar{p}_2(\eta) \sin^2\theta + \bar{p}_4(\eta) \sin^2\theta + \ldots\ldots$$

$$\bar{T}(\eta, \theta) = \bar{T}_o(\eta) + \bar{T}_2(\eta) \sin^2\theta + \ldots\ldots$$

$$\bar{\mu}(\eta, \theta) = \bar{\mu}_o(\eta) + \bar{\mu}_2(\eta) \sin^2\theta + \ldots\ldots \tag{26}$$

Substituting the various expansions of the flow variables viz., equation (26) in the governing equations (12) to (16), in boundary conditions (20) to (22), and collecting terms of like powers of θ, we get the following set of ordinary differential equations and the boundary conditions for the zeroth order terms.

Continuity Equation:

$$\frac{1 + n_{eo}\eta}{n_{eo}} \left(\bar{\rho}_o \bar{v}_o \right)' + 2\bar{\rho}_o \left(\bar{u}_o + \bar{v}_o \right) = 0 \qquad (27)$$

Radial Momentum Equation:

$$\frac{\bar{v}_o''}{n_{eo}^2} = \frac{3}{4} \frac{Re}{\bar{\mu}_o} \left(\frac{\bar{p}_o'}{n_{eo}} + \frac{\bar{\rho}_o \bar{v}_o \bar{v}_o'}{n_{eo}} \right) - \left(\frac{\bar{\mu}_o'}{n_{eo} \bar{\mu}_o} + \frac{2}{1 + \eta n_{eo}} \right) \frac{\bar{v}_o'}{n_{eo}}$$

$$- \frac{\bar{u}_o'}{2n_{eo}(1 + \eta n_{eo})} + \left(\frac{\bar{\mu}_o'}{n_{eo} \bar{\mu}_o} + \frac{7}{2(1+\eta\, n_{eo})} \right) \frac{\bar{u}_o + \bar{v}_o}{1 + \eta\, n_{eo}}$$

(28)

Transverse Momentum Equation:

$$\frac{\bar{u}_o''}{n_{eo}^2} = \frac{Re}{\bar{\mu}_o} \left[\frac{2\bar{p}_2}{1 + \eta n_{eo}} + \bar{\rho}_o \left(\frac{\bar{v}_o \bar{u}_o'}{n_{eo}} + \frac{\bar{u}_o (\bar{u}_o + \bar{v}_o)}{1 + \eta\, n_{eo}} \right) \right]$$

$$- \left(\frac{2}{1 + \eta\, n_{eo}} + \frac{\bar{\mu}_o'}{\bar{\mu}_o\, n_{eo}} \right) \frac{\bar{u}_o'}{n_{eo}} + \frac{1}{3} \frac{\bar{v}_o'}{n_{eo}(1 + \eta\, n_{eo})}$$

$$+ \frac{\bar{u}_o + \bar{v}_o}{1 + \eta n_{eo}} \left(\frac{8}{3(1 + \eta n_{eo})} + \frac{\bar{\mu}_o'}{\bar{\mu}_o\, n_{eo}} \right) \qquad (29)$$

Energy Equation:

$$\frac{\Lambda}{n_{eo}}\ (1+\eta n_{eo})^2\ \bar{\rho}_o\ \bar{v}_o\ \bar{T}_o' = \frac{(1+\eta n_{eo})^2}{n_{eo}}\bar{v}_o\bar{p}_o'$$

$$+\frac{1}{Re}\ \frac{(1+\eta n_{eo})}{Pr}\left[\Lambda\left\{2\ \frac{\bar{\mu}_o\ \bar{T}_o'}{n_{eo}} + \frac{(1+\eta n_{eo})}{n_{eo}^2}\left(\bar{\mu}_o'\ \bar{T}_o' + \bar{\mu}_o\ \bar{T}_o''\right)\right\}\right]$$

$$+\ 2\ \frac{(1+\eta n_{eo})^2}{n_{eo}^2}\ \frac{1}{Re}\ \bar{\mu}_o\ \bar{v}_o'^2 + \frac{4}{Re}\ \bar{\mu}_o\ (\bar{u}_o+\bar{v}_o)^2 \qquad (30)$$

Equation for p_2:

$$\frac{\bar{p}_2'}{n_{eo}} = -\frac{1}{2}\ \frac{\bar{p}_o'}{n_{eo}} + \frac{\bar{\rho}o\ \bar{u}_o}{(1+\eta\ n_{eo})}\ (\bar{u}_o+\bar{v}_o) + \frac{1}{2}\ \frac{\bar{\rho}_o\bar{v}_o\bar{v}_o'}{n_{eo}} \qquad (31)$$

$$\bar{p}_o = \frac{\gamma-1}{\gamma}\Lambda\bar{\rho}_o\ \bar{T}_o \qquad (32)$$

$$\bar{\mu}_o = \bar{\mu}_o\ (\bar{T}_o) \qquad (33)$$

In the present computations, square root law and Sutherland law, both have been used to relate viscosity with temperature.

The boundary conditions are:

At $\eta = 1$

$$\bar{u}_o = 1,\ \bar{v}_o = -1,\ \bar{\rho}_o = 1,\ \bar{T}_o = 1 - \frac{1}{2\Lambda},\ \bar{p}_2 = 0 \qquad (34)$$

At $\eta = 0$

Slip velocity is given by

$$\bar{u}_o = \sqrt{\frac{\pi\gamma}{2}} \frac{2-\sigma}{\sigma} \frac{M_\infty}{Re}\sqrt{\frac{T_\infty}{T_{o\infty}}} \frac{\bar{\mu}_o}{\bar{\rho}_o\sqrt{\bar{T}_o}}\left(\frac{1}{n_{eo}} \frac{d\bar{u}_o}{d\eta} - \bar{u}_o\right)_{\eta = 0} \tag{35}$$

$$\bar{v}_o = 0$$

Temperature jump is given by

$$\bar{T}_o = \bar{T}_w + \sqrt{\frac{\pi\gamma}{2}} \frac{2-\sigma}{\sigma} \frac{2\gamma}{\gamma+1} \frac{M_\infty}{Pr\ Re} \sqrt{\frac{T_\infty}{T_{o\infty}}} \frac{\bar{\mu}_o}{\bar{\rho}_o\sqrt{\bar{T}_o}}\left(\frac{1}{n_{eo}} \frac{d\bar{T}_o}{d\eta}\right)_{\eta = 0} \tag{36}$$

For adiabatic wall case

$$\left(\frac{d\bar{T}_o}{d\eta}\right)_{\eta = 0} = 0 \tag{38}$$

At $\eta = 0$, for noslip case

$$\bar{u}_o = \bar{v}_o = 0 \tag{39}$$

$$\bar{T}_o = \bar{T}_w \quad \text{or} \quad \frac{d\bar{T}_o}{d\eta} = 0 \tag{40}$$

In the above set of equations (27) to (33) and boundary conditions (34) to (40), a prime over a variable denotes the derivative with respect to η . The ellipic nature of the equations comes due to the presence of higher order terms, viz. u_2, T_2, ρ_2, p_2 etc. Jain[9] has shown that the effect of

this second order term near the stagnation region is small and these terms can be neglected in comparison to leading terms of the expansion in the vicinity of the stagnation point. The locally similar solutions transform the partial differential equations to a set of ordinary differential equations and boundary conditions. These differential equations are valid only for small values of Θ, i.e. in a small region near the stagnation point.

2.3 Concept of Effective Gamma

Ideal fluids obey the perfect gas law, $p = \rho RT$, while the real fluids depart from this law and obey $p = z'\rho RT$, were z' is the compressibly factor. In real fluids the thermodynamic quantities no longer remain constant. The real gas effects include ionization, dissociation and vibration degrees of freedom.

If the density ratio across the shock is given by ε, then

$$\varepsilon = \frac{\rho_\infty}{\rho_s} \tag{41}$$

From Rankine Hugoniot relation, as given by Probstein[4], we have

$$\varepsilon = \frac{p_s/\rho_s}{(h_s + e_s) - (h_\infty + e_\infty) - \frac{p_\infty}{\rho_s}} \tag{42}$$

Using hypersonic limiting case, i.e. when M_∞ approaches

infinity ($M_\infty \to \infty$), in front of the shock, p_∞ , h_∞, e_∞ all tend to zero

$$\varepsilon_{lim} = \frac{p_s/\rho_s}{h_s + e_s} \tag{43}$$

The ratio of specific heats, i.e. gamma, γ has no significance in the case of dissociating gas. In that case, we define γ_e , "effective ratio of specific heats", and it has a value different from 1.4 for a real gas.

From Rankine-Hugoniot relation[4], in the limiting case, $M_\infty \to \infty$, we have

$$\varepsilon_{lim} = \frac{\gamma - 1}{\gamma + 1} \tag{44}$$

If z denotes the degree of freedom which depends upon the motion of the molecule possesses[4], then

$$\varepsilon_{lim}^{-1} = z + 1 \tag{45}$$

For a monatomic gas, z = 3 (three translational degrees of freedom), and this gives $\varepsilon_{lim} = 1/4$. Similarly for a diatomic gas (three translational and two rotational degrees of freedom), $\varepsilon_{lim} = 1/6$. When the diatomic particle is excited to vibration, $\varepsilon_{lim} = 1/8$. Thus we observe that with introduction of real gas effects, ε_{lim} decreases, which in turn implies from equation (44) that the value of gamma, γ decreases. In other words, by decreasing the value of gamma, γ we can incorporate real gas effects upto some extent. With

real gas effects, at elevated temperatures, the value of ε_{lim} may be as low as 0.07 which implies a value of 1.15 for gamma, γ .

2.4 Mathematical Formulation for Ablation Problem

The slip flow boundary conditions without mass transfer were derived by Shidlovskiy[19] and Patterson[18]. These boundary conditions assume an impermeable surface and zero normal macroscopic velocity at the surface. They also assume that the mean free path although small is large enough so that there is no interaction between the incident and reflected molecules. But there occurs a small thin layer between the viscous layer and the body surface where the interaction among the molecules takes place and the velocity distribution of the molecules is affected. This thin layer is called the Knudsen layer (See Fig. B). v_I is the injection velocity.

To investigate the flow at low Reynolds number with ablation, it is necessary to consider boundary conditions with mass transport across the surface. The flow near the wall is non isentropic and we consider a non-Maxwellian distribution in the Knudsen layer.

If F denotes the Maxwell's velocity distribution function, then the non-Maxwellian distribution function in the Knudsen layer is given by F_s, where

$$F_s = F\,(1 + G) \tag{46}$$

and

$$F = N\,(2\pi RT)^{-3/2}\, e^{-\frac{1}{2}H^2} \tag{47}$$

G is a component of thermal velocities given by Patterson[17]

$$G = a_i H_i + \frac{1}{2}\, a_{ij}\, H_i H_j + \frac{1}{6}\, a_{ijk}\, H_i H_j H_k \tag{48}$$

The slip flow boundary conditions given by Shidlovskiy[19] were modified by Whitehead and Davis[22] for mass transport effects by assuming specular and diffused reflections at the surface. Lewis[14] used the same equations for calculating the HVSL flow with ablation. The various expressions for the transport of mass, momentum and energy across the Knudsen layer were derived by considering that the net flux at the outer edge of the Knudsen layer equals the incident flux, plus the specularly and diffusely reflected fluxes at the wall.

Let the number of diffusely reflected molecules be proportional to Θ and the number of molecules which have undergone specular reflection is proportional to $(1 - \Theta)$. The number of diffusely reflected molecules are further subdivided into those that reflect diffusely from the solid portion of the surface (proportional to $1-\beta$) and those that pass through the pores of the surface and reflect diffusely from the interior of the body (proportional to β) where

$$\beta \propto \frac{\text{Injection area}}{\text{Total surface area}} \tag{49}$$

For specular reflection

$$F_s' (U, V, W) = F_s (U, -V, W) \tag{50}$$

The mass transport equation can now be written as

$$m \int_{-\infty}^{\infty}\int_{-\infty}^{\infty}\int_{-\infty}^{\infty}(V+v)\, F_s\, dU\, dV\, dW = m \int_{-\infty}^{\infty}\int_{-\infty}^{-V}\int_{-\infty}^{\infty}(V+v)\, F_s\, dU\, dV\, dW$$

$$+ (1-\Theta)\, m \int_{-\infty}^{\infty}\int_{-V}^{\infty}\int_{-\infty}^{\infty}(V+v)\, F_s'\, dU\, dV\, dW$$

$$+ \beta\Theta\, m \int_{-\infty}^{\infty}\int_{-V_I}^{\infty}\int_{-\infty}^{\infty}(V+v_I)\, F_w\, dU\, dV\, dW$$

$$+ (1-\beta)\,\Theta\, m \int_{-\infty}^{\infty}\int_{0}^{\infty}\int_{-\infty}^{\infty} V\, F_w\, dU\, dV\, dW \tag{51}$$

The term on the L.H.S. represents the net mass transported at the outer edge of the Knudsen layer across a unit area in a unit time. The first term on the R.H.S. gives the mass transported across the Knudsen layer by the molecules incident on the surface. The second term on R.H.S. represents the mass flow of molecules undergoing specular reflection.

The third term gives the mass of molecules which are diffusely reflected from the interior of the surface with a Maxwellian distribution relative to the injection velocity v_I. The fourth term gives the mass of molecules diffusely reflected from the solid surface with zero macroscopic velocity.

In the similar way the equations for momentum and energy transport across the surface can be derived.as done by Whitehead and Davis[22]. After non-dimensionalising these equations in the manner shown in equations (11) and reducing them by considering small injection velocity (Ref. 22), we have

Mass Transport

$$N_s \sqrt{\frac{\gamma-1}{\gamma}\bar{T}_s}\left[\sqrt{2\pi}\ \bar{v}' + 2 - \beta \frac{N_I}{N_s}\sqrt{\frac{\bar{T}_w}{\bar{T}_s}}\ (2+\sqrt{2\pi}\ \bar{v}_I')\right]$$

$$= 2(1-\beta)\ N_w \sqrt{\frac{\gamma-1}{\gamma}\bar{T}_w} \qquad (52)$$

Normal Momentum Transport

$$\bar{P}_s = \beta\bar{P}_I\left[1 + 2\sqrt{\frac{2}{\pi}}(\bar{v}_I' - \bar{v}')\right] + (1-\beta)\ \bar{P}_w\left[1-2\sqrt{\frac{2}{\pi}}\ \bar{v}'\right]$$

$$+ \frac{\bar{\mu}}{Re}\sqrt{\frac{\pi}{2}}\frac{15}{16}\frac{2-\varrho}{\varrho}\sqrt{\frac{\gamma-1}{\gamma}\frac{\Lambda}{\bar{T}_s}}\ \frac{1}{n_{eo}}\ \frac{\partial\bar{T}_s}{\partial\eta} \qquad (53)$$

Tangential Momentum Transport

$$\bar{u}_s = \frac{5\pi}{16}\sqrt{\frac{\bar{\pi}}{2}}\left(\frac{2-\Theta}{\Theta}\right)\frac{\bar{\mu}}{\bar{p}\,Re}\sqrt{\frac{\gamma-1}{\gamma}\Lambda\,\bar{T}_s}\left(\frac{1}{n_{eo}}\frac{\partial\bar{u}}{\partial\eta}-\bar{u}_s\right) \tag{54}$$

Energy Transport

$$\bar{T}_s = \bar{T}_w\left[\left(1-\beta\frac{N_I}{N_s}\sqrt{\frac{\bar{T}_w}{\bar{T}_s}}\right)\left\{1+\left(-5\sqrt{\frac{2\pi}{8}}\frac{(2-\alpha)}{\alpha}\bar{v}'\right.\right.\right.$$

$$+\beta\frac{N_I}{N_s}\left(\frac{\bar{T}_w}{\bar{T}_s}\right)^{3/2}\frac{5\sqrt{2\pi}}{8}\bar{v}_I'$$

$$\left.+\left(\frac{2-\alpha}{\alpha}\right)\frac{75\pi}{256}\frac{\sqrt{2\pi}}{n_{eo}\,Re}\sqrt{\frac{\gamma-1}{\gamma}\frac{\Lambda}{\bar{T}_s}}\frac{\bar{\mu}}{\bar{p}}\frac{\partial\bar{T}}{\partial\eta}\right)\Big/\left(1-\beta\frac{N_I}{N_s}\left(\frac{\bar{T}_w}{\bar{T}_s}\right)^{3/2}\right)\Big\}$$

$$\left.+\sqrt{\frac{\pi}{2}}\bar{v}'-\beta\frac{N_I}{N_s}\sqrt{\frac{\bar{T}_w}{\bar{T}_s}}\sqrt{\frac{\pi}{2}}\bar{v}_I'\right]\left[\frac{1}{1-\beta\frac{N_I}{N_s}\left(\frac{\bar{T}_w}{\bar{T}_s}\right)^{3/2}}\right] \tag{55}$$

Here

$$\bar{v}' = \frac{\bar{v}}{\sqrt{\frac{\gamma-1}{\gamma}\Lambda\,\bar{T}_s}}, \quad \bar{v}_I' = \frac{\bar{v}_I'}{\sqrt{\frac{\gamma-1}{\gamma}\Lambda\,\bar{T}_w}} \tag{56}$$

In the present investigations, we envisaged that the surface material ablates through the efflux of gases from the surface. For ablation, we assume the area of the porous wall is zero (i.e. $\beta = 0$). Using this in the above equations we got the

following expressions for slip and temperature jump for ablation (Ref. 14):

$$\bar{u}_s = \frac{5\pi}{16}\sqrt{\frac{\pi}{2}}\left(\frac{2-\Theta}{\Theta}\right)\frac{\bar{\mu}}{\bar{p}\,Re}\sqrt{\frac{\gamma-1}{\gamma}\Lambda\,\bar{T}_s}\left(\frac{1}{n_{eo}}\frac{\partial\bar{u}}{\partial\eta} - \bar{u}\right) \qquad (57)$$

$$\bar{T}_s = 4\,\bar{T}_w\,\frac{C}{A} + \frac{B}{A} \qquad (58)$$

where

$$A = 8 + 5\sqrt{2\pi}\,\frac{2-\alpha}{\alpha}\,\bar{v}'$$

$$B = \frac{2-\alpha}{\alpha}\,\frac{75\pi}{32}\,\frac{\bar{\mu}}{\bar{p}}\,\frac{\sqrt{2\pi}}{Re}\sqrt{\frac{\gamma-1}{\gamma}\Lambda\,\bar{T}_s}\,\frac{1}{n_{eo}}\,\frac{\partial\bar{T}}{\partial\eta}$$

$$C = 2 - \sqrt{2\pi}\,\bar{v}'$$

For $v = 0$, the above conditions reduce to the expression for no ablation.

In the present investigation, surface slip and temperature jump conditions given by equations (57) and (58) are used in the computation of the governing equations (27) to (33).

2.5 Numerical Method of Integration

The present set of equations consists of three second order equations, viz. equations (28) to (30). The equation of continuity (27) is of first order. In the above set of

equations, the first order derivatives in the merged layer equations, viz. (27) to (31) are replaced by central differences and the end point first order derivatives in the boundary conditions (34) to (40) are replaced by three point one-sided differencing. This way, a second order accuracy is achieved throughout the calculations. If X_N represents the value of any variable (u, v or T) at the N^{th} mesh point, then

$$X'_N = \frac{X_{N+1} - X_{N-1}}{2\Delta} \tag{59}$$

and

$$X''_N = \frac{X_{N+1} - 2X_N + X_{N-1}}{\Delta^2} \tag{60}$$

where $\Delta = \frac{1}{NDIV}$ and NDIV denote the grid-size and the number of divisions into which the merged layer has been divided. Here N = 1 represents the surface and corresponds to $\eta = 0$ while N = NDIV + 1 represents the free stream location corresponding to $\eta = 1$. The resulting algebric equations are solved by the method of Accelerated Successive Replacement (Ref. 8).

Using the finite differencing the boundary conditions (34) to (40) become

$$\bar{u}_o(1) = \sqrt{\frac{\pi\gamma}{2}} \frac{2-\sigma}{\sigma} \frac{M_\infty}{Re} \sqrt{\frac{T_\infty}{T_{o\infty}}} \frac{\bar{\mu}_o(1)}{\bar{\rho}_o(1)\sqrt{\bar{T}_o(1)}}$$

$$\left[\frac{1}{n_{eo}} \frac{4\bar{u}_o(2) - \bar{u}_o(3) - 3\bar{u}_o(1)}{2\Delta} - \bar{u}_o(1) \right] \tag{61}$$

$$\bar{v}_o(1) = 0 \tag{62}$$

$$\bar{T}_o(1) = \bar{T}_w + \left(\sqrt{\frac{\pi\gamma}{2}}\ \frac{2-\alpha}{\alpha}\ \frac{2\gamma}{\gamma+1}\ \frac{M_\infty}{Pr\ Re}\sqrt{\frac{T_\infty}{T_{o\infty}}}\ \frac{\bar{\mu}_o(1)}{\bar{\rho}_o(1)\ \sqrt{\bar{T}_o(1)}}\right)x$$

$$\frac{1}{n_{eo}}\ \frac{4\bar{T}_o(2) - \bar{T}_o(3) - 3\bar{T}_o(1)}{2\Delta}\Bigg) \tag{63}$$

$$\bar{u}_o\ (NDIV+1) = 1,\ \bar{v}_o\ (NDIV+1) = -1,\ \bar{T}_o\ (NDIV+1) = 1 - \frac{1}{2\Lambda}$$

$$\bar{\rho}_o(NDIV+1) = 1,\ \ \bar{p}_2\ (NDIV+1) = 0 \tag{64}$$

For no slip case

$$\bar{u}_o(1) = \bar{v}_o(1) = 0,\ \ \bar{T}_o(1) = \bar{T}_w \tag{65}$$

$$\bar{u}_o\ (NDIV+1) = 1,\ \bar{v}_o\ (NDIV+1) = -1,\ \bar{T}_o\ (NDIV+1) = 1 - \frac{1}{2\Lambda}$$

$$\bar{\rho}_o\ (NDIV+1) = 1,\ \ \bar{p}_2\ (NDIV+1) = 0 \tag{66}$$

Accelerated Successive Replacement Method (ASR)

The ASR method, originally developed by Liberstein[13], has been applied by Jain and Adimurthy[6] to hypersonic flows in stagnation region. They found the results to be reasonably accurate for a wide variety of parameters. As the name implies, the scheme replaces the old values of the variables as soon as the new values are available. Also, the correction procedure involves a parameter 'ω' known as

the acceleration parameter. The way this parameter is evaluated ensures that the correction applied to the variables is always small. As such, the iteration procedure does not diverge even under quite stringent conditions. The correction to a variable at the N^{th} mesh point in $(k+1)^{th}$ iteration is applied in the following manner:

$$x_N^{k+1} = x_N^k - \omega \frac{X_N}{\frac{dX_N}{dx_N}} \tag{67}$$

where x_N denotes any variable u, v, T at the N^{th} grid point and X_N $(u_o, v_o \ldots\ldots, n_{eo}) = 0$ is a typical zeroth order equation. 'ω' is calculated in the following manner to avoid divergence of the iterative scheme:

$$\left| \frac{x_N^{k+1} - x_N^k}{x_N^k} \right| = \omega \left| \frac{X_N}{x_N^k \frac{dX_N}{dx_N}} \right| < \varepsilon \tag{68}$$

where ε is a small parameter.

Let

$$\sigma = \frac{x_N^k \varepsilon}{X_N} \frac{dX_N}{dx_N} \tag{69}$$

If $\sigma < 1$, then we take $\omega = \sigma$

and if $\sigma \geq 1$, then we take $\omega = 1$.

This procedure ensures that correction applied at each iteration is never greater than ε times the value of the variable at that point in the previous iteration. The

correction for each variable starts from N = 2 to N = NDIV. In this procedure, boundary conditions are always satisfied in each global iterations.

Solution Procedure

To start with, an initial profile satisfying the boundary conditions and a value of parameter n_{eo} is prescribed. Then we proceed to solve the differential equations. The corrections are first made to $\bar{v}_o$, $\bar{u}_o$, $\bar{T}_o$ for grid points 2 to NDIV by using equations (28), (29) and (30) respectively. These $\bar{p}_o$ and $\bar{\mu}_o$ are calculated from the equation of state and μ-T relation respectively. $\bar{\rho}_o$ and $\bar{p}_2$ are obtained by numerical integration of the first order equations (27) and (31) respectively. These equations are integrated from the free stream to the surface. At the last but one point from the free stream, the values of $\bar{\rho}_o$ and $\bar{p}_2$ are calculated using Trapezoidal rule. The values at the next four subsequent points are found by Simpson's rule and at the rest of the points except that on body surface (η= 0) by Weddle's rule.

From equation (27) we have

$$\int \frac{\bar{\rho}_o'}{\bar{\rho}_o} \, d\eta = \int \frac{n_{eo}}{(1 + \eta n_{eo})\bar{v}_o} \left(-2\bar{u}_o - 2\bar{v}_o - \frac{1+\eta n_{eo}}{n_{eo}} \bar{v}_o'\right) d\eta \tag{70}$$

It is observed that for $\bar{v}_o(1) = 0$, there occurs a singularity and the density at the surface becomes infinite, unless the

following condition is used:

$$\bar{v}_o' = -2n_{eo}\,\bar{u}_o(1) \quad \text{for slip case}$$

$$= 0 \quad \text{for noslip case.}$$

The above condition is used to improve upon the value of $\bar{v}_o$ at the second grid point.

Pressure at the surface is calculated from the following expression:

$$\bar{p}_o(1) = \bar{p}_o(2) - \Delta\bar{p}_o'(1) \tag{71}$$

where $\bar{p}_o'(1)$ is calculated from normal momentum equation evaluated at the surface, viz.

$$\bar{p}_o'(1) = \frac{4\,\bar{\mu}_o(1)}{3n_{eo}\,Re}\left[\bar{v}_o''(1) + \left(2 + \frac{\bar{\mu}_o'(1)}{n_{eo}\,\bar{\mu}_o(1)}\right)\bar{v}_o'(1)n_{eo} + \frac{\bar{u}_o'(1)n_{eo}}{2}\right.$$

$$\left. - \left(\frac{7}{2} + \frac{\bar{\mu}_o'(1)}{n_{eo}\,\bar{\mu}_o(1)}\right)\bar{u}_o(1)\,n_{eo}^2\right] \tag{72}$$

Then knowing the pressure at the wall, the density at the wall is evaluated from the equation of state.

For convergence, we define ERR1 and ERR2 as the maximum difference in the value of tangential velocity and temperature respectively between the current and previous iteration at the N^{th} mesh point. When ERR1 and ERR2 are

both less than 0.001, the results are considered to be converged. The converged results at a particular Reynolds number may be used as the initial profile for a higher Reynolds number. This reduces the C.P.U. time significantly.

However, the following difficulties arose, especially at very high Reynolds number: (i) Due to infinitesimally thin shock, there are inadequate number of grid points in the shock structure zone. For such cases, convergence became difficult to attain. (ii) Under such conditions, the convergence upto third decimal place was also accepted when it was observed that the values of the parameters n_{eo}, C_H and $(C_F/\mathrm{Sin}\Theta)$ have stabilized sufficiently. In a few cases, the number of iterations were extended upto 4000 in order to ensure that the computations did not diverge. (iii) It was observed that the initial profile did have an effect on the results. For such cases, the initial profile for computation of the results of higher Reynolds number was changed to another converged profile at a low Re. (iv) In a few cases, the ML thickness n_{eo} was not permitted to grow. Using this technique, we were able to achieve convergence upto fourth decimal place in most of the cases and upto third decimal place in some cases of very high Reynolds number.

For ablation also, the above numerical technique of ASR method was used. Here, a constant value of n_{eo} was given for both noslip and slip case in order to study the effect of ablation on the flow characteristics. Again, for higher normal velocity at the surface. We feel that the numerical

technique has to be modified if massive blowing is to be applied. This may be due to the fact that hypersonic rarefied flow is very sensitive to extraneous disturbances and the numerical method develops instability when a normal velocity is imposed at the surface.

SECTION III

DISCUSSION OF RESULTS

In the present investigation, an attempt has been made to understand the basic nature of the flow around the stagnation point of a space vehicle under hypersonic rarefied conditions. An effort has been made to imbibe the real gas effects through the concept of effective γ (gamma) and to simulate the different fluid flow conditions in the wind tunnels. Also, the effect of ablation on the flow field is studied in detail. This study helps in providing useful information to the designer.

Calculations have been carried out to study the effect of the variation of the surface temperature $\bar{T}_w$, gamma (γ), Prandtl number (Pr) and the viscosity-temperature (μ-T) relations on the detailed structure and overall characteristics of the flow field. In most of the cases, computations have been carried out for shuttle reentry conditions at 104.93 Kms and 92.35 Kms which respectively represent a rarefied limit of the continuum regime and a flow at high Reynolds number. For each prescribed ambient condition given in Table 1, stagnation Reynolds number has been calculated using Sutherland law for viscosity-temperature relation.

3.1 Effect of the Variation of the Surface Temperature

The effect of variation of free stream Mach number (M_∞) and free stream Reynolds number (Re_∞) on the flow characteristics and surface quantities has already been considered by Jain and

Adimurthy[6] and Jain and Prabha[8]. Their calculations were carried out for a very cold wall case and it was observed that the heat transfer coefficient, C_H, with the surface slip conditions was more in comparison to the values without the surface slip conditions for a wide range of Reynolds number. Liu[6] carried out the calculations for a hot wall case and found the values of the heat transfer coefficient, C_H, without the surface slip conditions to be more than the values with surface slip conditions. In the present investigation, we have tried to resolve this controversy. In Figs. 1-3, we have plotted the variation of the heat transfer coefficient, C_H, against the wall temperature, $\bar{T}_w$, for the prescribed reentry conditions of the shuttle at an altitude of 104.93 Kms and 92.35 Kms. From Fig. 1, it was found that for a very cold wall case ($\bar{T}_w \leq 0.15$), the surface slip conditions increased the stagnation point heat transfer coefficient, C_H, while for a relatively hot wall case ($\bar{T}_w \geq 0.15$), the surface slip conditions decreased the heat transfer coefficient in comparison to the noslip values of C_H.

Stagnation point heat transfer coefficient is given by

$$C_H = \frac{2\Lambda\ \bar{\mu}_o\ (1)}{Pr\quad Re}\quad \frac{\partial \bar{T}}{\partial \bar{r}}$$

For a given ambient condition and Prandtl number, the value of C_H depends essentially on the product of the viscosity at the surface ($\bar{\mu}_o(1)$) and the temperature gradient $(\frac{\partial \bar{T}}{\partial \bar{r}})$. Figs. 2 and 3 respectively show the variation of

$\bar{\mu}_o(1)$ and $(\frac{\partial \bar{T}}{\partial \bar{r}})$ against the wall temperature $\bar{T}_w$. It was observed that the product of the two quantities, viz. $\bar{\mu}_o(1)$ and $(\frac{\partial \bar{T}}{\partial \bar{r}})$, for a very cold wall case ($\bar{T}_w \leq 0.15$) with surface slip conditions happened to be more than the value of the product of $\bar{\mu}_o(1)$ and $\frac{\partial \bar{T}}{\partial \bar{r}}$ without surface slip conditions. For a relatively hot wall case ($\bar{T}_w \geq 0.15$), the value of this product with surface slip conditions decreased in comparison to the case of no slip conditions. This may be the reason for the increase in the stagnation point heat transfer coefficient with the surface slip conditions for a very cold wall case and decrease in the value of C_H for a hot wall case in comparison to the noslip values of heat transfer coefficient. In order to confirm these results, we further carried out a similar study for Re = 50 and $M_\infty = 20$ (Table 2.2). Fig. 4 shows a similar kind of behaviour of the heat transfer coefficient, C_H, with the variation in wall temperature $\bar{T}_w$. Fig. 5 gives the variation of the skin-friction coefficient parameter, $C_F/\text{Sin}\Theta$, with surface temperature $\bar{T}_w$ (See Table 2.1). The skin-friction coefficient parameter is also found to behave in a way, similar to the variation of the heat transfer coefficient, C_H, with surface temperature $\bar{T}_w$. It was also observed, that the difference in the values of stagnation point heat transfer coefficient, C_H, and the skin-friction coefficient parameter, $C_F/\text{Sin}\Theta$, for slip and noslip cases becomes small at higher values of the Reynolds number in comparison to the difference at lower Reynolds number. Figs. 6 and 7 respectively showed the

variation of surface slip and the temperature values against the wall temperature $\bar{T}_w$. We found that as the wall temperature increased, the values of the surface slip, $\bar{u}_s$, and temperature $\bar{T}_s$, increased for both the altitudes. As expected, the values of $\bar{u}_s$ and $\bar{T}_s$ are higher for a rarer atmosphere at 104.93 Kms than for a denser atmosphere at 92.35 Kms. We further noted that for the rarer atmosphere $\bar{u}_s$ and $(\bar{T}_s - \bar{T}_w)$ are not equal to zero even for a very cold wall.

Another interesting feature observed from the above analysis (Figs. 1-4) was that the adiabatic wall temperature with surface slip conditions was found to be more than the free stream stagnation temperature for a rarefied flow (104.93 Kms altitude), while for a denser flow (92.35 Kms altitude), the surface temperature tends to become equal to the free stream stagnation temperature (See Tables 2.1 and 2.2). In the rarer region, due to inadequate number of collisions, the molecules strike the surface at an angle of incidence ($\Theta > 0$) and as such carry more translational energy E_i to the wall, while the emitted molecules carry energy E_w corresponding to the wall temperature. The energy transferred to the wall at any instant is $E = E_i - E_w$, which raises the equilibrium temperature. In denser region,the molecules suffer enough collisions and lose their entire normal momentum by the time they reach the wall. Thus, the molecules come at an angle of incidence $\Theta = 0$. As such, they carry a relatively lesser

amount of translational energy to the wall, viz., $E = E_i - E_w$ will be less in the denser medium than in the rarer medium. This partially explains the phenomenon observed above.

3.2 Effect of Different Viscosity-temperature Relations

From kinetic theory considerations, Bird[1] has found that the viscosity-temperature variation is of the nature of $\mu \propto T^{\omega}$, where the parameter ω depends upon the model of the gas and intermolecular forces. He further found, that $\omega = 0.5$ for a hard sphere model. Jain[9] carried out extensive studies for different $\omega = 0.5$, 0.75 and 1 using the present code and found that for $\omega = 0.5$, the results of the maximum temperature in the ML agreed with those of DSMC results of Vogenitz and Takata[21]. In the present investigation, the results with $\omega = 0.5$ have been compared with Sutherland law of μ-T relation. The present results thus supplement the results of Jain[9].

Figure 8 shows the tangential velocity ($\bar{u}$) and normal velocity ($-\bar{v}$) profiles with the square-root law and Sutherland law of μ-T relation at $\gamma = 1.4$, $Pr = 0.72$ and at an altitude of 104.93 Km. Considerable difference was found in the velocity profiles for Sutherland law and square-root law of viscosity. Fig. 9 gives the temperature profiles obtained from the two viscosity laws with and without surface slip and temperature jump conditions. In comparison to the square-root law, the results with

Sutherland law gave (i) an increase in merged layer thickness, (ii) decrease in maximum temperature and the shift in maximum temperature towards the outer edge of the merged layer and (iii) a diffused shock. These differences in the flow characteristics with two μ-T relations diminished significantly as the ambient atmosphere became dense at 92.35 Kms (Fig. 10). From Table 5 (See Section VI), we found that the values of the heat transfer coefficient, C_H, with Sutherland viscosity law are more than the values of C_H with square-root law of viscosity by about 16% at altitude 104.93 Kms, 26% at 99.49 Kms. and 35% at 92.35 Kms. Similarly, the skin-friction coefficient parameter, $C_F/\text{Sin}\Theta$, has more value with Sutherland law than with the square-root law of viscosity and the percentage difference goes on increasing with the increase in Reynolds number.

Figure 11 shows a smooth curve for the stagnation point heat transfer coefficient at different altitudes of the shuttle flight conditions for the Sutherland and square-root law of viscosity relations. This curve compared well with the results obtained from AFE Trajectory[10] and Fay and Riddle's empirical formula. We call this curve a universal curve in the sense that it is valid for all values of stagnation Reynolds number.

3.3 Effect of the Variation in Gamma and Prandtl Number on the Flow Quantities

In Figs. 12-28, an exhaustive study has been carried out to determine the effect of the variation in Prandtl number and gamma on the structure and the overall characteristics of the flow field.

(a) Effect of Variation of Prandtl Number

Figure 12 shows the variation of the heat transfer coefficient, C_H, against Prandtl number for different values of gamma, γ with and without surface slip conditions at an altitude of 104.93 Kms of the reentry conditions of the space shuttle. It was observed that with decrease in Prandtl number, the values of stagnation point heat transfer coefficient increased. It was further noticed that as gamma, γ decreased, the values of the heat transfer coefficient increased for all Prandtl numbers. Figs. 11 (b, c, d, e) show the variation of the heat transfer coefficient, C_H with Prandtl number for $\gamma = 1.4, 1.3, 1.2$ and 1.1 respectively. It was observed that the values of the heat transfer coefficient, C_H, with surface slip conditions were more than the values with noslip conditions. But with decrease in gamma γ, the values of C_H with the slip and noslip conditions came close to each other mainly because $\frac{T_{o\infty}}{T_\infty}$ ($\frac{T_{o\infty}}{T_\infty} = 1 + \frac{\gamma-1}{2} M_\infty^2$) decreased, which resulted in an increase in the wall temperature ratio $\bar{T}_w$ ($\bar{T}_w = \frac{T_w}{T_{o\infty}}$).

With decrease in the Prandtl number, the other changes observed in the merged layer were (i) the merged layer thickness

increased slightly (Fig. 13), (ii) the maximum temperature decreased (Fig. 14), (iii) and there was little effect on the location of the maximum temperature in the merged layer under the prescribed conditions (Fig. 15). (Also see Tables 3.1, 3.2).

A similar kind of study was carried out at an altitude of 92.35 Kms of the shuttle flight conditions in order to confirm the above drawn conclusions. Figs. 16 and 17 respectively show the variations of the heat transfer coefficient, C_H, and the temperature profiles with different Prandtl numbers (See Table 3.3 and 3.4).

Prandtl number is given by the following relation:

$$Pr = \frac{\mu C_p}{\kappa}$$

where κ represents the coefficient of thermal conductivity. With decrease in Prandtl number, the conductivity increases thereby causing more diffusion of heat towards the outer edge of the merged layer. As a result, the merged layer thickness increases and the maximum temperature decreases. Also, larger amount of heat is transferred to the wall, thus increasing the heat transfer coefficient, C_H, at the wall.

Figures 18 and 19 respectively show the variation of the skin-friction coefficient parameter, $C_F/\mathrm{Sin}\Theta$, with the Prandtl number at altitude 104.93 Kms and 92.35 Kms. As expected, the skin-friction coefficient parameter is observed to follow the similar kind of variation as shown by the heat transfer coefficient, C_H.

(b) Effect of the Variation in Gamma

Figures 20-28 show the effect of the variation in gamma γ, on the structure of the merged layer and its overall characteristics.

Figure 20 shows the variation of the stagnation point heat transfer coefficient, C_H with gamma for Pr = 0.6, 0.8, 1.0 at an altitude of 104.93 Kms, with and without surface slip conditions. The figure shows an increase in the heat transfer coefficient, C_H, with decrease in the value of gamma. Figs. 20(b, c, d) show the variation of C_H with gamma for Pr = 0.6, 0.8 and 1.0 for surface slip and noslip cases. The difference between the two curves with and without slip decreased as gamma decreased.

From Figs. 21-23, it was observed that at the altitude of 104.93 Kms, the decrease in gamma resulted in (i) decrease in the merged layer thickness, (ii) decrease in the maximum temperature and (iii) the shift in the location of the maximum temperature towards the wall. From Fig. 23 we found that the effect of the change in gamma was realised more in the shock wave like zone of the merged layer, than in the inner viscous layer. Figs. 24 and 25 respectively show the tangential velocity profiles and the temperature profiles for various values of gamma at Pr = 0.8 with surface slip conditions at 104.93 Kms altitude. In Figs. 26-28, a similar kind of study has been done for the reentry space shuttle conditions at the altitude 92.35 Kms.The results at high Reynolds number (altitude = 92.35 Kms) are similar to the results at low

Reynolds number (altitude = 104.93 Kms). However, the increase in the value of the heat transfer coefficient, C_H, with decrease in gamma was observed to be much smaller at high Reynolds number than at low Reynolds number. Figs. 29 and 30 respectively show the variation of the skin-friction coefficient parameter, $C_F/\mathrm{Sin}\Theta$, with gamma at altitudes of 104.93 Kms and 92.35 Kms. The skin-friction coefficient parameter, $C_F/\mathrm{Sin}\Theta$, is observed to behave in a way similar to the behaviour of the heat transfer coefficient, C_H.

We can physically explain the effect of gamma γ , on the flow characteristics as follows:

Gamma, is given by the ratio of the specific heats, viz., $\gamma = \frac{C_p}{C_v}$ where C_p and C_v are specific heats at constant pressure and volume respectively. With decrease in gamma, the specific heat at constant volume, C_v, increases more rapidly than the specific heat at constant pressure, C_p. For the same energy content ($e = C_vT$), the maximum temperature will decrease with increase in C_v. As explained earlier, by decreasing gamma, we are to some extent simulating the real gas effects which involve ionization and dissociation processes. Also, a decrease in γ increases density in the merged layer. For the same mass flow rate, the increase in density implies a decrease in merged layer thickness due to which the heat transfer coefficient, C_H, increases.

3.4 Comparison of the Results from Present Investigation with the Available Experimental Data and Theoretical Results

Figures 31-35 show the comparison of the present results with the available experimental and theoretical results. The overall characteristics of the flow field from the present calculations for monatomic and diatomic gases have also been compared.

Figure 31 shows the variation of the heat transfer coefficient, C_H, with the stagnation Reynolds number for different altitudes of the shuttle flight conditions at $\gamma = 1.4$ and $\gamma = 1.66$ with surface slip conditions. These results were compared with the Direct Simulation Monte-Carlo Technique (DSMC) results of Moss and Bird[9] and with values of the heat transfer coefficient obtained from the empirical formula of Fay and Riddle (See Table 4, Section VI). It was observed that the values of C_H for a monatomic gas ($\gamma = 1.66$) fell below the values of C_H for a diatomic gas ($\gamma = 1.4$). The curve for the heat transfer coefficient, C_H from the present results at $\gamma = 1.4$ when compared with the DSMC results of Moss and Bird[9] shows a reasonably good agreement upto an altitude of 104.93 Kms of shuttle flight conditions. The maximum difference between the two results is 8 percent at 104.93 Kms altitude. The present results are also found to be in fairly good agreement with Fay and Riddle values of heat transfer coefficient, C_H, upto an altitude of 104.93 kms.

Figure 32 shows the variation of the skin-friction parameter, $C_F/Sin\Theta$, for different shuttle flight conditions (See Table 1, Section VI) at $\gamma = 1.4$ and $\gamma = 1.66$. The figure showed that $C_F/Sin\Theta$ followed a trend similar to the heat transfer coefficient, C_H in Fig. 31.

In Fig. 33, wall pressure was plotted against stagnation Reynolds number for a monatomic gas ($\gamma = 1.66$) and a diatomic gas ($\gamma = 1.4$) at Pr = 0.75 for different shuttle flight conditions. It was observed that the wall pressure for the monatomic gas had lower values in comparison to that of diatomic gas. With decrease in stagnation Reynolds number, the wall pressure increased and the increase was faster at low Reynolds number. Experimental results of Potter and Bailey[17] for $\gamma = 1.4$, $T_w = T_{o\infty}$, $M_\infty = 3.9\text{-}6.0$ and for $\gamma = 1.66$ with $T_w = T_{o\infty}$ and $M_\infty = 4.3\text{-}5.7$, were also plotted. Potter and Bailey[17] carried out the experiments for a flat-nosed probe and found that the impact pressure for monatomic gas dipped to lower values as compared to the diatomic gas. The trend shown by the results from present investigation compares well with the experimental results of Potter and Bailey[17] and Sherman[7]. Fig. 34 shows the variation of the wall pressure for different shuttle flight conditions at Pr = 0.75 and Pr = 1.0. It was observed that the curve for Pr = 1.0 falls below the curve for Pr = 0.75 and the two curves merged into each other at high Reynolds number indicating negligible effect of Prandtl number variation on surface pressure in the denser region of atmosphere.

3.5 Effect of Ablation

Figures 35-40 give the affect of ablation on the flow variables and overall characteristics of the flow field. This study has been done at Re = 50, M_∞ = 20 and $\bar{T}_w$ = 0.2 with and without surface slip conditions. As pointed out in the text, the slip conditions modified for the mass transport across the Knudsen layer have been used. Fig. 35 shows the velocity and temperature profiles with and without ablation for surface slip. The surface temperature $\bar{T}_s$ decreased with ablation. This is very much evident from the relation of $\bar{T}_s$ from equation (53). It was noticed that the gradients of the flow parameter reduced and merged layer thickness increased with ablation. Fig. 36 shows the pressure and density profiles. Pressure fluctuations near the wall were observed and an increase in the pressure and density was noticed in the shockwave like zone of the merged layer. The study for the noslip case (Figs. 37 and 38) gave a similar kind of variation. Figs. 39 and 40 show a decrease in the values of the heat transfer coefficient and skin-friction coefficient parameter with increase in the mass transfer parameter, M ($M = \bar{\rho}\bar{v}$). The present results for ablation were found to be consistent with the results of Moss[15] who carried out the calculations for the noslip conditions.

In the present study for ablation, very small amount of injection velocity could be achieved ($\bar{v}_I = 0.002$) and for larger injection velocities the process becomes unstable. The calculations were carried out for a constant value of n_{eo}. A modification in the numerical technique for the present code is recommended to apply larger injection velocities.

SECTION IV

SUMMARY

The present study deals with the solution of the NS equations to investigate the stagnation point merged layer flow past the spherical nose of a space vehicle.

An attempt has been made to understand the basic nature of the flow with variations in the surface temperature, viscosity - temperature relations, gamma and Prandtl number. Particular emphasis has been placed in simulating the real gas effects through the concept of effective gamma, γ. Various graphs and tables are presented to show the changes in the structure and the overall characteristics of the flow field under shuttle reentry conditions.

In the present investigation, we found that slip and temperature jump conditions had considerable effect on the flow quantities. For a very cold wall case, the surface slip condition increased the heat transfer coefficient and the skin-friction coefficient parameter from their value with noslip conditions while the reverse was true for a relatively hot wall. The viscosity-temperature relation was also observed to affect the structure and the overall characteristics of the flow field. The affect of μ-T relation was quite significant at low Reynolds number.

Further, it was observed that a decrease in gamma γ, resulted in a decrease in the merged layer thickness and the maximum temperature in the merged layer while the heat transfer coefficient, C_H increased. A decrease in the Prandtl number increased the heat transfer coefficient C_H, and the merged layer thickness but the maximum temperature in the merged layer decreased. The comparison of the present results with the experimental results of Potter and Bailey[17] led us to conclude that the surface pressure for monatomic gases are lower than the surface pressure for diatomic gases. Finally, we found that ablation led to a decrease in the heat transfer coefficient, C_H, and skin friction coefficient parameter, $C_F/\text{Sin}\theta$. Certain modifications will be necessary in the numerical technique in the present formulation if one wants to apply massive blowing.

SECTION V

REFERENCES

(1) Bird, G.A., "Definition of mean free path for Real gases", Physics of Fluids, Vol. 26, 1983, pp.3222-3223.

(2) Davis, R.T., "Numerical Solution of the Hypersonic Viscous Shock-Layer Equations", AIAA J., Vol. 8., No.5, 1970, pp. 843-851.

(3) Hayes, W.D. and Probstein, R.F., "Hypersonic Flow Theory", Academic Press Inc., New York, 1959.

(4) Hayes, W.D. and Probstein, R.F., "Hypersonic Flow Theory", Vol. 1,1966.

(5) Jain, A.C. and Prabha, S., "A Comparative Study of Stagnation Point Hypersonic Viscous Shock Layer and Hypersonic Merged Layer Flows", 14th Int. Symp. on RGD, edited by H. Oguchi, 1984, pp. 241-248.

(6) Jain, A.C. and Adimurthy, V., "Hypersonic Merged Stagnation Shock Layers", Part I : Adiabatic Wall Case, pp. 342-347; Part II : Cold Wall Case, pp. 348-354; AIAA J., Vol. 12, No.3,1974.

(7) Jain, A.C., "Lectures on Reentry Aerodynamics", May-June, 1980.

(8) Jain, A.C. and Prabha, S., "Hypersonic Second Order Merged Layer on Blunt Bodies", Submitted to the Department of Space Govt. of India , Aug., 1982.

(9) Jain, A.C., "Hypersonic Merged Layer Flow over a Sphere", AIAA Paper 85-1031, 1985.

(10) Jain, A.C. and Hamilton G. Woods, "Investigation of Hypersonic Rarefied Flow on a Spherical Nose of AOTV", NASA SBIR, Phase 1, Final Report submitted to NASA under contract NASA - 37305, July 1987.

(11) Kao, H.C., "Hypersonic Viscous Flow Near the Stagnation Streamline of a Blunt Body", AIAA J., Vol. 2, 1964, pp. 1896-1906.

(12) Levinsky, F.S. and Yoshihara, H., "Rarefied Hypersonic Flow Over a Sphere", Hypersonic Flow Research, edited by F.R. Riddel, Academic Press, New York, 1962, pp. 81-106.

(13) Liberstein, H.M., "A Course in Numerical Analysis", Harper and Row Publishers, Inc., New York, 1986, p. 113.

(14) Murray, A.L. and Lewis, C.H., "Heat and Mass-Transfer Effects on Three Dimensional Viscous Shock Layer Flows", 2nd AIAA/ASME Thermophysics and Heat Transfer Conference, May 24-26, 1978.

(15) Moss, J.N., "Reacting Viscous-Shock Layer Solutions with Multicomponent Diffusion and Mass Injection", NASA TR R-411.

(16) Probstein, R.F. and Kemp, N.H., "Viscous Aerodynamic Characteristics in Hypersonic Rarefied Gas Flows", J. Aerospace Sci., Vol. 27, pp. 174-192 (1960).

(17) Potter, J.L. and Bailey, A.B., "Pressure in the Stagnation Region of Blunt Bodies in the Viscous Layer to Merged Layer Regimes of Rarefied Flow", AEDC - TDR - 63 - 168, Sept., 1983.

(18) Patterson, G.N., "Molecular Flow of Gases", John Wiley and Sons, Inc., New York, 1956.

(19) Shidlovskiy, V.P., "Introduction to the Dynamics of Rarefied Gases", American Elsevier Publishing Company, Inc., New York, 1967.

(20) Van Dyke, M., "Second-order compressible boundary layer theory with application to blunt bodies in hypersonic flow", ARS Progress in Astronautics and Rocketry : Hypersonic Flow Research, edited by F.R. Riddell (Academic Press, New York, 1962), Vol. 7, pp. 37-76.

(21) Vogenitz, F.W. and Takata, G.Y., "Monte-Carlo Study of Blunt Body Hypersonic Viscous Shock Layer", 7th RGD Symposium, 1972, pp. 911-918.

(22) Whitehead, R.E. and Davis, R.T., "Surface Conditions in Slip Flow with Mass Transfer", SC - CR - 69 - 3289.

(23) Yuan, S.W., "Foundations of Fluid Mechanics", Prentice Hall, 1976.

SECTION VI

Tables

1. Ambient conditions for Shuttle Flight

Table 1

$\gamma = 1.4$, $Pr = 0.7$

Altitude Kms	U_∞ Km/sec	ρ_∞ gm/cm^3	T_∞ ^oK	r_B cms	Re_∞	M_∞	T_w ^oK
109.75	7.47	0.115×10^{-9}	249.0	136.2	73.148	23.613	387.0
104.93	7.47	0.246×10^{-9}	223.0	136.2	171.65	24.95	506.5
99.49	7.50	0.591×10^{-9}	190.0	136.2	474.617	27.14	705.0
92.35	7.50	0.218×10^{-8}	180.0	129.61	1750.85	27.88	921.5
85.74	7.53	0.637×10^{-8}	198.9	132.2	4791.76	26.63	1190.0

2. Values of stagnation point heat transfer coefficient, C_H and skin-friction coefficient parameter $C_F/\text{Sin}\Theta$ with surface temperature variation

Table 2.1

$Re = 10$, $M_\infty = 20$, $\gamma = 1.4$, $Pr = 0.7$

WALL TEMPERATURE $\bar{T}_w$ =	0.05	0.1	0.2	0.4	0.6	0.8	0.9	1.0	1.1	1.15
NOSLIP C_H	0.6336	0.643	0.628	0.5014	0.368	0.233	0.165	0.097	0.03	-0.002
$C_F/\text{Sin}\Theta$	0.46	0.548	0.608	0.644	0.669	0.69	0.70	0.711	0.723	0.728
SLIP C_H	0.644	0.60	0.552	0.383	0.26	0.144	0.09	0.036	-0.013	-
$C_F/\text{Sin}\Theta$	0.5549	0.558	0.542	0.547	0.522	0.536	0.535	0.532	0.530	-

Table 2.2

Re = 50, M_∞ = 20, γ= 1.4, Pr = 0.7

WALL TEMPERATURE $\bar{T}_w$ =		0.05	0.1	0.2	0.4	0.6	0.8	1.0	1.1
NOSLIP	C_H	0.28	0.292	0.275	0.206	0.139	0.074	0.011	-0.02
	$C_F/Sin\Theta$	0.202	0.228	0.249	0.262	0.271	0.279	0.287	0.29
SLIP	C_H	0.304	0.295	0.256	0.198	0.111	0.048	-0.012	-
	$C_F/Sin\Theta$	0.23	0.24	0.243	0.24380	0.251	0.254	0.256	-

3. Values of C_H, $C_F/Sin\Theta$, $\bar{T}_{max}$ and n_{eo} with variation in gamma, and Prandtl number, Pr

Table 3.1

Altitude = 104.93 Kms (without surface slip conditions)

Gamma (γ) =		1.4	1.3	1.2	1.1
Pr = 0.6	C_H	0.4557	0.4991	0.5606	0.6752
	$C_F/Sin\Theta$	0.3352	0.3675	0.4141	0.5178
	$\bar{T}_{max}$	0.6011	0.5814	0.5579	0.5528
	n_{eo}	0.484	0.407	0.326	0.248
Pr = 0.8	C_H	0.394	0.44	0.4915	0.579
	$C_F/Sin\Theta$	0.321	0.356	0.397	0.4836
	$\bar{T}_{max}$	0.706	0.684	0.653	0.622
	n_{eo}	0.457	0.383	0.3	0.215
Pr = 1.0	C_H	0.3584	0.3954	0.4539	0.5508
	$C_F/Sin\Theta$	0.319	0.349	0.397	0.4652
	$\bar{T}_{max}$	0.789	0.766	0.734	0.688

Table 3.2

Altitude = 104.93 Kms (with surface slip conditions)

GAMMA (γ) =		1.4	1.3	1.2	1.1
Pr=0.6	C_H	0.704	0.7047	0.7102	0.6814
	$C_F/\sin\Theta$	0.546	0.543	0.5438	0.566
	$\bar{T}_{max}$	0.648	0.622	0.59	0.572
	n_{eo}	0.506	0.423	0.336	0.254
Pr=0.8	C_H	0.61755	0.634	0.64	0.658
	$C_F/\sin\Theta$	0.546	0.549	0.5488	0.5573
	$\bar{T}_{max}$	0.7579	0.7298	0.6913	0.6477
	n_{eo}	0.477	0.397	0.31	0.213
Pr=1.0	C_H	0.549	0.568	0.573	0.6073
	$C_F/\sin\Theta$	0.55	0.549	0.546	0.557
	$\bar{T}_{max}$	0.8401	0.8121	0.7728	0.7183
	n_{eo}	0.455	0.379	0.296	0.2

Table 3.3

Altitude = 92.35 Kms (without surface slip conditions)

GAMMA (γ) =		1.4	1.3	1.2	1.1
Pr=0.6	C_H	0.1956	0.2174	0.2474	0.2919
	$C_F/\sin\Theta$	0.1235	0.1322	0.1441	0.1642
	$\bar{T}_{max}$	0.9645	0.963	0.956	0.94
	n_{eo}	0.166	0.135	0.102	0.068
Pr=0.8	C_H	0.1655	0.179	0.205	0.2423
	$C_F/\sin\Theta$	0.1223	0.13045	0.1430	0.1623
	$\bar{T}_{max}$	0.9888	0.9859	0.9835	0.972
	n_{eo}	0.146	0.129	0.097	0.063
Pr=1.0	C_H	0.144	0.1539	0.17728	0.2093
	$C_F/\sin\Theta$	0.119	0.12831	0.1407	0.16038
	$\bar{T}_{max}$	1.02	0.7986	0.999	0.9894
	n_{eo}	0.146	0.126	0.094	0.061

Table 3.4

Altitude = 92.35 Kms (with surface slip conditions)

GAMMA (γ)		1.4	1.3	1.2	1.1
Pr=0.6	C_H	0.2315	0.2466	0.2639	0.2932
	C_F /SinΘ	0.1515	0.1543	0.16	0.169
	$\bar{T}_{max}$	0.964	0.9635	0.958	0.94
	n_{eo}	0.1665	0.1355	0.1035	0.0675
Pr=0.8	C_H	0.198	0.2049	0.2223	0.2427
	C_F /SinΘ	0.1505	0.153	0.158	0.1685
	$\bar{T}_{max}$	0.9887	0.9852	0.9851	0.9736
	n_{eo}	0.1485	0.1285	0.0975	0.0635
Pr=1.0	C_H	0.176	0.177	0.192	0.2156
	C_F /SinΘ	0.1486	0.1511	0.1565	0.168
	$\bar{T}_{max}$	1.018	0.9986	0.999	0.987
	n_{eo}	0.1485	0.1275	0.0945	0.0595

4. Universal C_H curve: In this table, the values of the heat transfer coefficient with surface slip for space shuttle reentry conditions (using Sutherland and square-root law of viscosity), AFE trajectory and Fay and Riddle's empirical formula are compared. Fay and Riddle's formula is given as follows:

$$C_H = \frac{q}{\frac{1}{2}\rho_\infty U_\infty^3} = (2^{1/4} \times 0.94)\left(\frac{p_{eo}}{p_\infty} \cdot \frac{T_\infty}{T_{eo}}\right)^{0.5} \times \left(\sqrt{\frac{T_{eo}}{T_w}}\right)^{0.1}$$

$$\times \frac{1}{\sqrt{M_\infty \times Re}} \times \left(1 + \frac{2}{(\gamma-1)\,M_\infty^2}\right) \times \left(1 - \frac{T_w}{T_{eo}}\right)$$

$$\times \left(\frac{\frac{p_{eo}}{p_\infty} - 1}{\frac{p_{eo}}{p_\infty} \cdot \frac{T_\infty}{T_{eo}}}\right)^{1/4}$$

where Re is the stagnation Reynolds number

$$\frac{p_{eo}}{p_\infty} = \left[\frac{\gamma + 1}{2\gamma M_\infty^2 - (\gamma-1)}\right]^{\frac{1}{\gamma-1}} \times \left[\frac{(\gamma+1)\,M_\infty^2}{(\gamma-1)M_\infty^2 + 2}\right]^{\frac{\gamma}{\gamma-1}} \times \left(1 + \frac{\gamma-1}{2} M_\infty^2\right)^{\frac{}{\gamma-}}$$

and $$\frac{T_{eo}}{T_\infty} = 1 + \frac{\gamma-1}{2} M_\infty^2$$

$\gamma = 1.4$, Pr = 0.72

Table 4

SHUTTLE VALUES		FAY & RIDDLE VALUES	AFE TRAJECTORY	
Re	C_H	C_H	Re	C_H
4.8132	0.8479	0.9774	10	0.69
6.92	0.7607	0.8152	16.6	0.55
10.288	0.6528	0.656	31.62	0.4
15.321	0.5522	0.5378	56.23	0.3
24.762	0.43284	0.41291	100	0.2
38,99	0.3419	0.32906	158.48	0.145
139.95	0.1498	0.169	182	0.13
258.81	0.0998	0.1222		

5. Values of the heat transfer coefficient, C_H, and skin-friction coefficient parameter, $C_F/\sin\theta$ with different μ-T relations for surface slip conditions

Table 5

$\gamma = 1.4$, Pr = 0.72

Altitude Kms	Square-root law of viscosity	Sutherland law of viscosity
104.93	$C_H = 0.5574$ $C_F/\sin\theta = 0.45165$	$C_H = 0.64824$ $C_F/\sin\theta = 0.54438$
99.49	$C_H = 0.34307$ $C_F/\sin\theta = 0.259$	$C_H = 0.43417$ $C_F/\sin\theta = 0.3412$
92.35	$C_H = 0.1498$ $C_F/\sin\theta = 0.10685$	$C_H = 0.20314$ $C_F/\sin\theta = 0.14727$

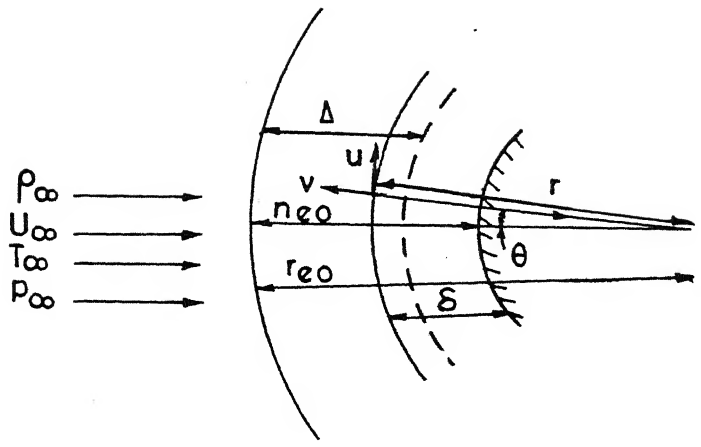

FIG. A CO ORDINATE SYSTEM AND SYMBOLS

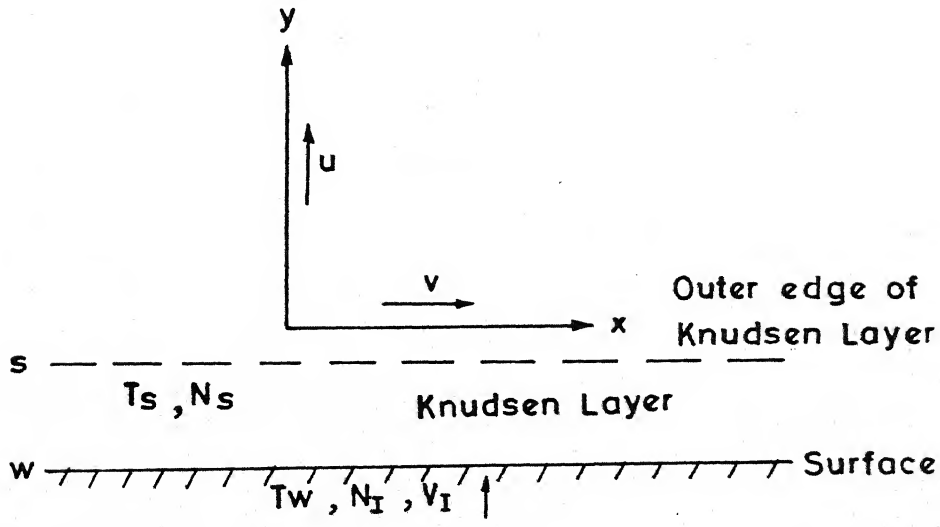

FIG. B COORDINATE SYSTEM FOR SLIP FLOW BOUNDARY CONDITIONS

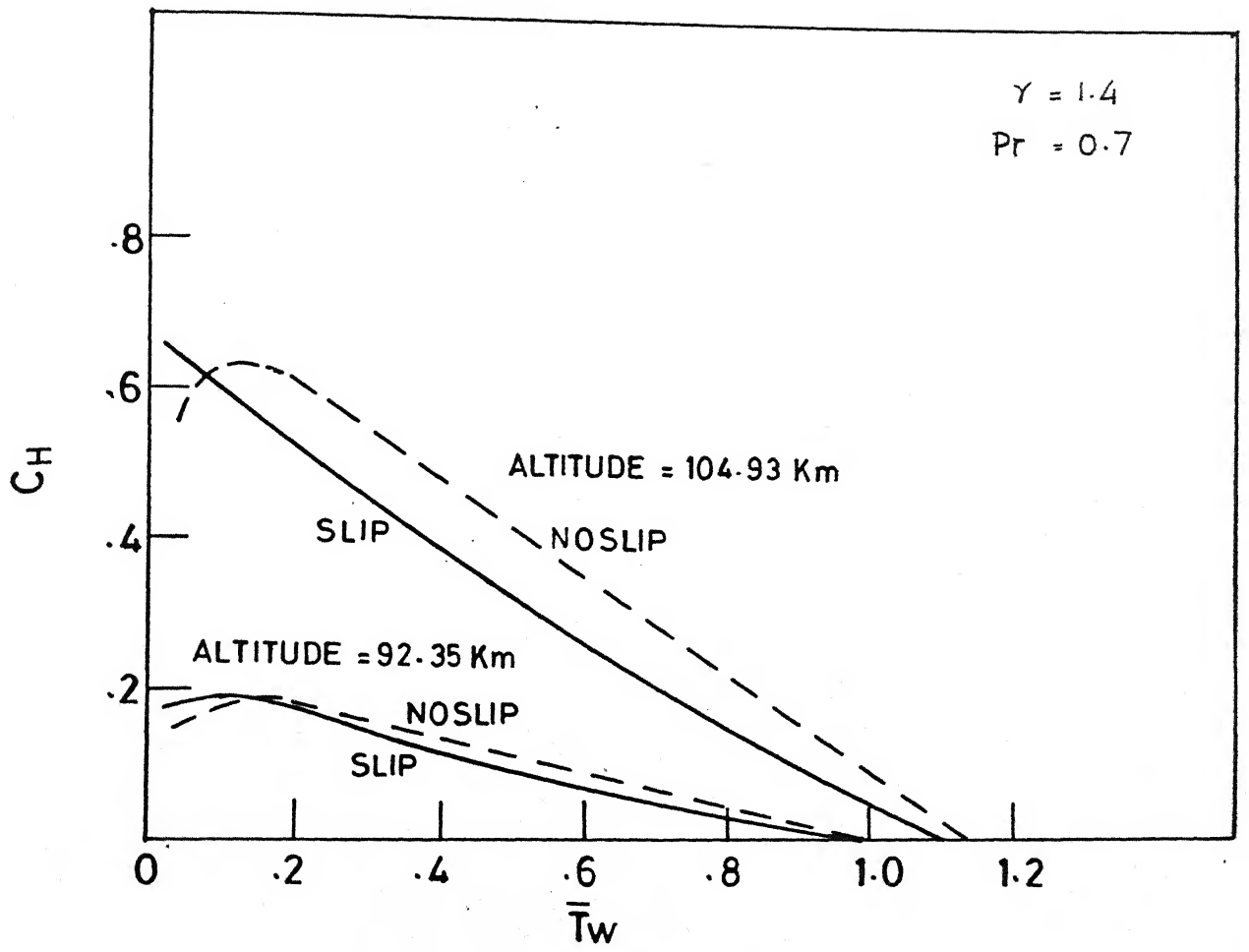

FIG. 1 VARIATION OF THE HEAT TRANSFER COEFFICIENT, C_H, WITH WALL TEMPERATURE FOR SURFACE SLIP AND NOSLIP CONDITIONS

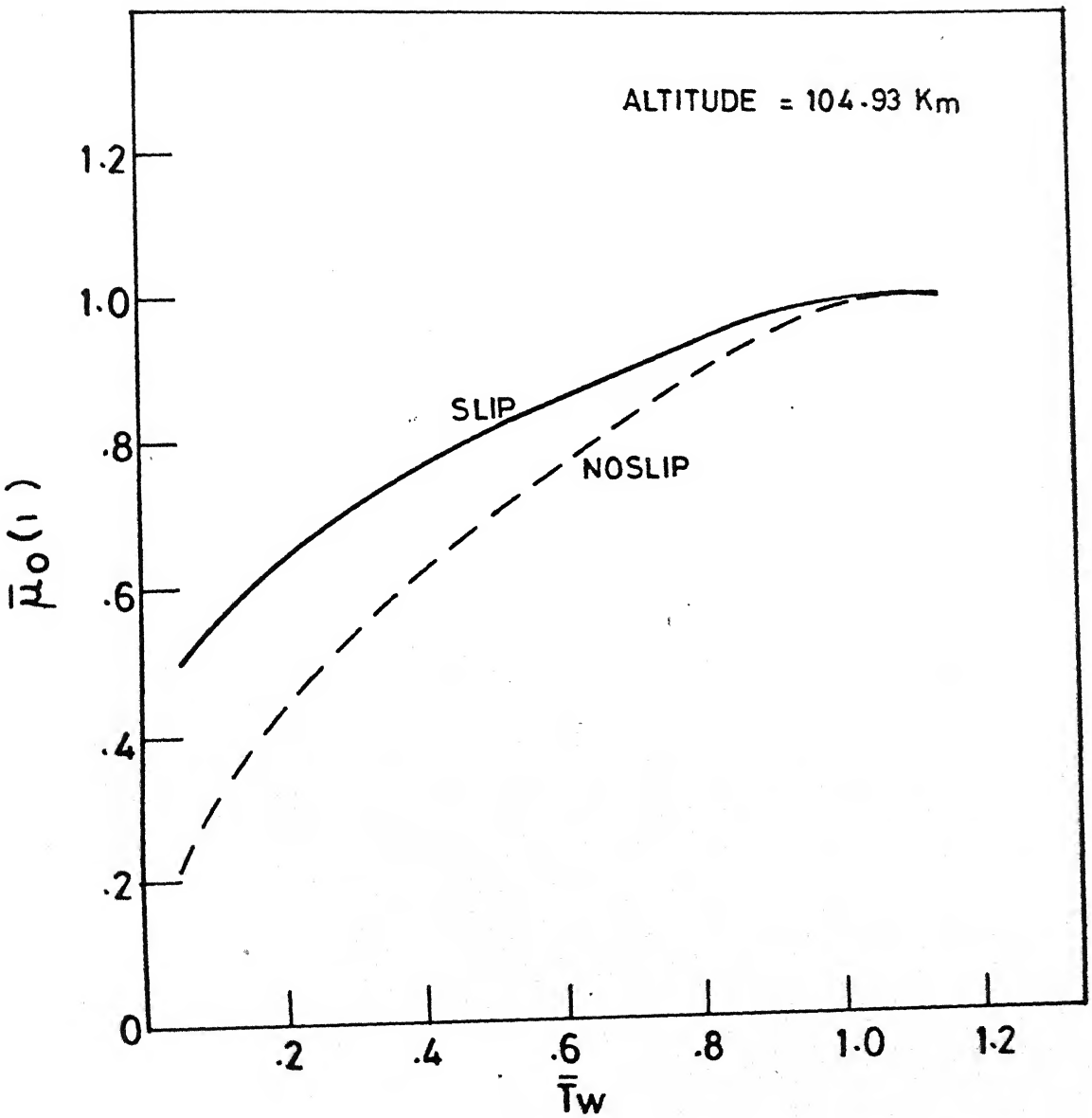

FIG. 2 VARIATION OF VISCOSITY AT THE SURFACE WITH WALL TEMPERATURE FOR SURFACE SLIP AND NO SLIP CONDITIONS

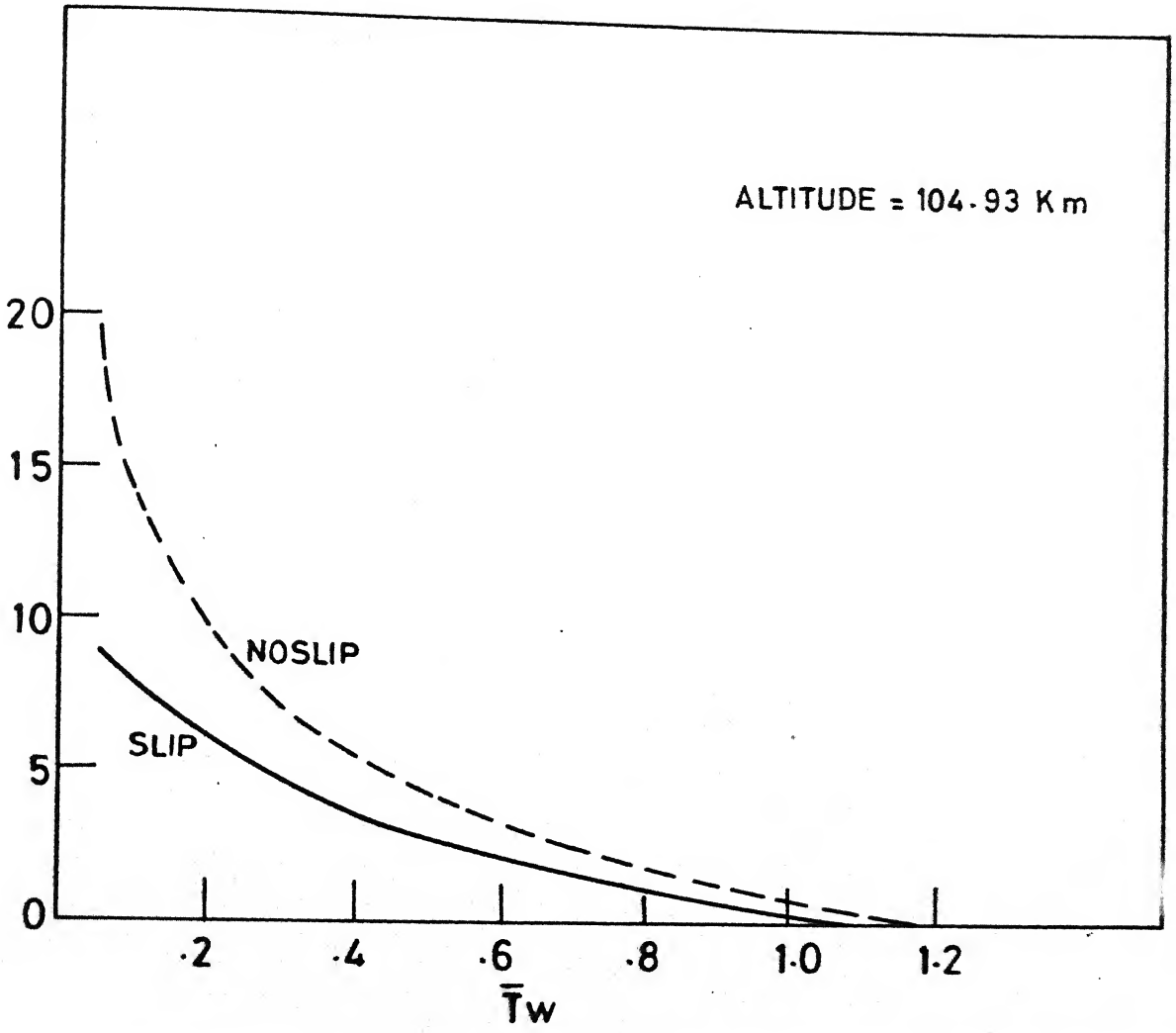

. 3 COMPARISON OF TEMPERATURE GRADIENT WITH WALL TEMPERATURE FOR SURFACE SLIP AND NO SLIP CONDITIONS

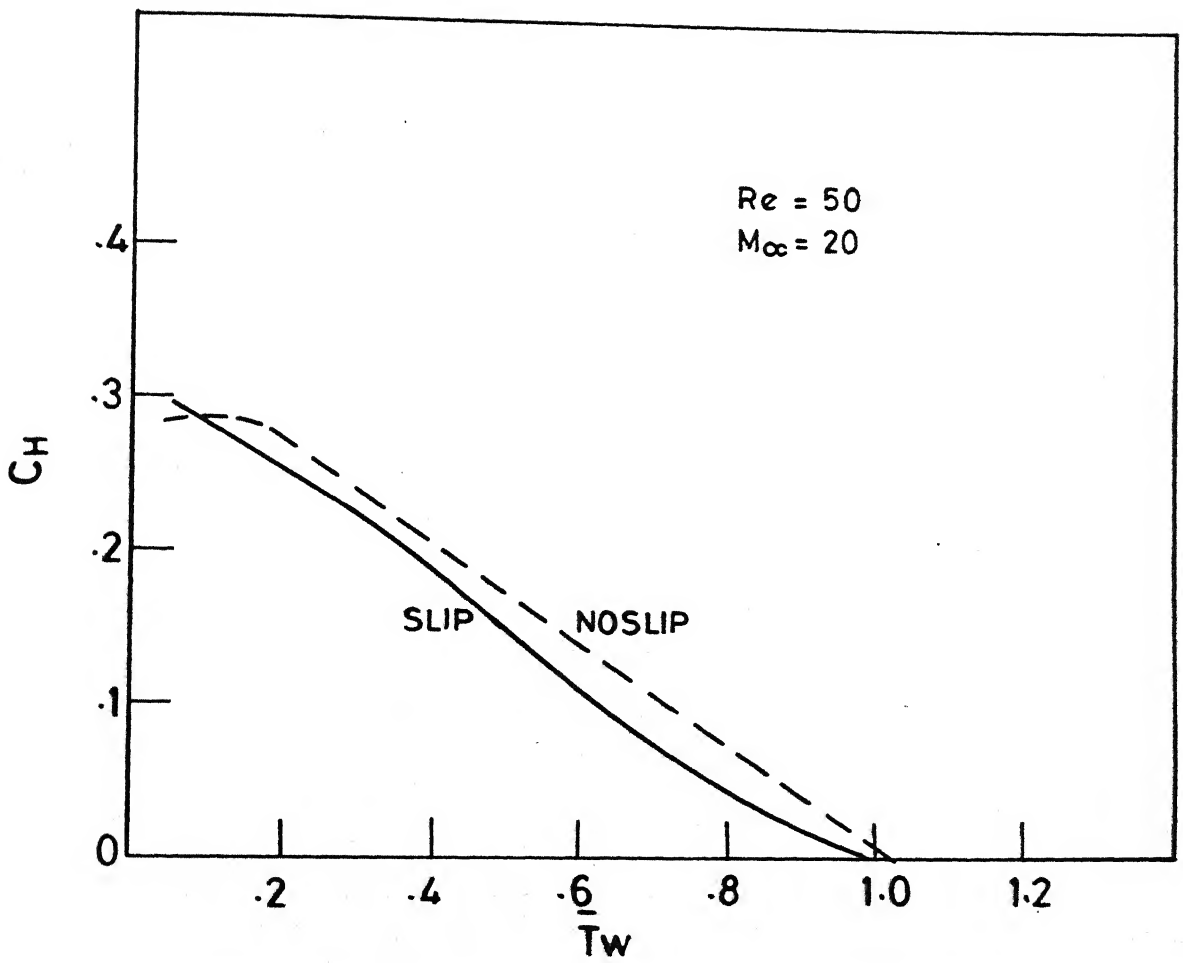

FIG. 4 VARIATION OF THE STAGNATION POINT HEAT TRANSFER COEFFICIENT C_H WITH WALL TEMPERATURE, $\bar{T}w$ FOR SURFACE SLIP AND NOSLIP CONDITIONS

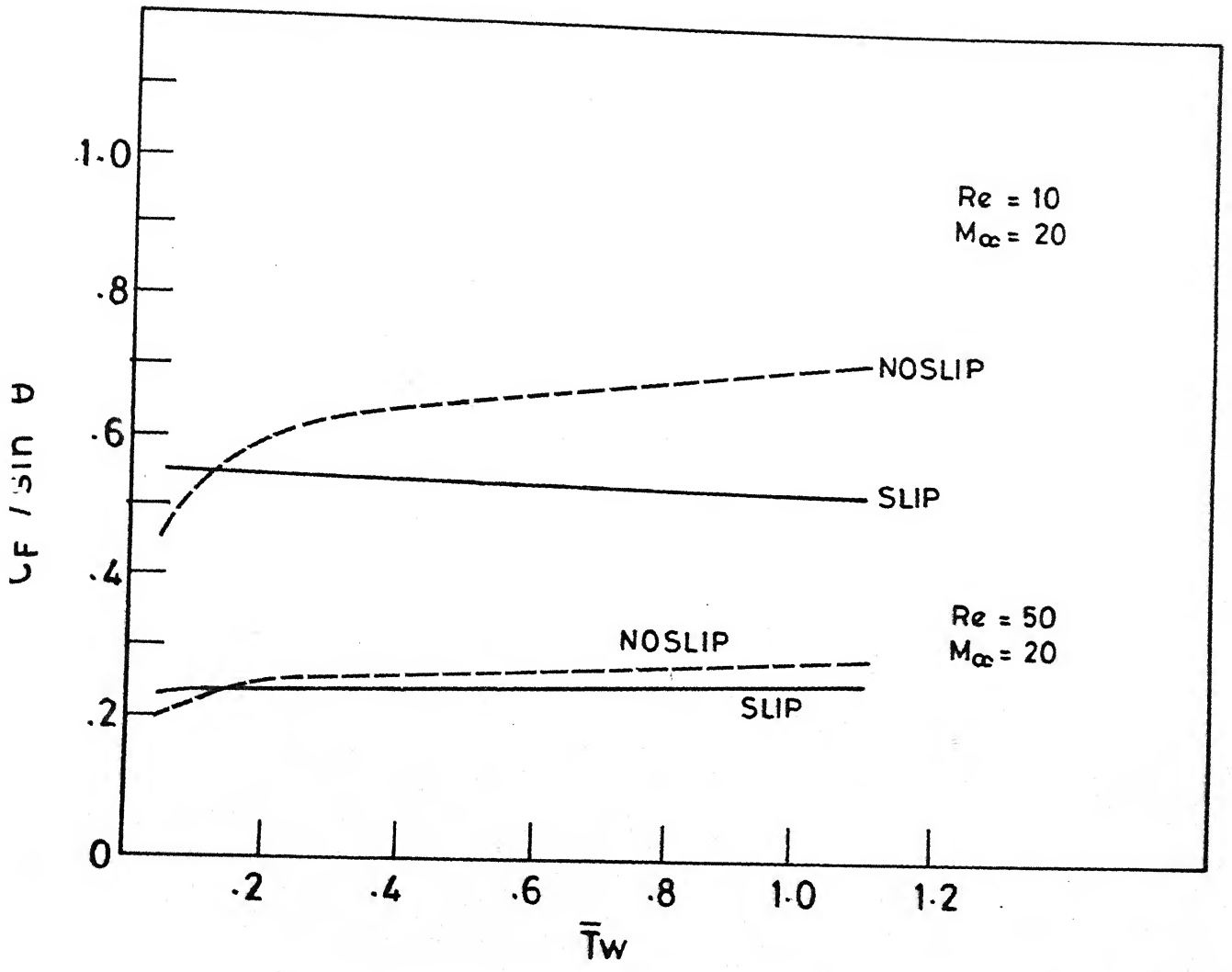

FIG. 5 VARIATION OF SKIN-FRICTION COEFFICIENT PARAMETER, $C_F / \sin\theta$, WITH WALL TEMPERATURE, $\bar{T}w$, FOR SURFACE SLIP AND NOSLIP CONDITIONS

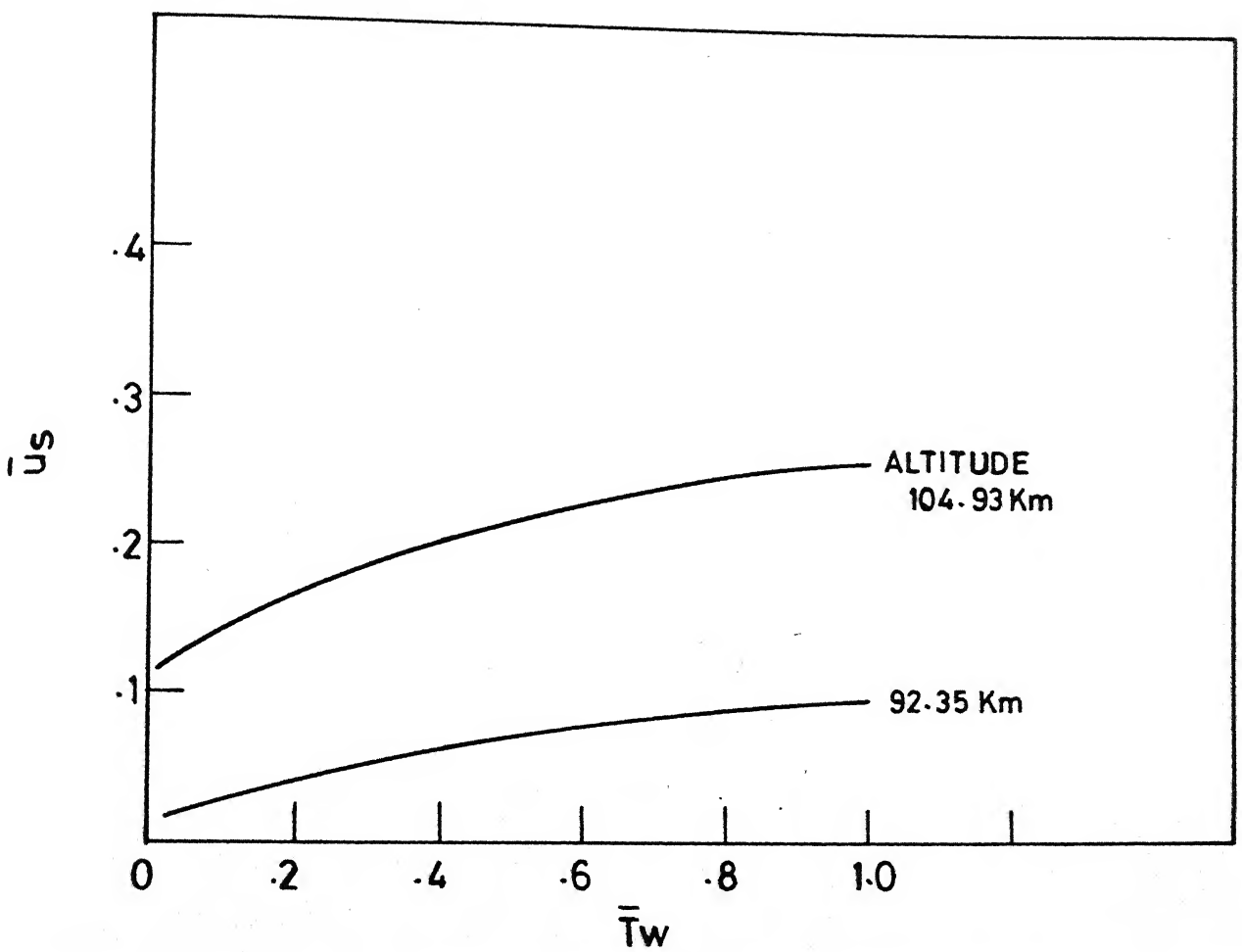

FIG. 6 VARIATION OF SLIP VELOCITY AT THE SURFACE WITH WALL TEMPERATURE FOR SHUTTLE CONDITIONS AT 104.93 AND 92.35 Kms.

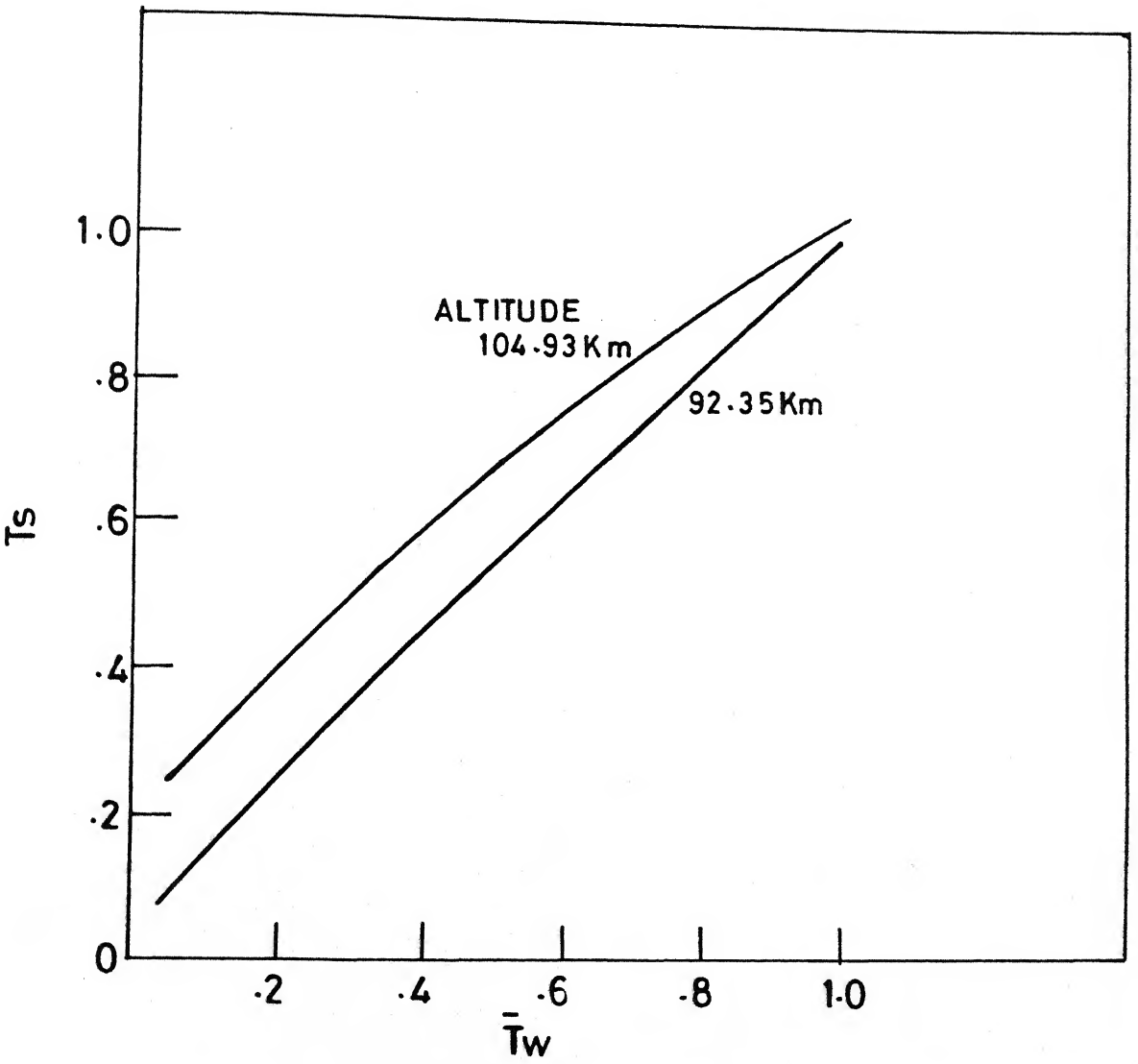

FIG. 7 VARIATION OF THE TEMPERATURE AT THE BASE OF THE VISCOUS LAYER WITH WALL TEMPERATURE, $\bar{T}w$ FOR SHUTTLE CONDITIONS AT 104.93 AND 92.35 Kms

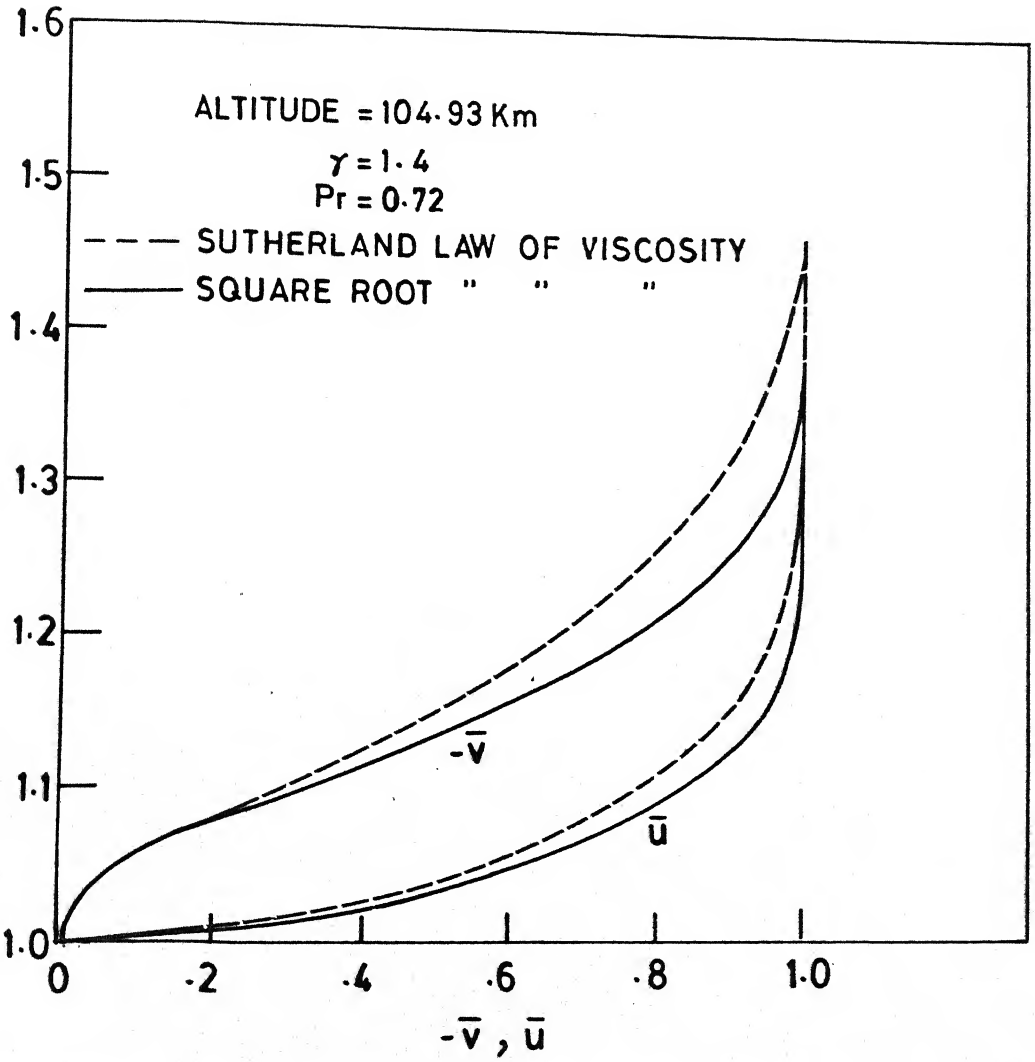

FIG. 8 STAGNATION POINT TANGENTIAL VELOCITY AND NORMAL VELOCITY PROFILES FOR DIFFERENT VISCOSITY TEMPERATURE RELATIONS

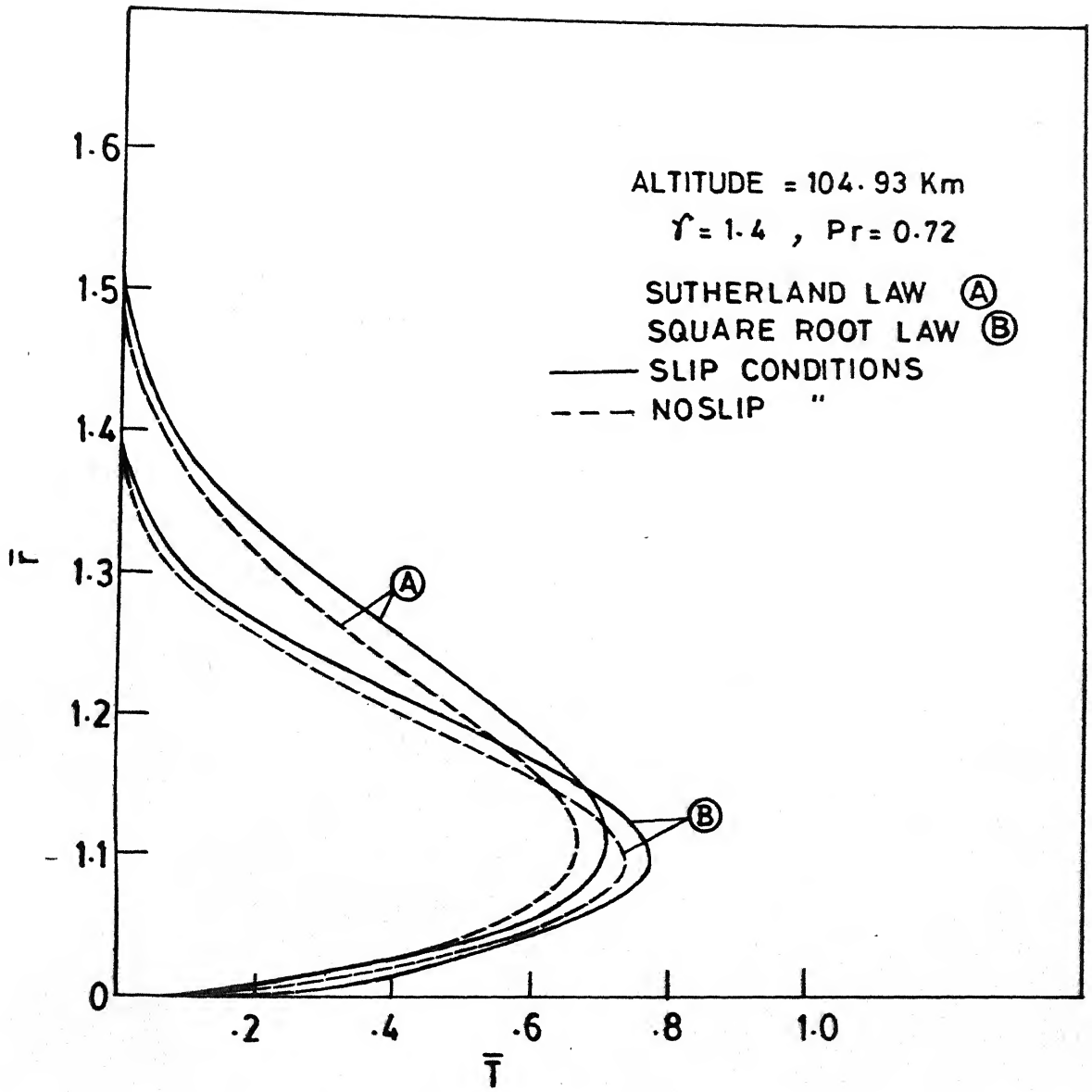

FIG. 9 STAGNATION POINT TEMPERATURE PROFILES FOR DIFFERENT VISCOSITY TEMPERATURE RELATIONS WITH AND WITHOUT SURFACE SLIP CONDITION

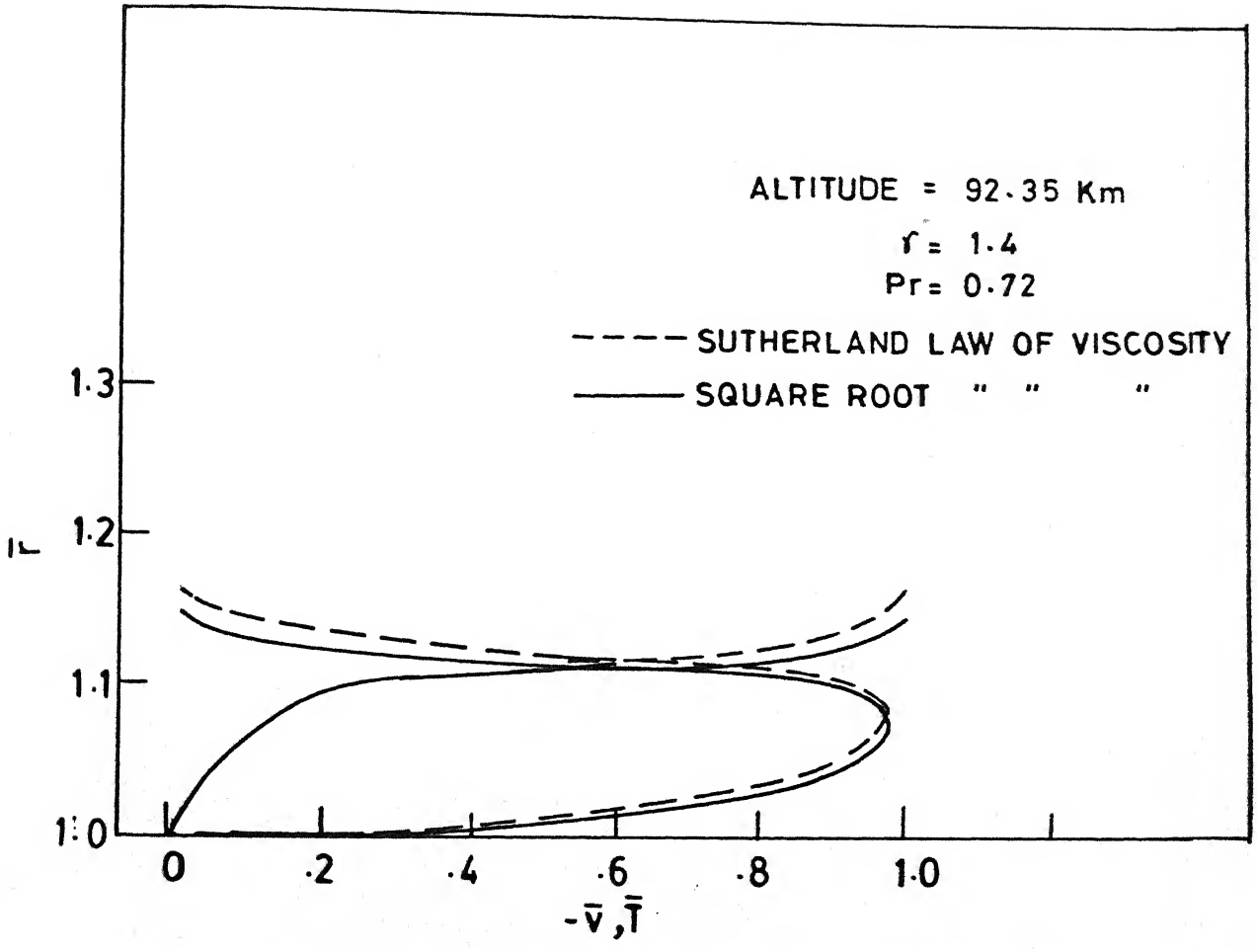

FIG.10 STAGNATION POINT TEMPERATURE AND NORMAL VELOCITY PROFILES WITH DIFFERENT VISCOSITY-TEMPERATURE RELATIONS

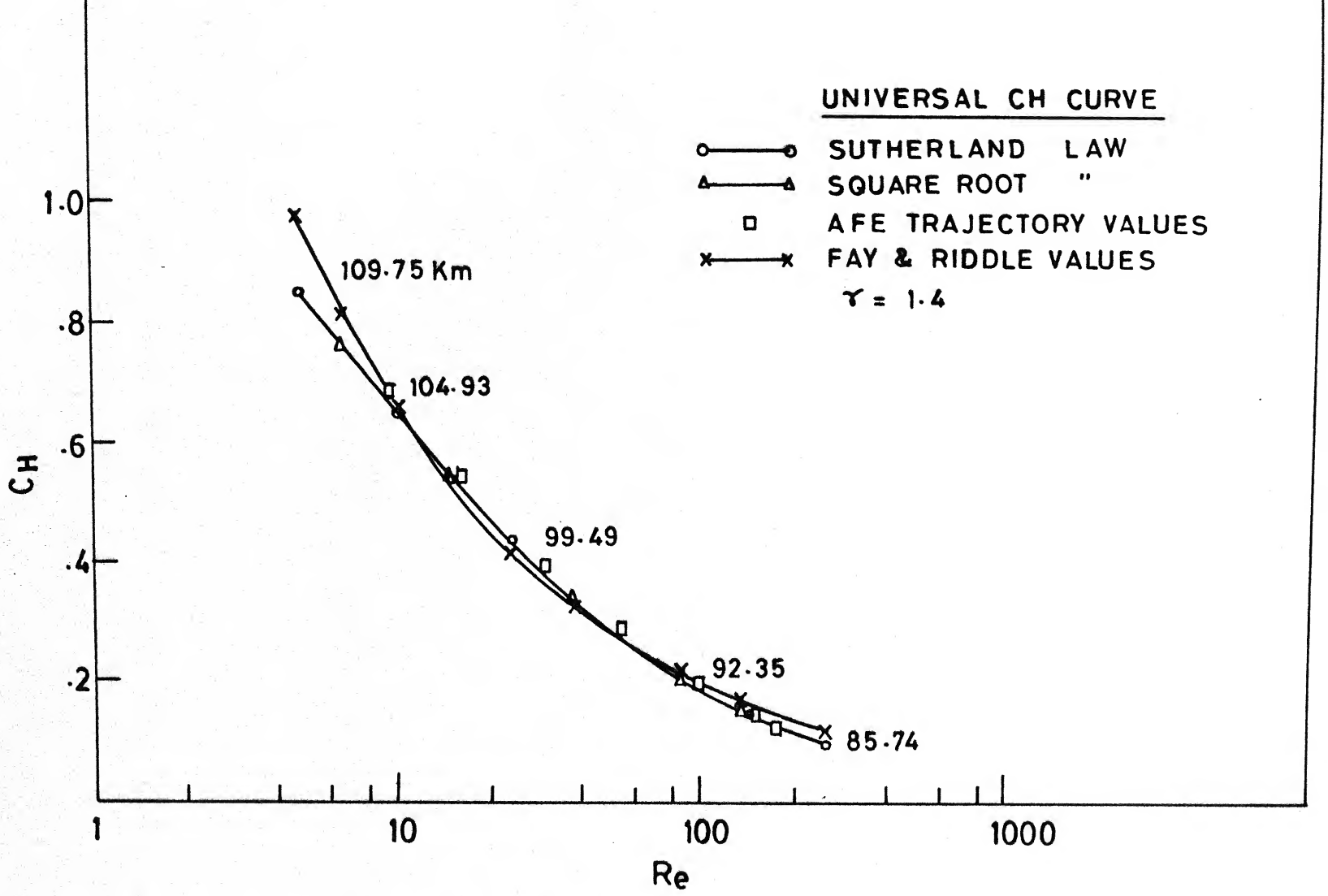

FIG. 11 COMPARISON OF THE STAGNATION POINT HEAT TRANSFER COEFFICIENT FROM THE PRESENT RESULTS FOR REENTRY SPACE SHUTTLE FLIGHT CONDITIONS AND AFE FLIGHT CONDITIONS WITH FAY AND RIDDLE VALUES

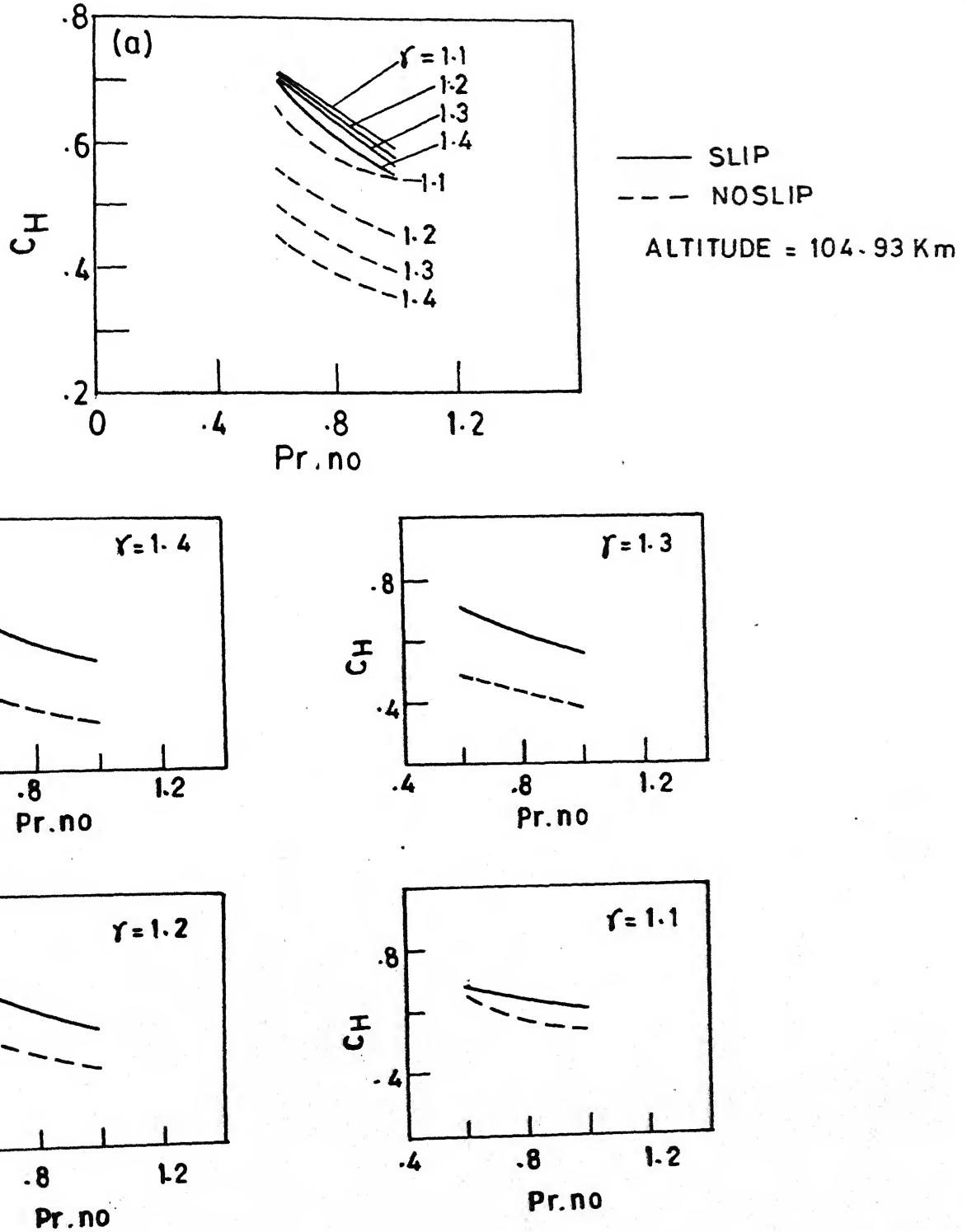

VARIATION OF THE STAGNATION POINT HEAT TRANSFER COEFFICIENT, C_H WITH PRANDTL NUMBERS AND ALSO WITH AND WITHOUT SURFACE SLIP CONDITIONS

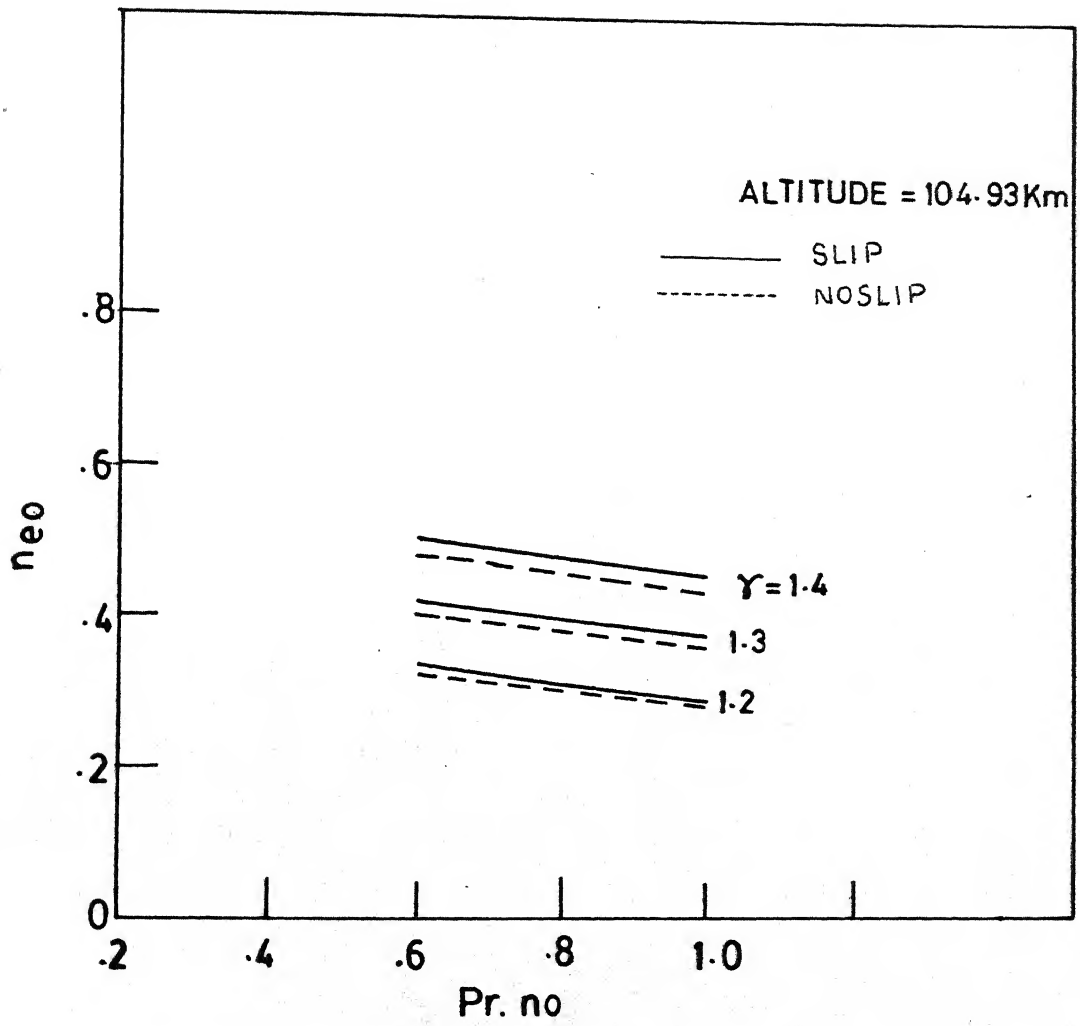

FIG. 13 VARIATION OF THE MERGED LAYER THICKNESS neo WITH PRANDTL NUMBER USING SURFACE SLIP AND NO-SLIP CONDITIONS

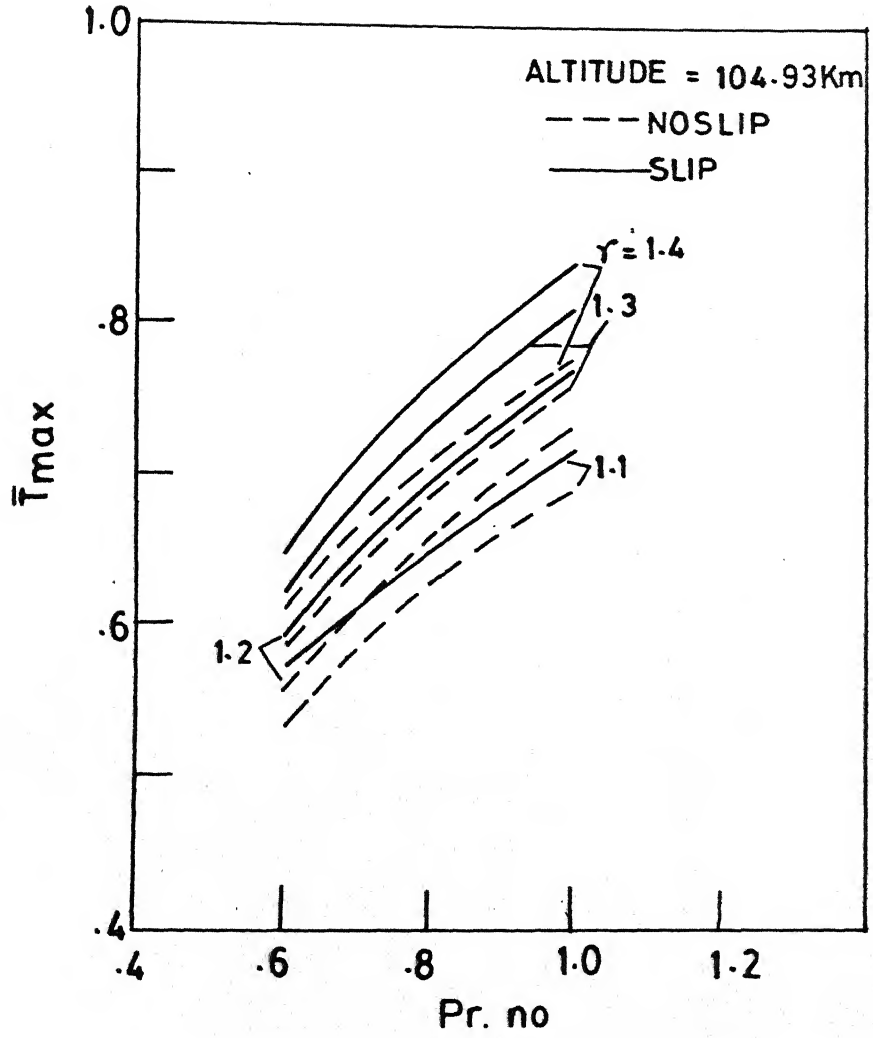

FIG. 14 VARIATION OF THE MAXIMUM TEMPERATURE, $\bar{T}max$, WITH PRANDTL NUMBER AND USING SURFACE SLIP AND NOSLIP CONDITIONS

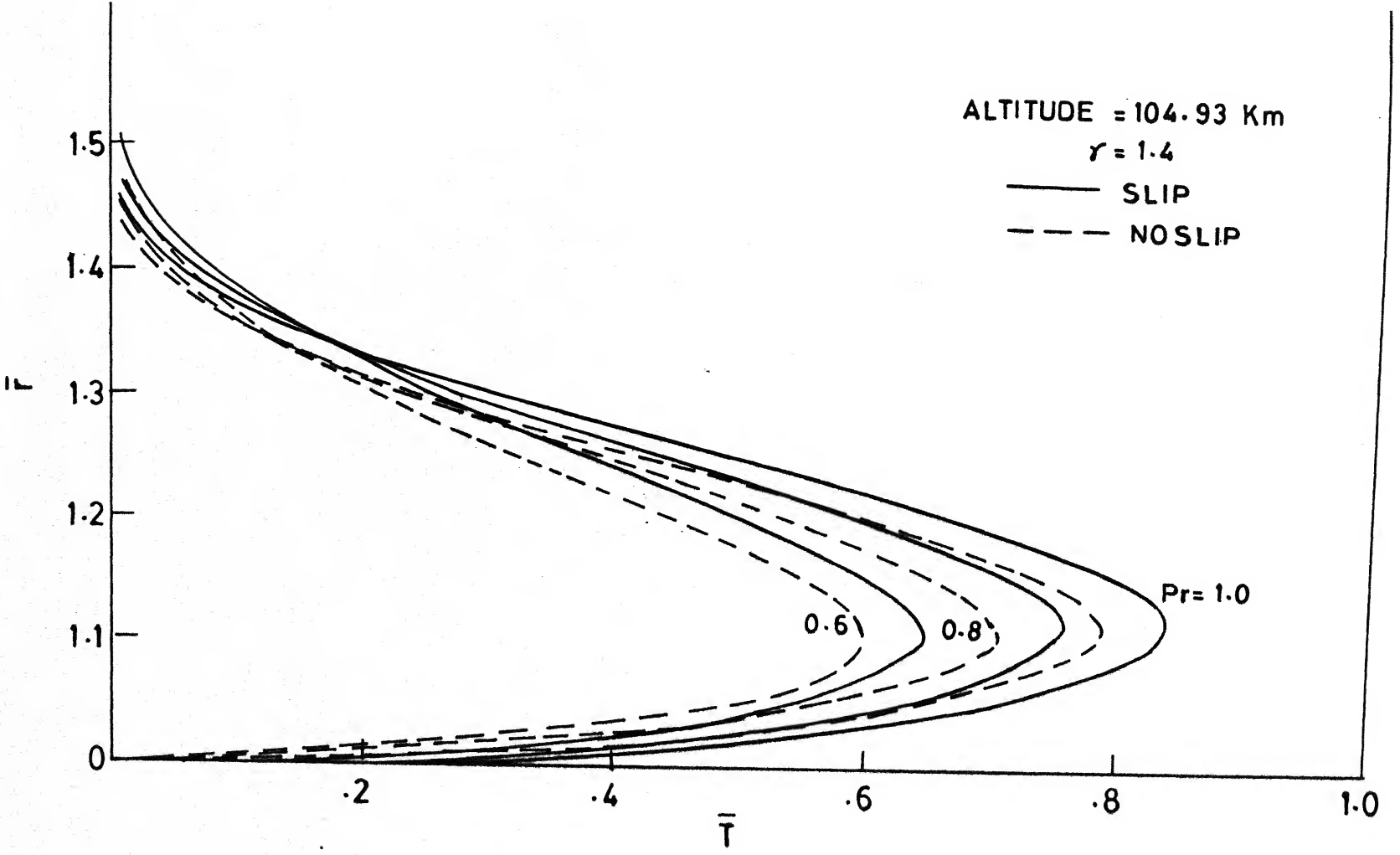

FIG. 15 STAGNATION POINT TEMPERATURE PROFILES WITH AND WITHOUT SURFACE SLIP CONDITION FOR DIFFERENT VALUES OF PRANDTL NUMBER

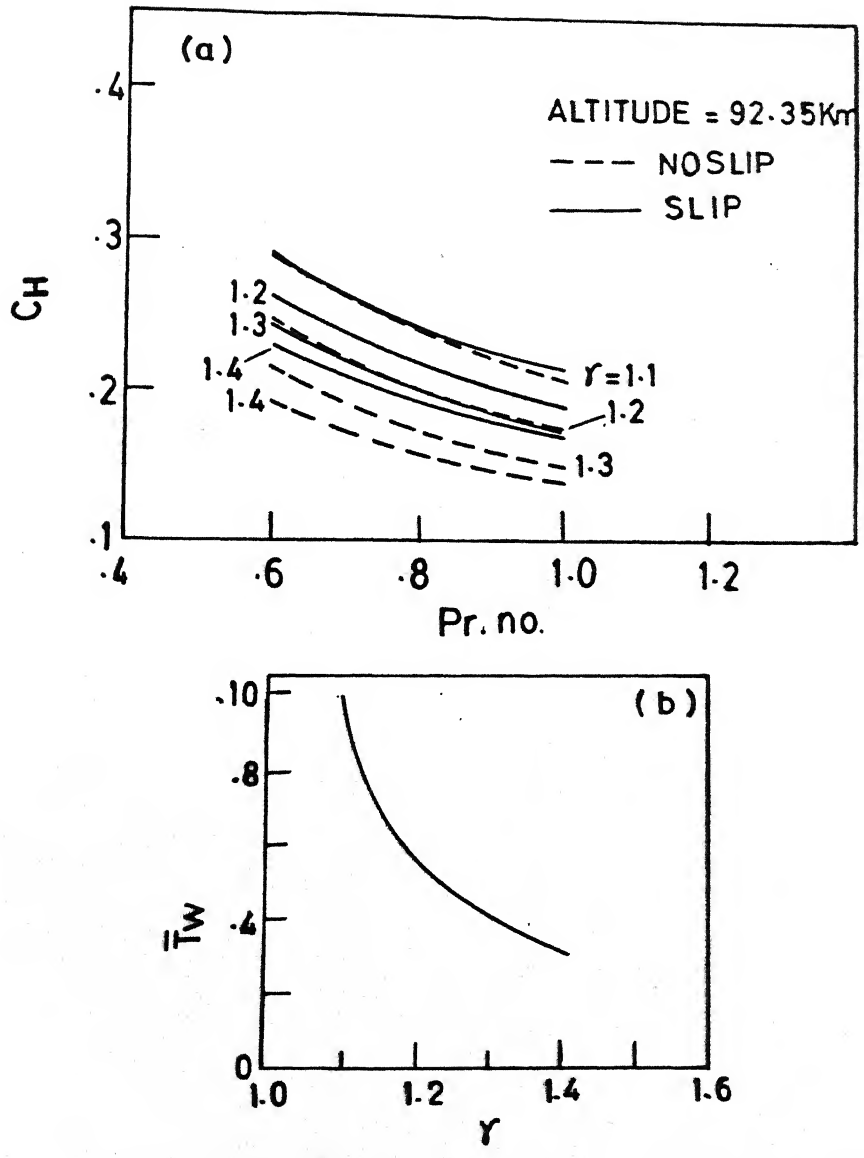

FIG. 16 VARIATION OF THE STAGNATION POINT HEAT TRANSEER COEFFICIENT C_H WITH PRANDTL NUMBER FOR A GIVEN VALUE OF GAMMA WITH AND WITHOUT SURFACE SLIP CONDITION

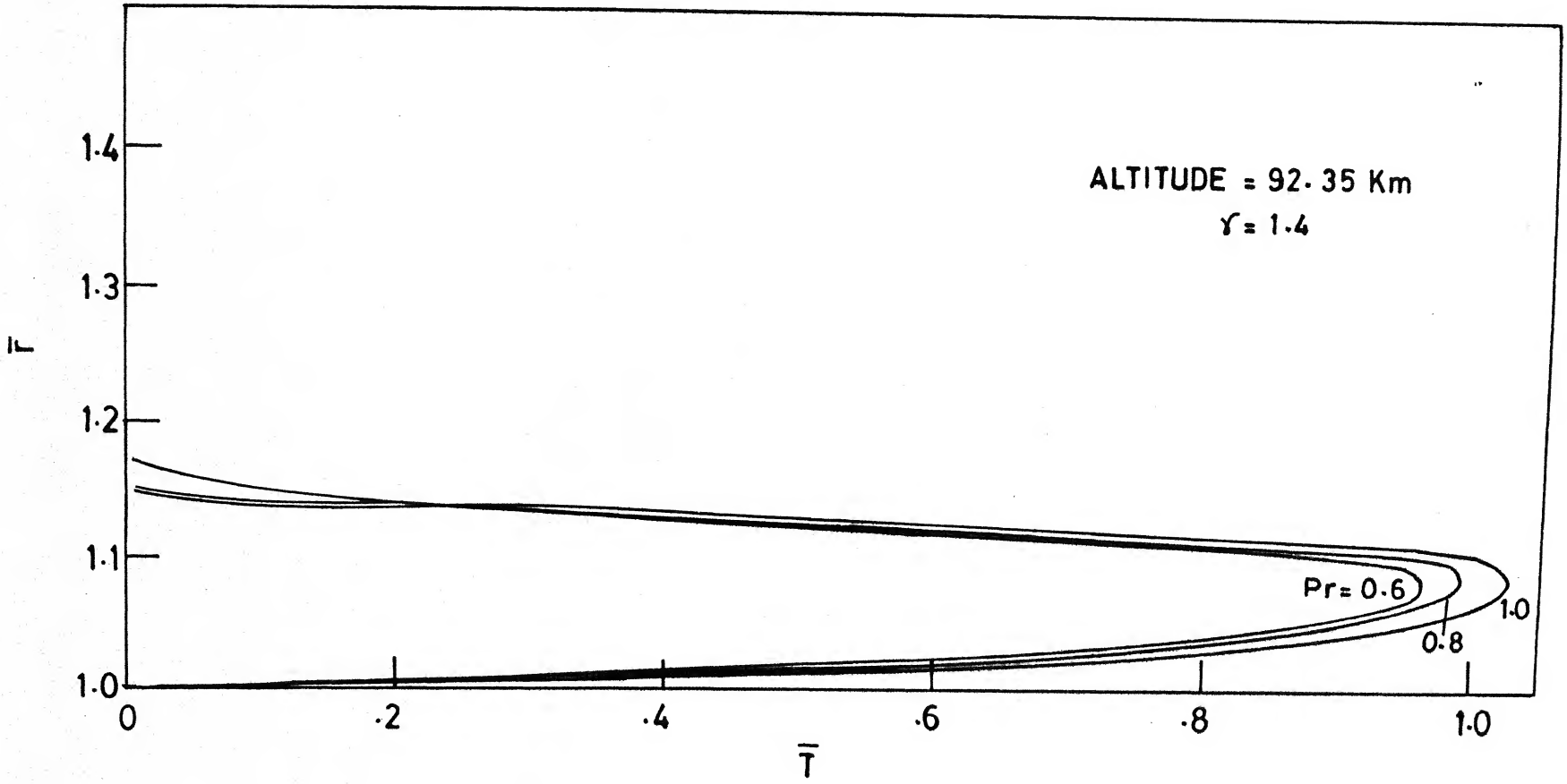

FIG. 17 STAGNATION POINT TEMPERATURE PROFILES FOR VARIOUS PRANDTL NUMBERS

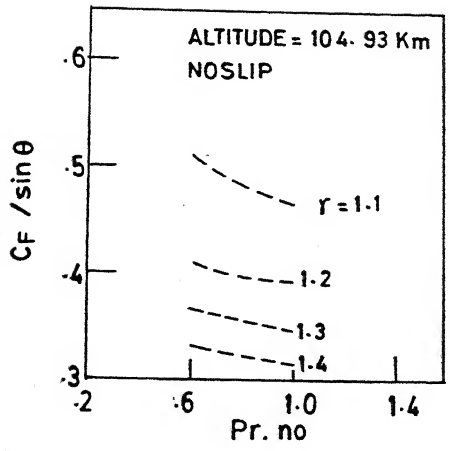

FIG. 18

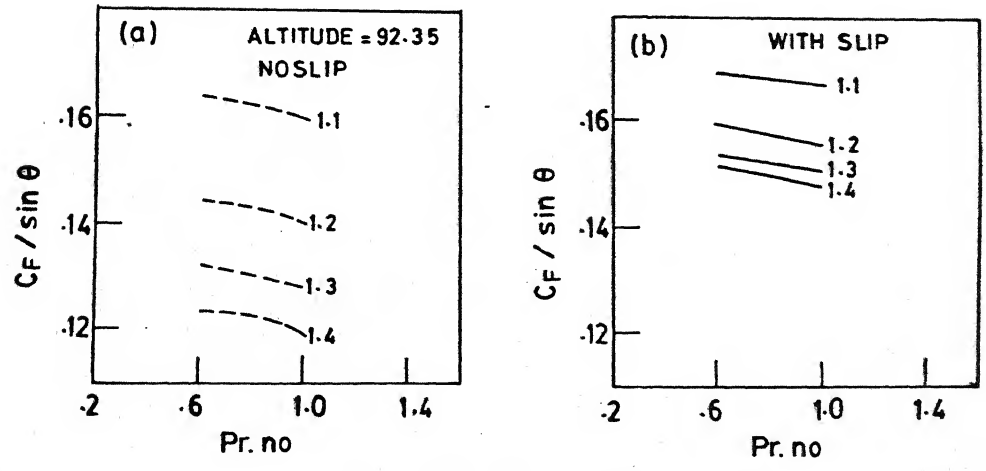

FIG. 19

FIG. 18 VARIATION OF STAGNATION POINT SKIN FRICTION COEFFICIENT PARAMETER, C_F / sin θ, WITH PRANDTL NUMBER FOR NOSLIP CASE

FIG. 19 VARIATION OF STAGNATION POINT SKIN FRICTION COEFFICIENT PARAMETER, C_F / sin θ, AGAINST Pr. no. WITH AND WITHOUT SURFACE SLIP CONDITIONS

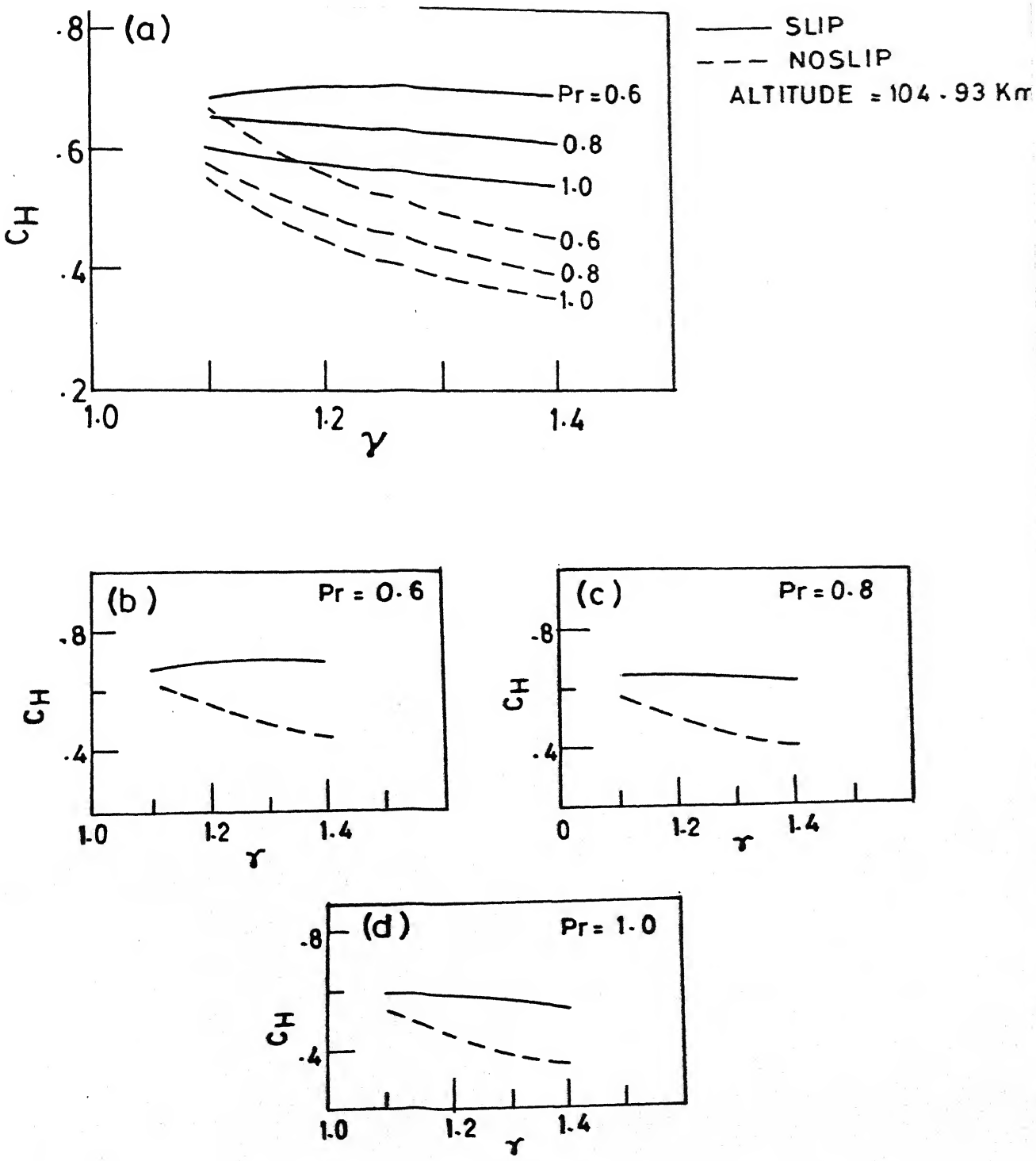

FIG. 20 VARIATION OF THE STAGNATION POINT HEAT TRANSFER COEFEICIENT C_H AGAINST GAMMA WITH AND WITHOUT SURFACE SLIP CONDITIONS

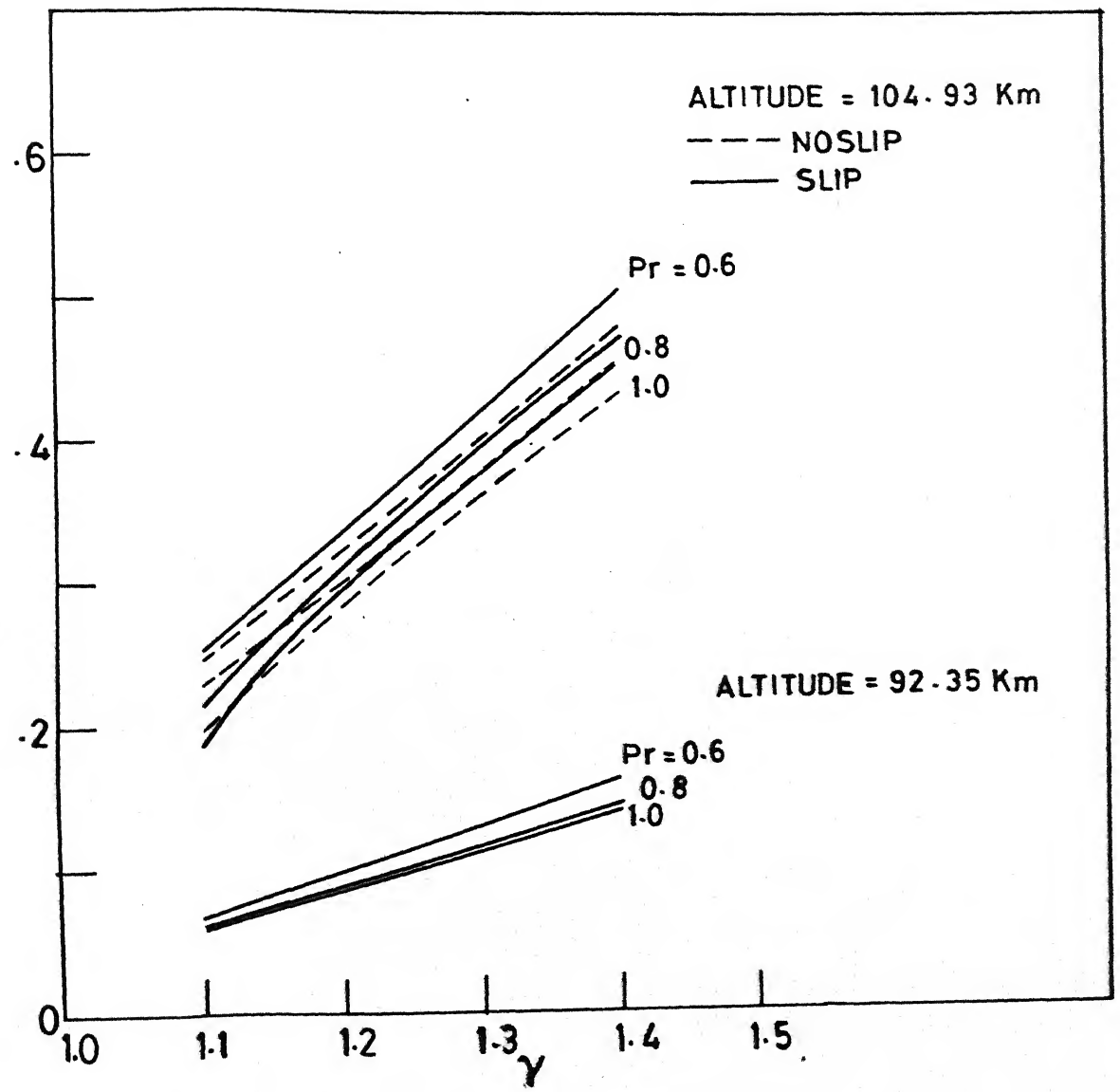

G. 21 VARIATION OF THE MERGED LAYER THICKNESS AGAINST GAMMA WITH AND WITHOUT SURFACE SLIP CONDITIONS

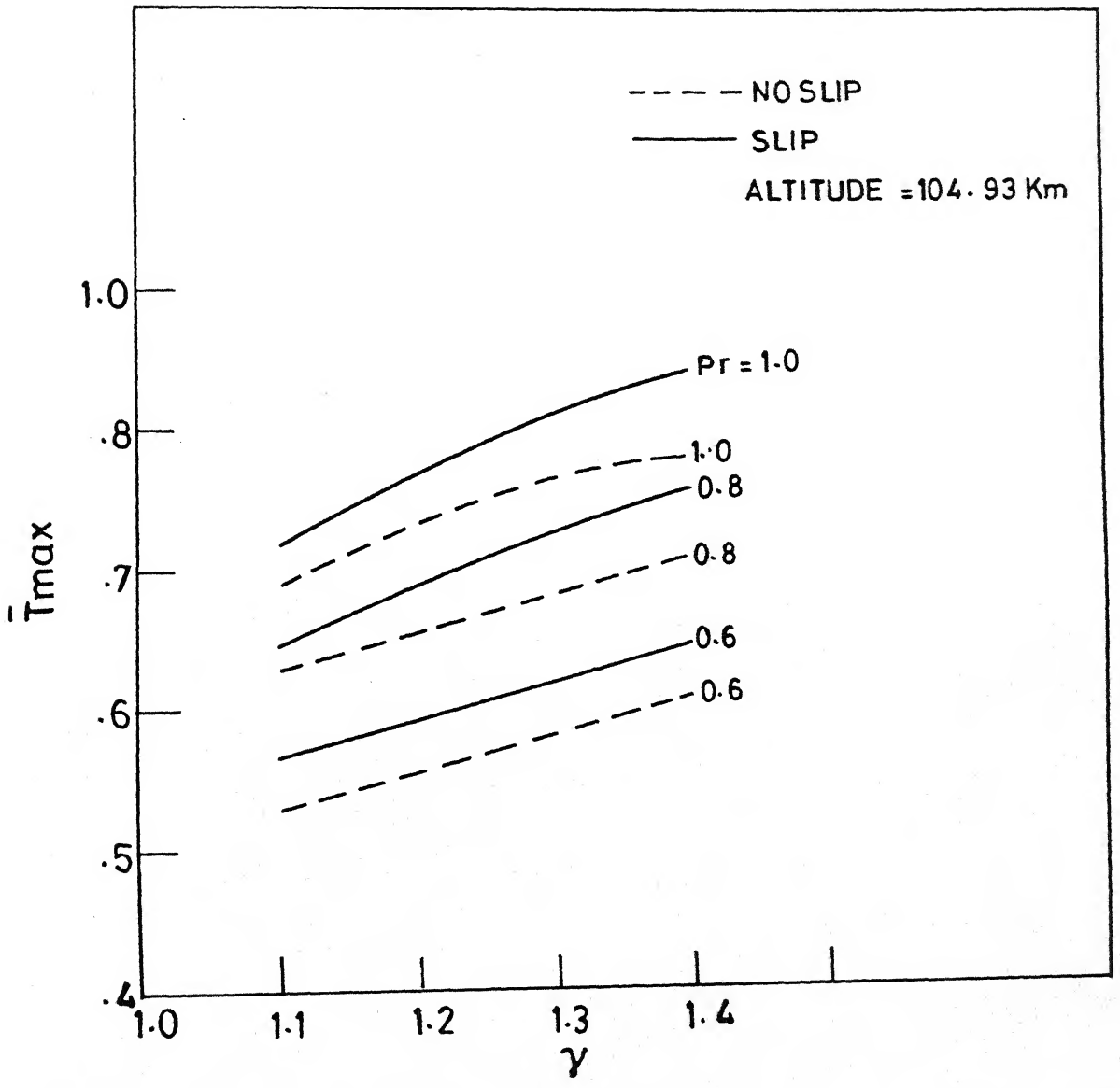

FIG. 22 VARIATION OF THE MAXIMUM TEMPERATURE WITH GAMMA FOR DIFFERENT VALUES OF PRANDTL NUMBER USING SLIP AND NOSLIP SURFACE CONDITIONS

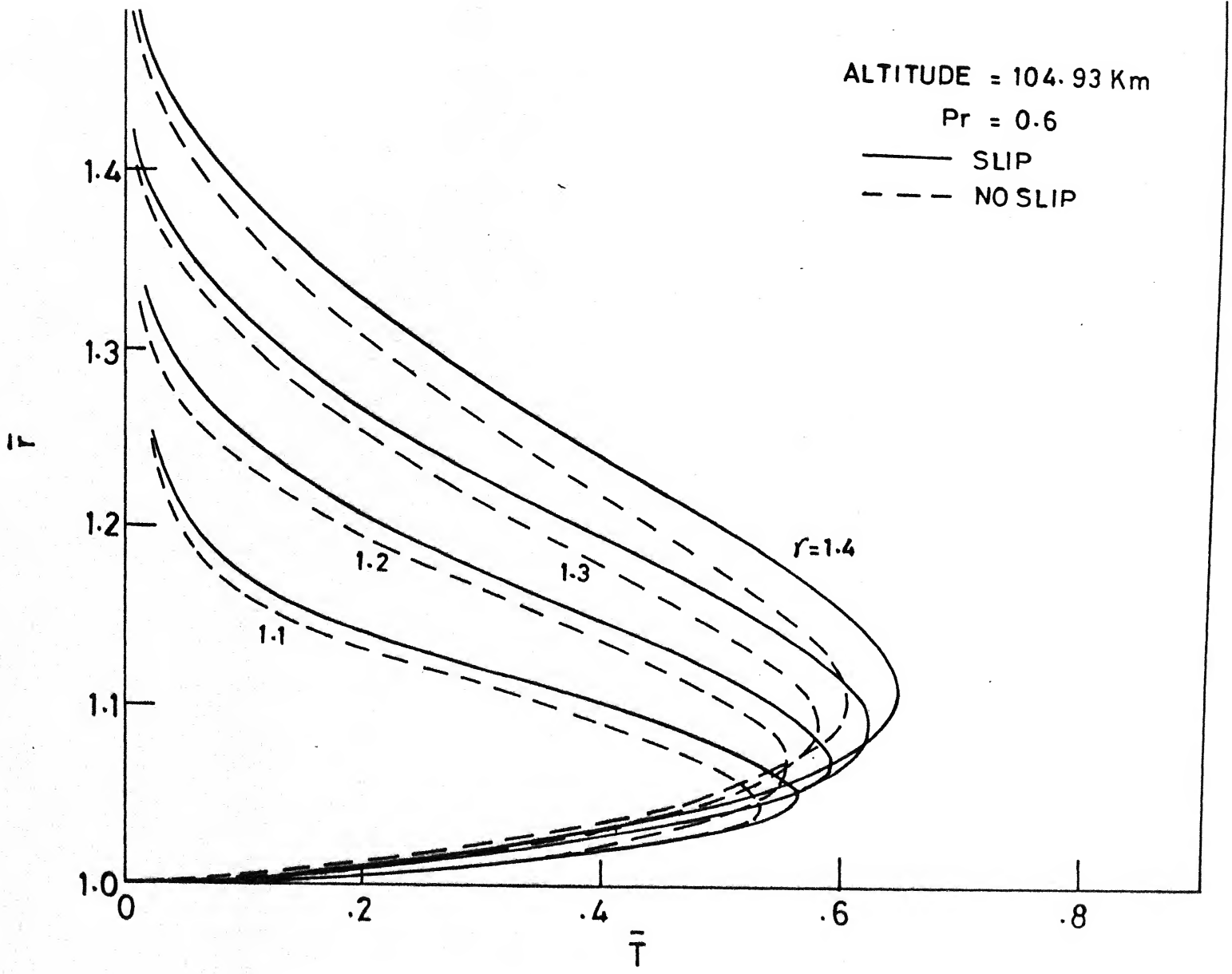

FIG. 23 STAGNATION POINT TEMPERATURE PROFILES WITH AND WITHOUT SURFACE SLIP CONDITION FOR DIFFERENT VALUES OF GAMMA

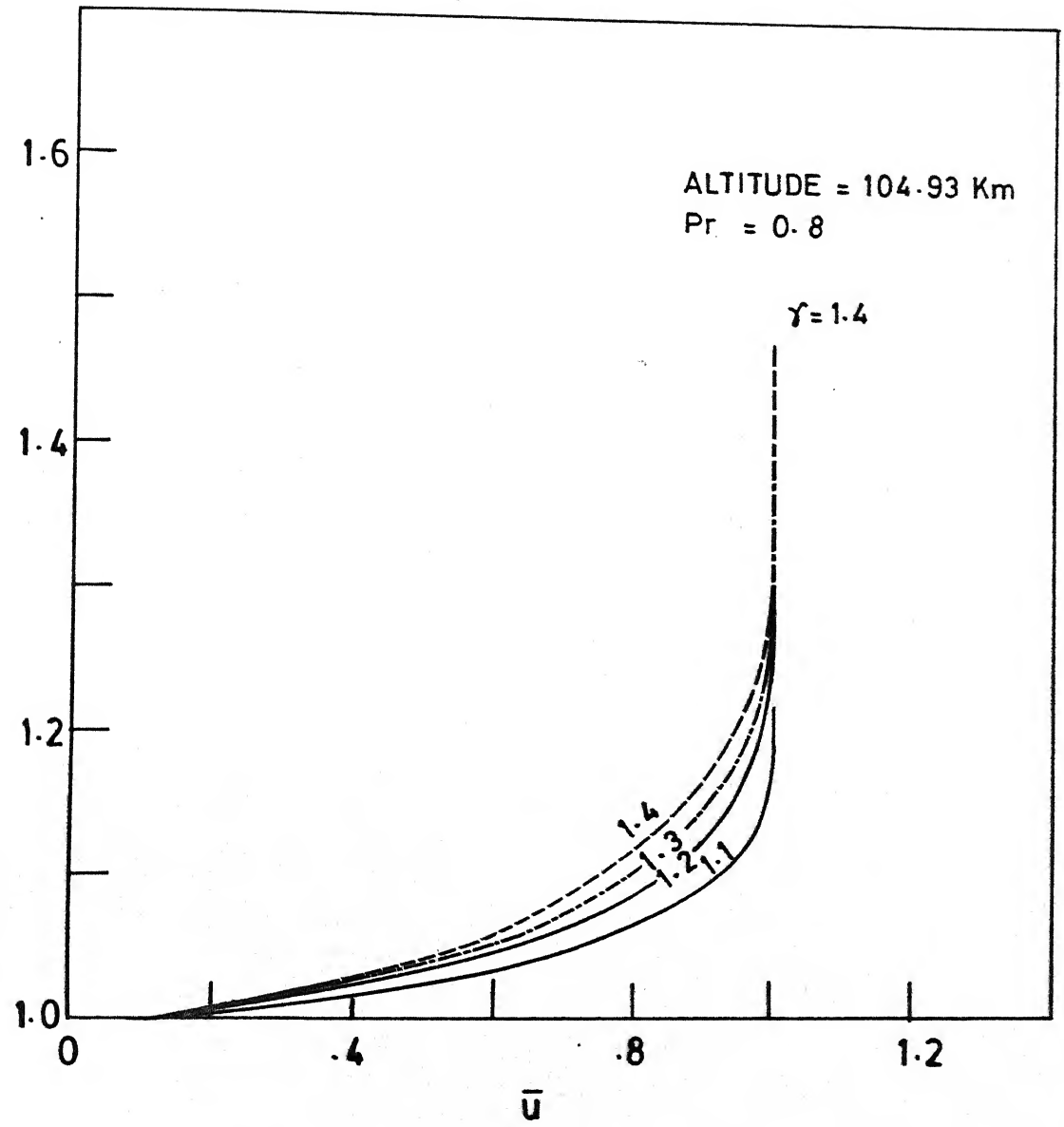

. 24 STAGNATION POINT TANGENTIAL VELOCITY PROFILES FOR DIFFERENT VALUES OF GAMMA WITH SURFACE SLIP CONDITIONS

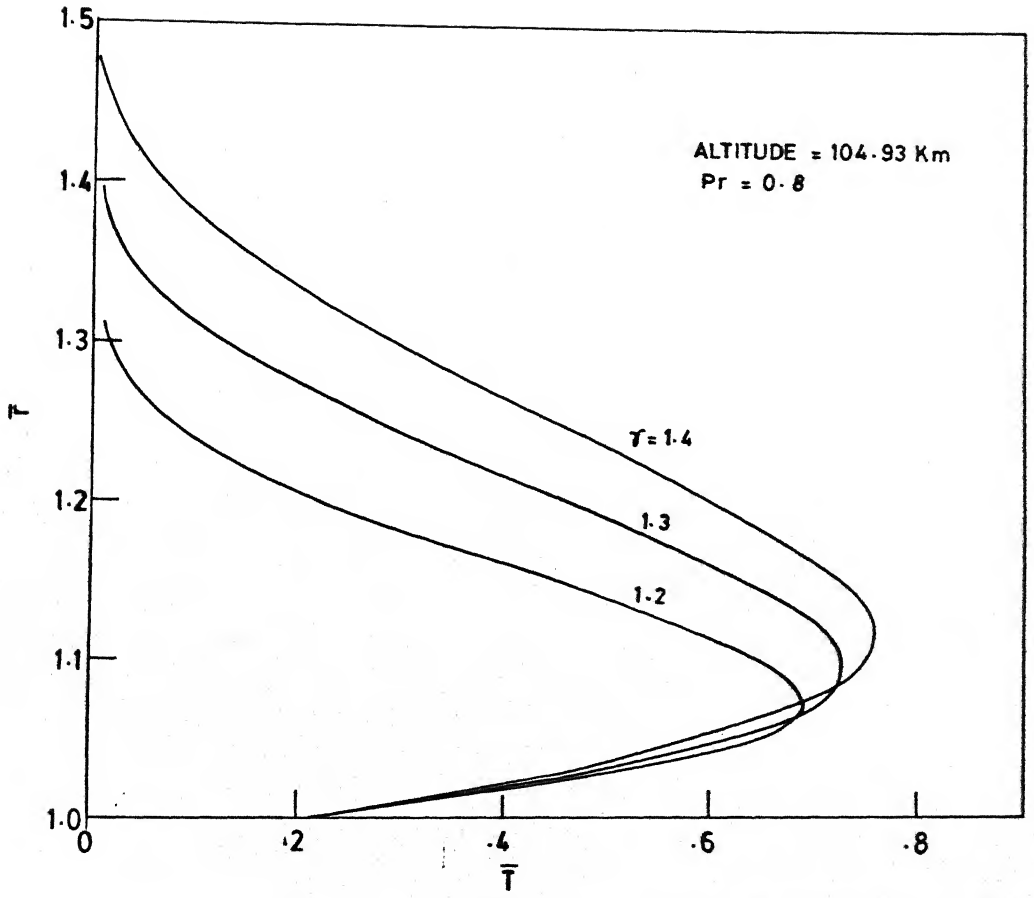

FIG. 25 STAGNATION POINT TEMPERATURE PROFILES WITH SURFACE SLIP FOR DIFFERENT VALUES OF GAMMA

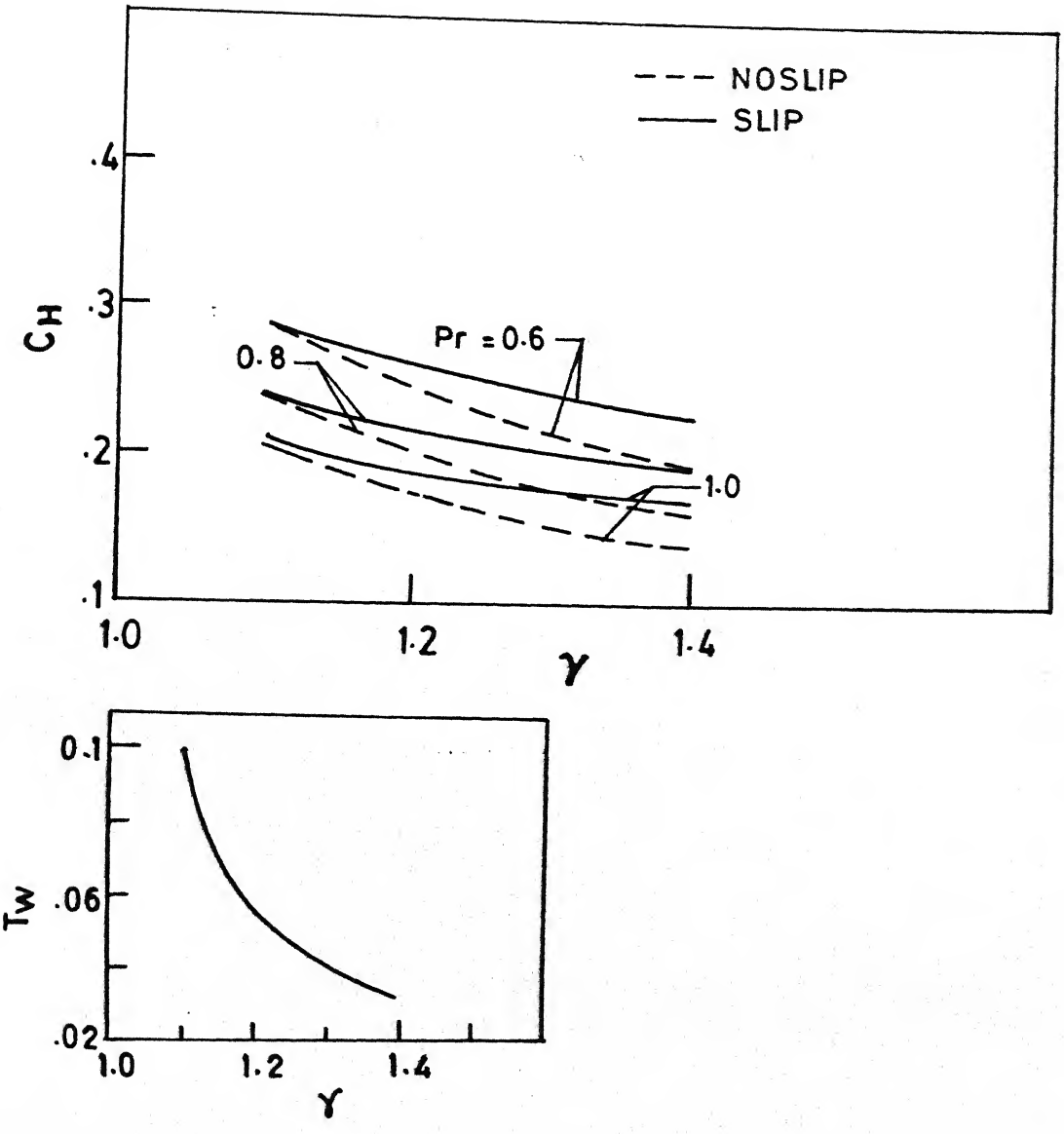

. 26 VARIATION OF THE STAGNATION POINT HEAT TRANSFER COEFFICIENT C_H WITH GAMMA USING SURFACE SLIP AND NO SLIP CONDITION

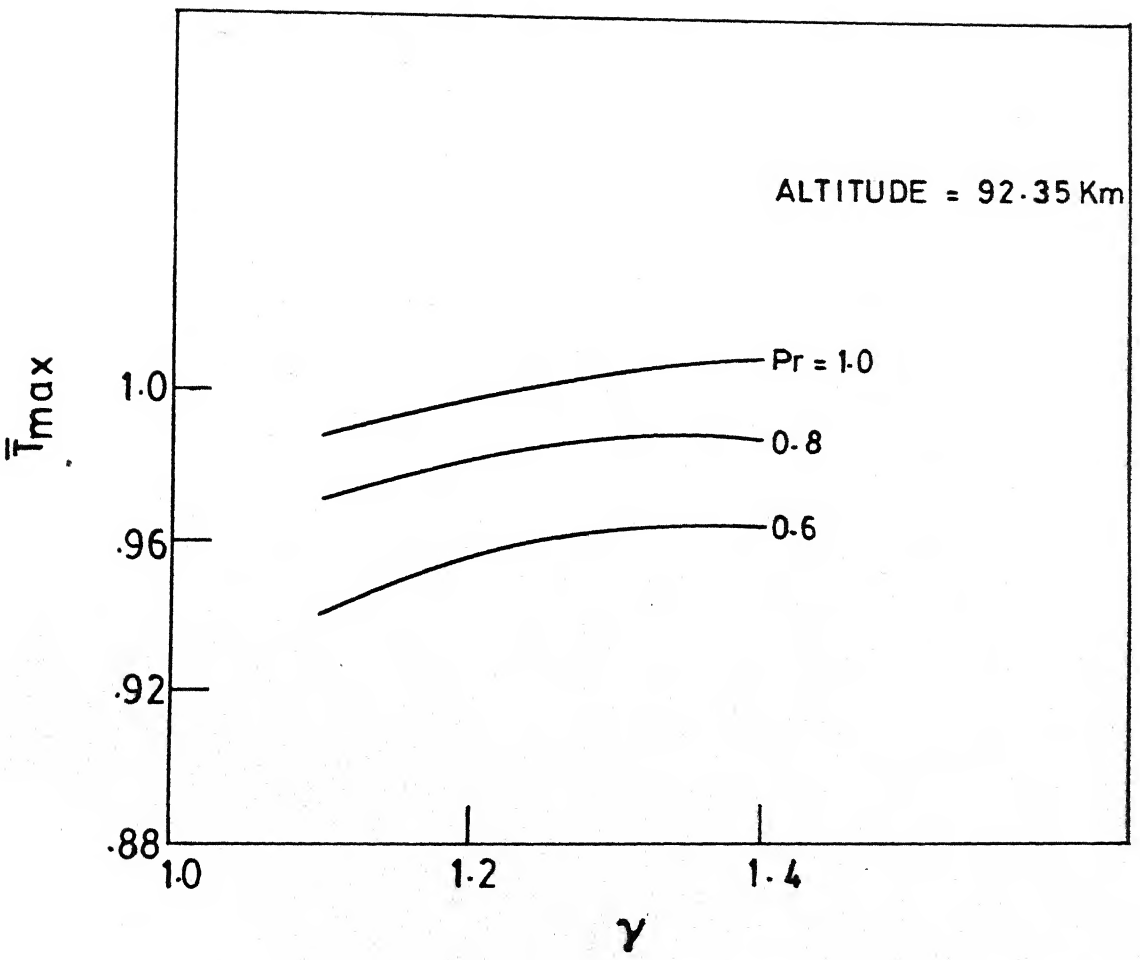

FIG. 27 VARIATION OF THE MAXIMUM TEMPERATURE WITH GAMMA FOR DIFFERENT VALUES OF PRANDTL NUMBERS FOR SURFACE SLIP CONDITIONS

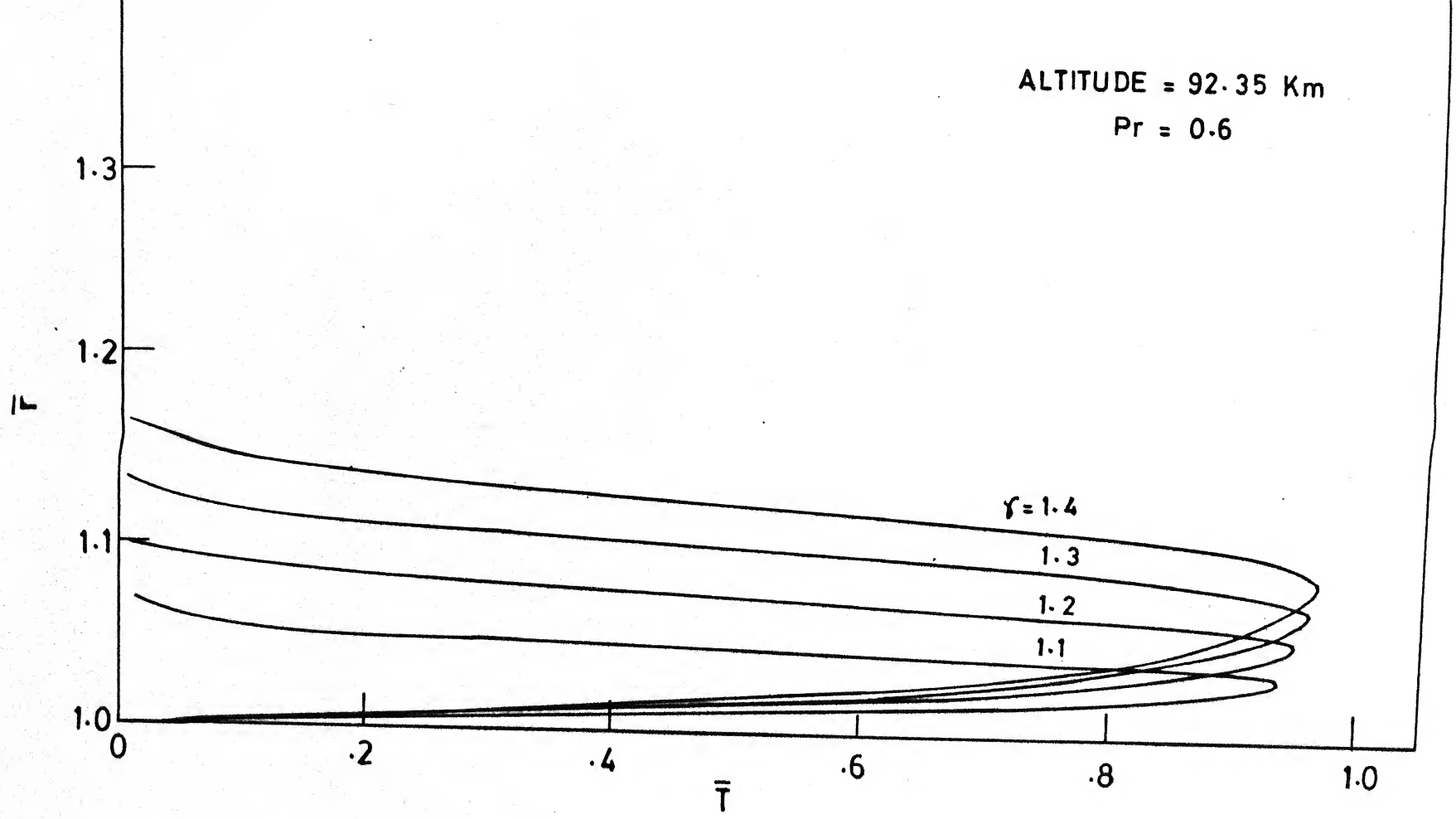

FIG. 28 STAGNATION POINT TEMPERATURE PROFILES FOR DIFFERENT VALUES OF GAMMA

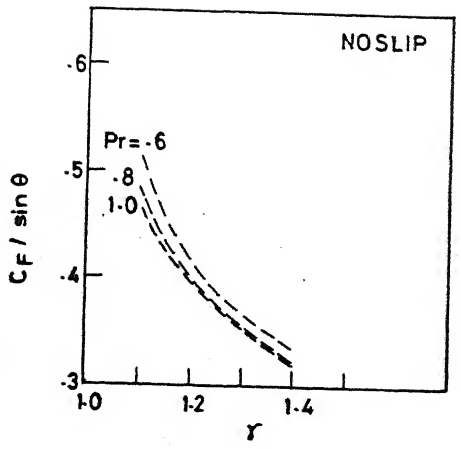

FIG. 29

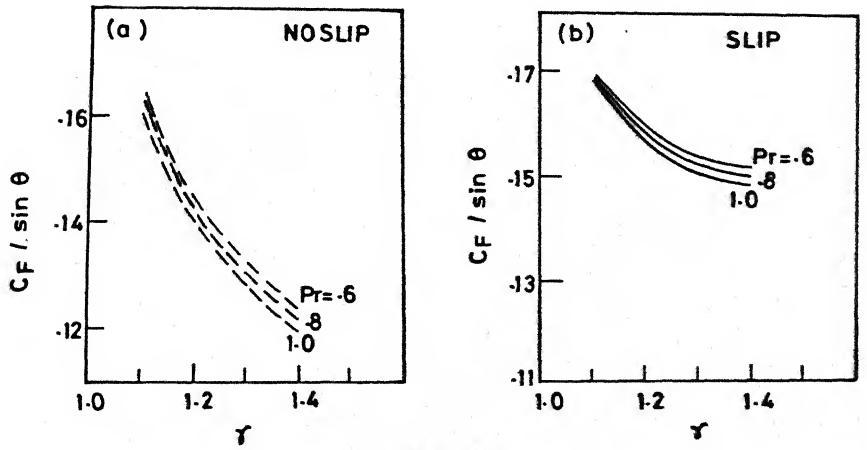

FIG. 30

FIG. 29 VARIATION OF STAGNATION POINT SKIN-FRICTION COEFFICIENT PARAMETER, $C_F/\sin\theta$, WITH GAMMA FOR NOSLIP CASE

FIG. 30 VARIATION OF STAGNATION POINT SKIN-FRICTION COEFFICIENT PARAMETER, $C_F/\sin\theta$, AGAINST GAMMA WITH AND WITHOUT SURFACE SLIP CONDITION

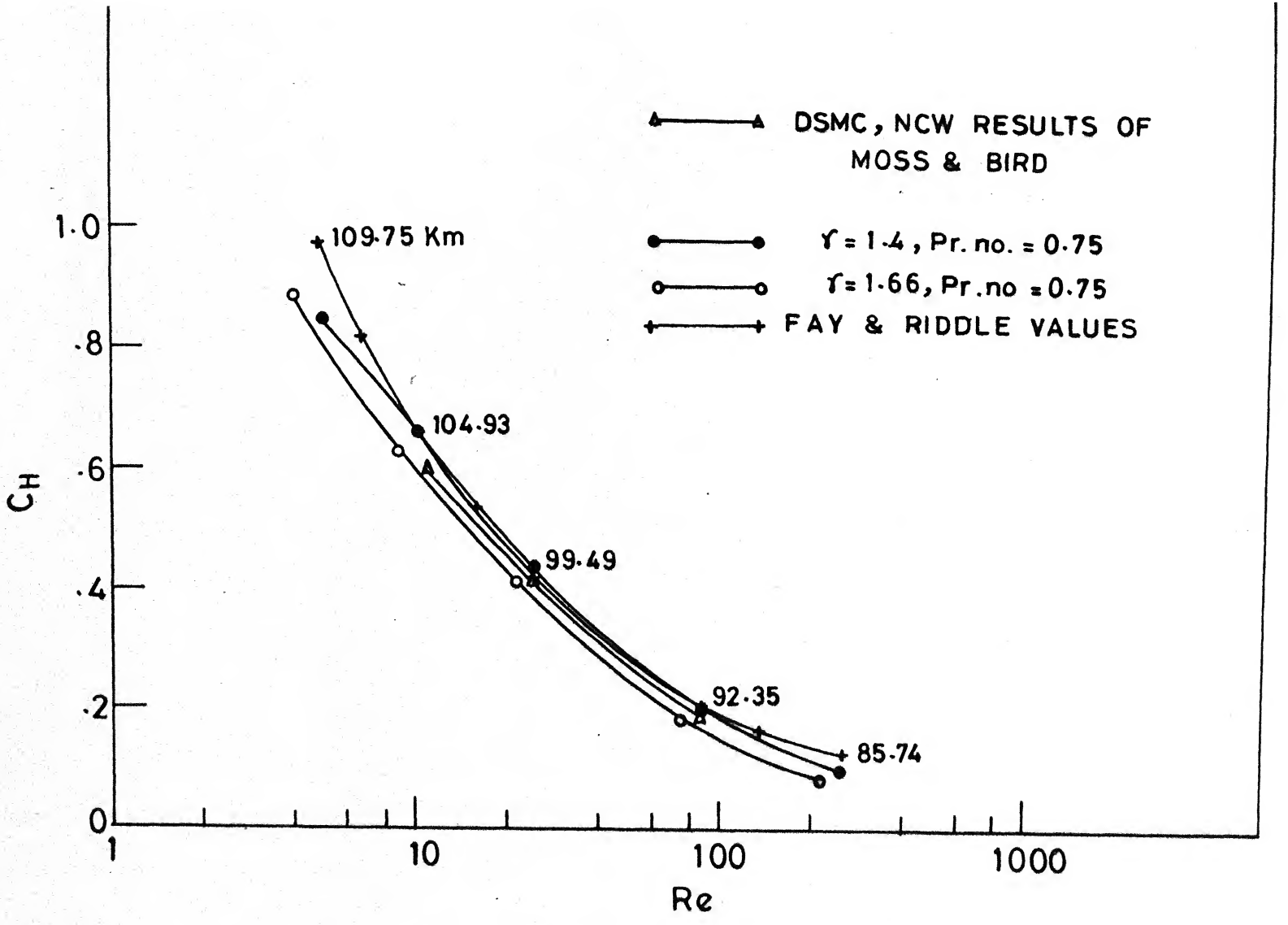

FIG. 31 COMPARISON OF STAGNATION POINT HEAT TRANSFER COEFEICIENT AT DIFFERENT VALUES OF GAMMA FROM PRESENT RESULTS WITH DSMC RESULTS (Ref. 9)

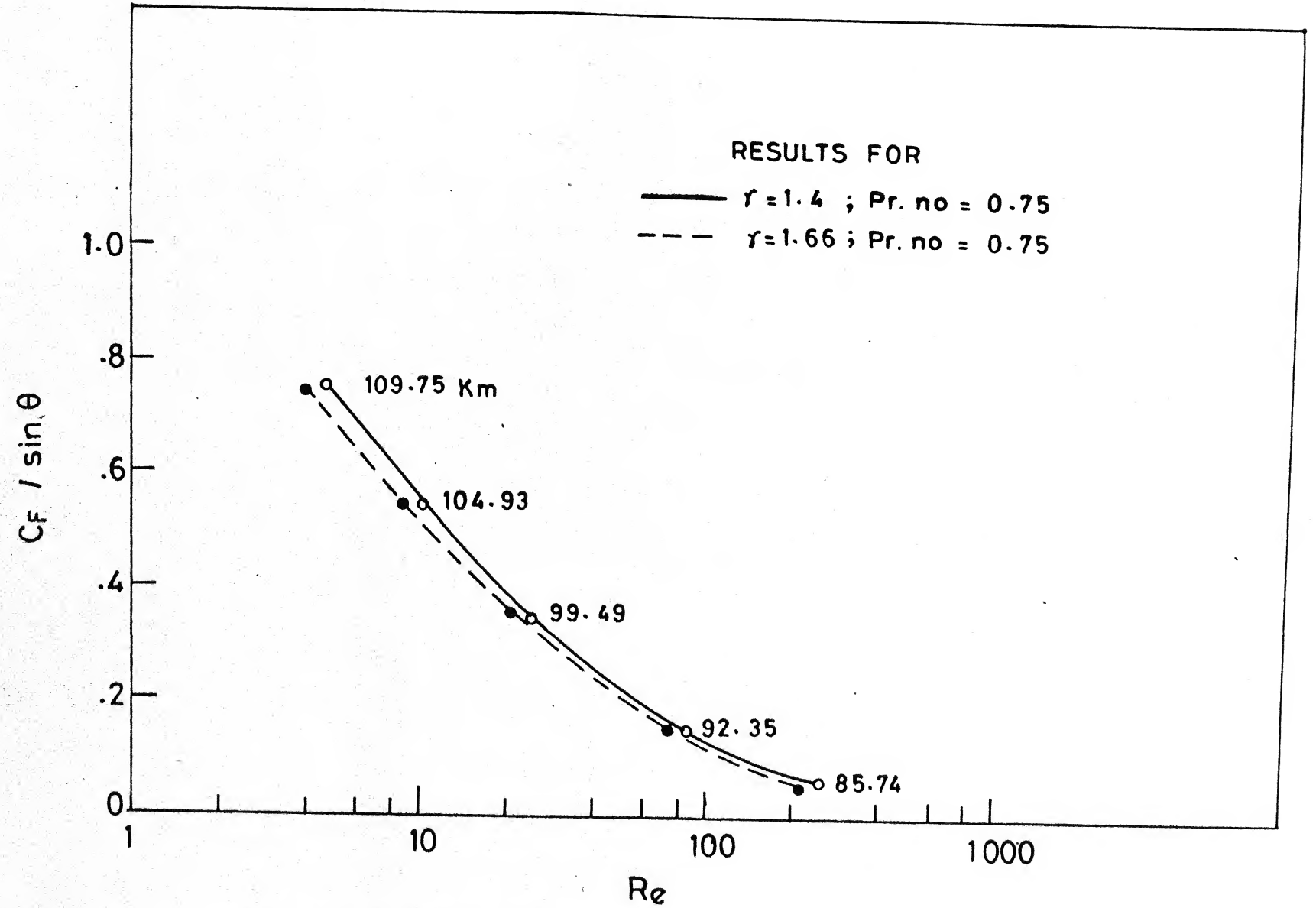

FIG. 32 COMPARISON BETWEEN STAGNATION POINT SKIN-FRICTION COEFFICIENT PARAMETER C_F / sin θ FOR DIFFERENT VALUES OF GAMMA FOR VARIOUS SPACE SHUTTLE RE ENTRY CONDITIONS

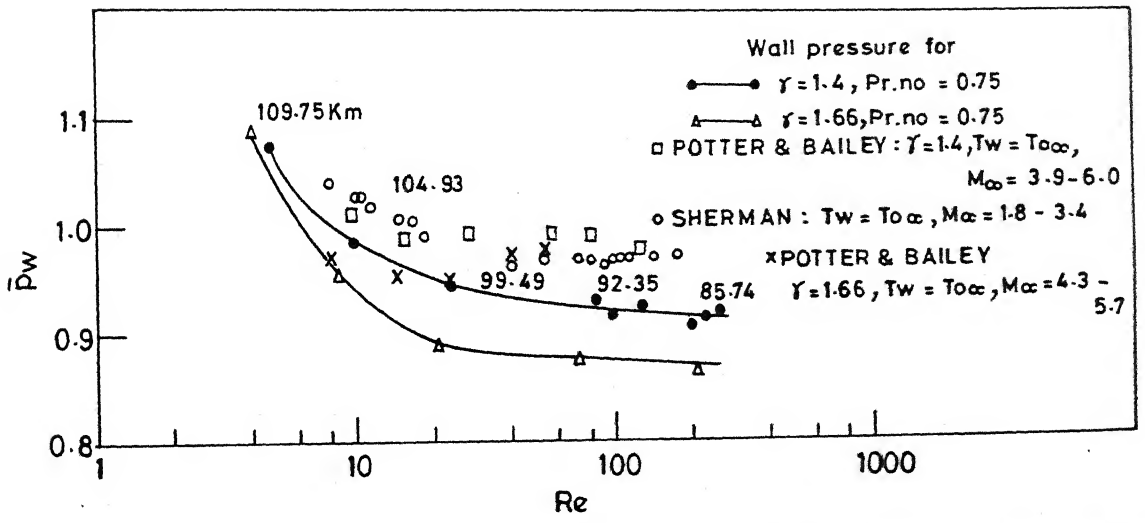

FIG. 33 VARIATION OF WALL PRESSURE WITH REYNOLDS NUMBER FOR DIFFERENT VALUES OF GAMMA FOR SHUTTLE REENTRY CONDITIONS

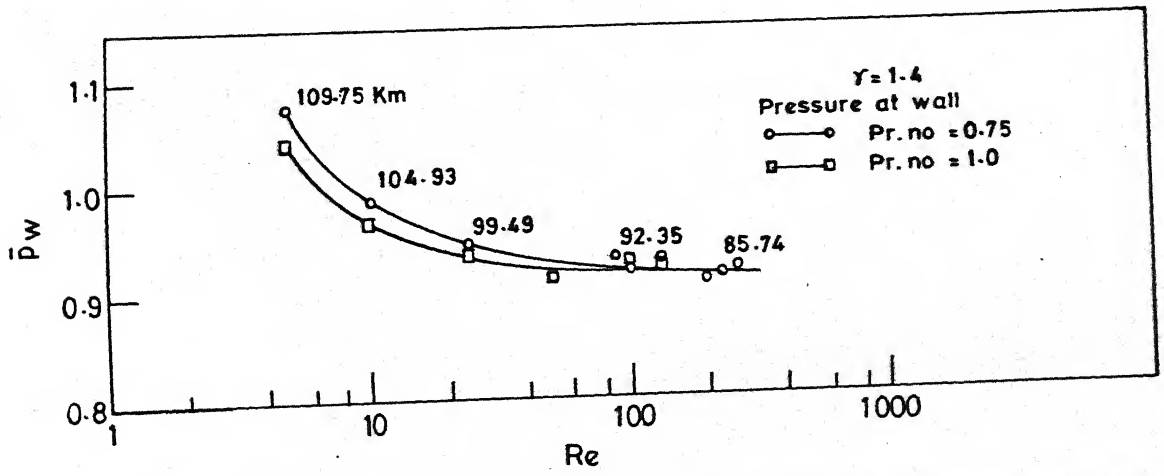

FIG. 34 VARIATION OF WALL PRESSURE WITH REYNOLDS NUMBER FOR DIFFERENT VALUES OF PRANDTL NUMBER

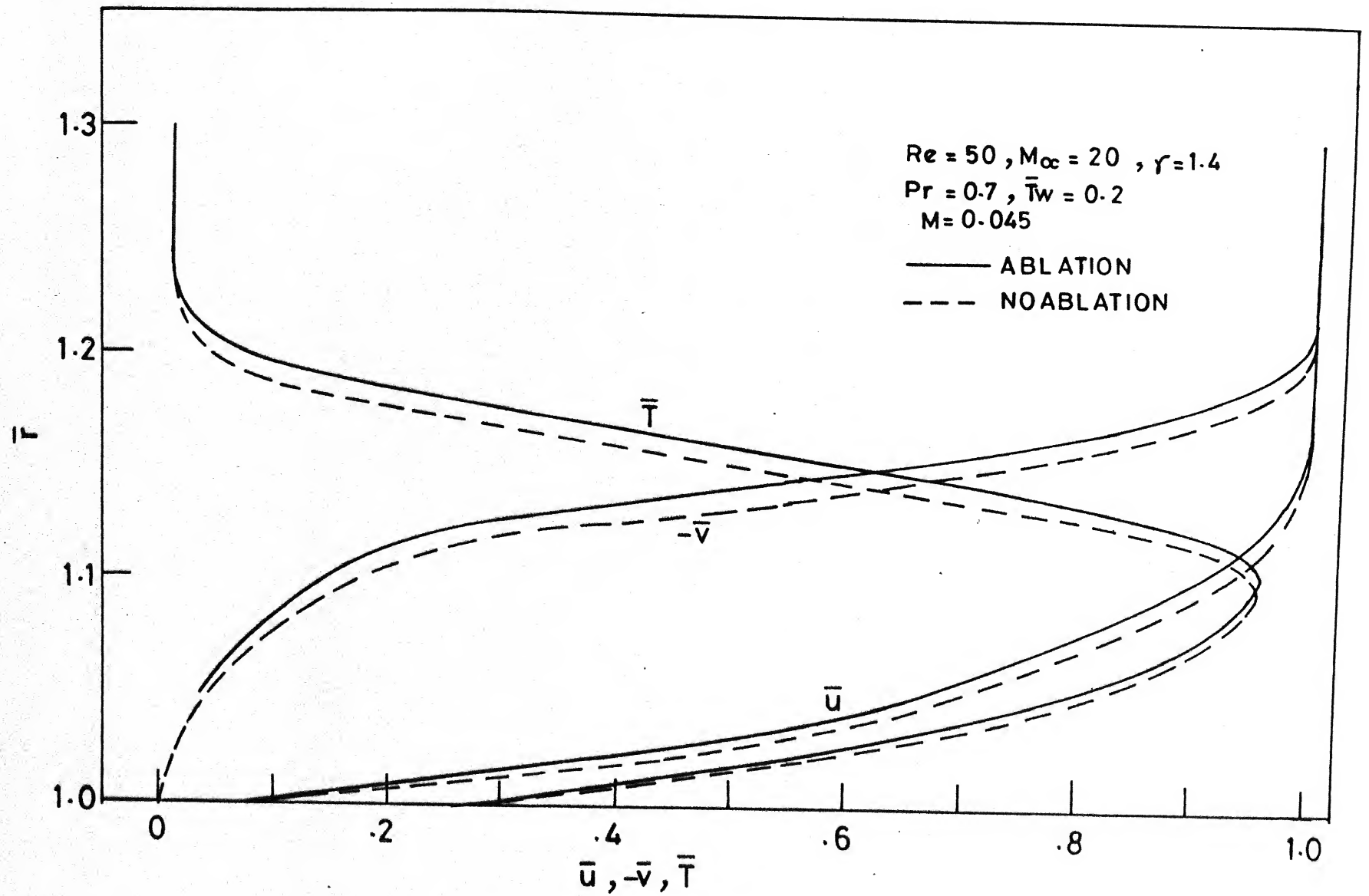

FIG. 35 STAGNATION POINT TEMPERATURE AND VELOCITY PROFILES WITH AND WITHOUT ABLATION USING SURFACE SLIP CONDITIONS

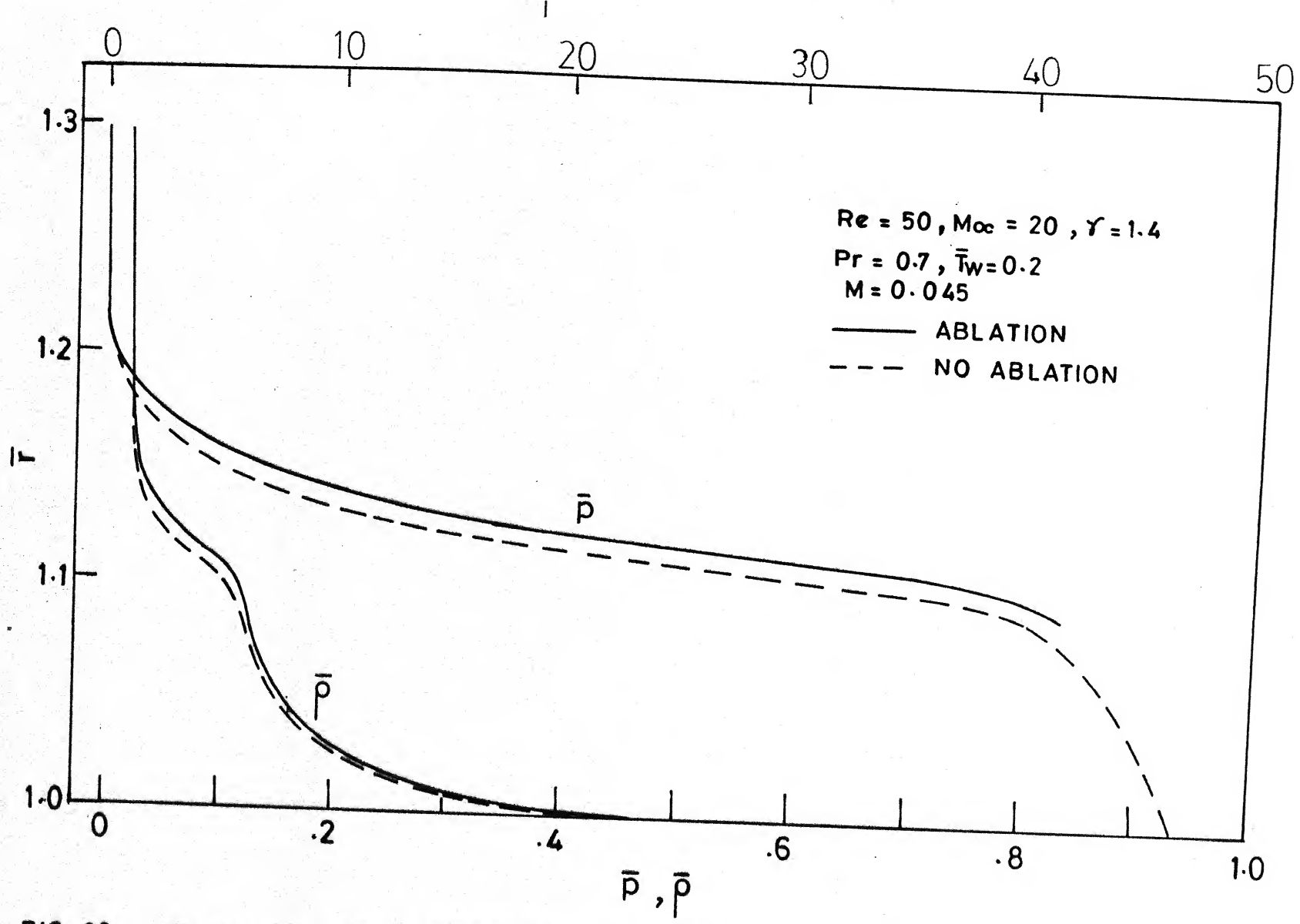

FIG. 36 STAGNATION POINT PRESSURE AND DENSITY PROFILES WITH AND WITHOUT ABLATION USING SURFACE SLIP CONDITION

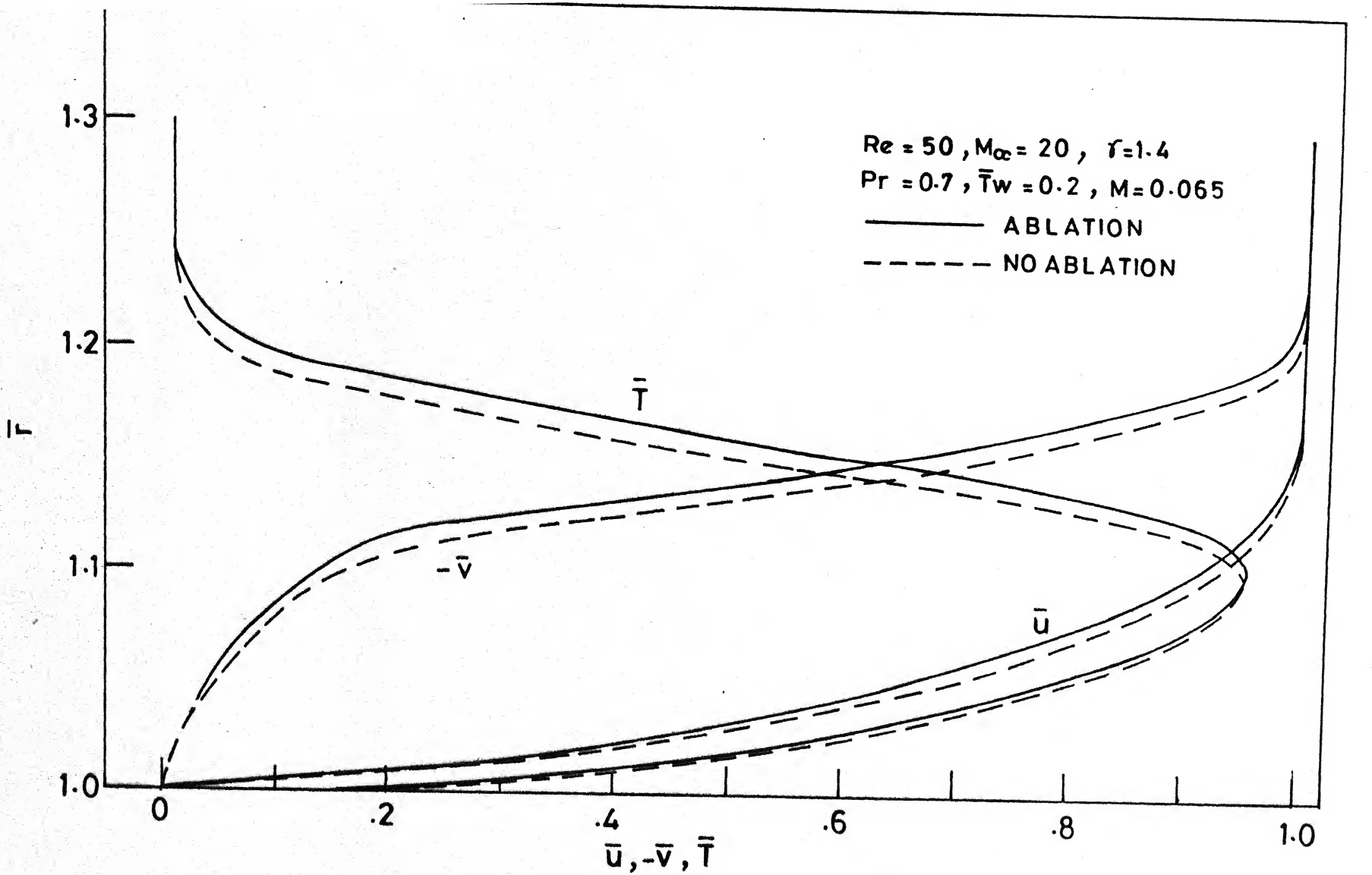

FIG. 37 STAGNATION POINT TEMPERATURE AND VELOCITY PROFILES WITH AND WITHOUT ABLATION WITH NOSLIP SURFACE CONDITIONS

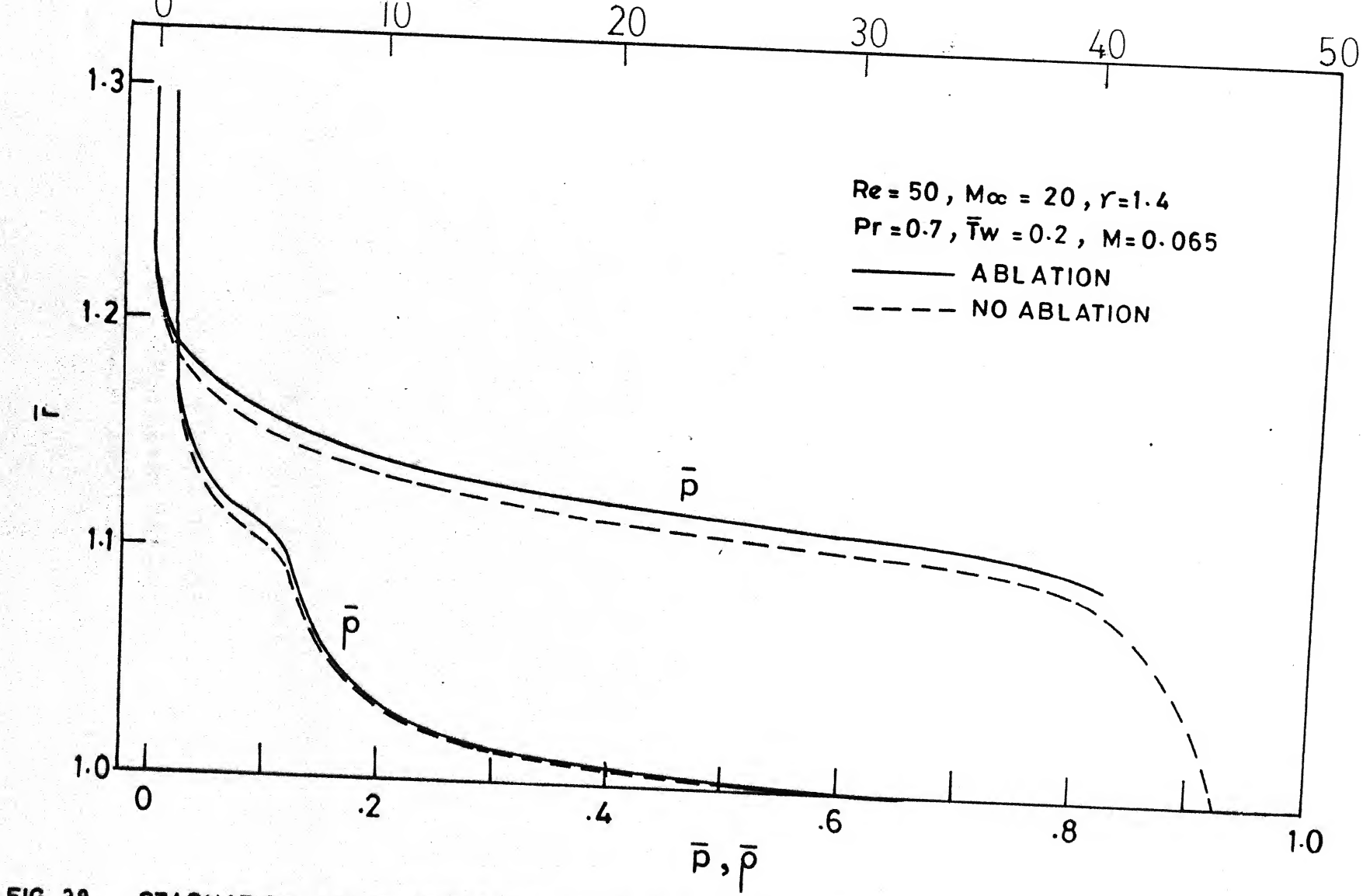

FIG. 38 STAGNATION POINT PRESSURE AND DENSITY PROFILES WITH AND WITHOUT ABLATION USING NOSLIP SURFACE CONDITIONS

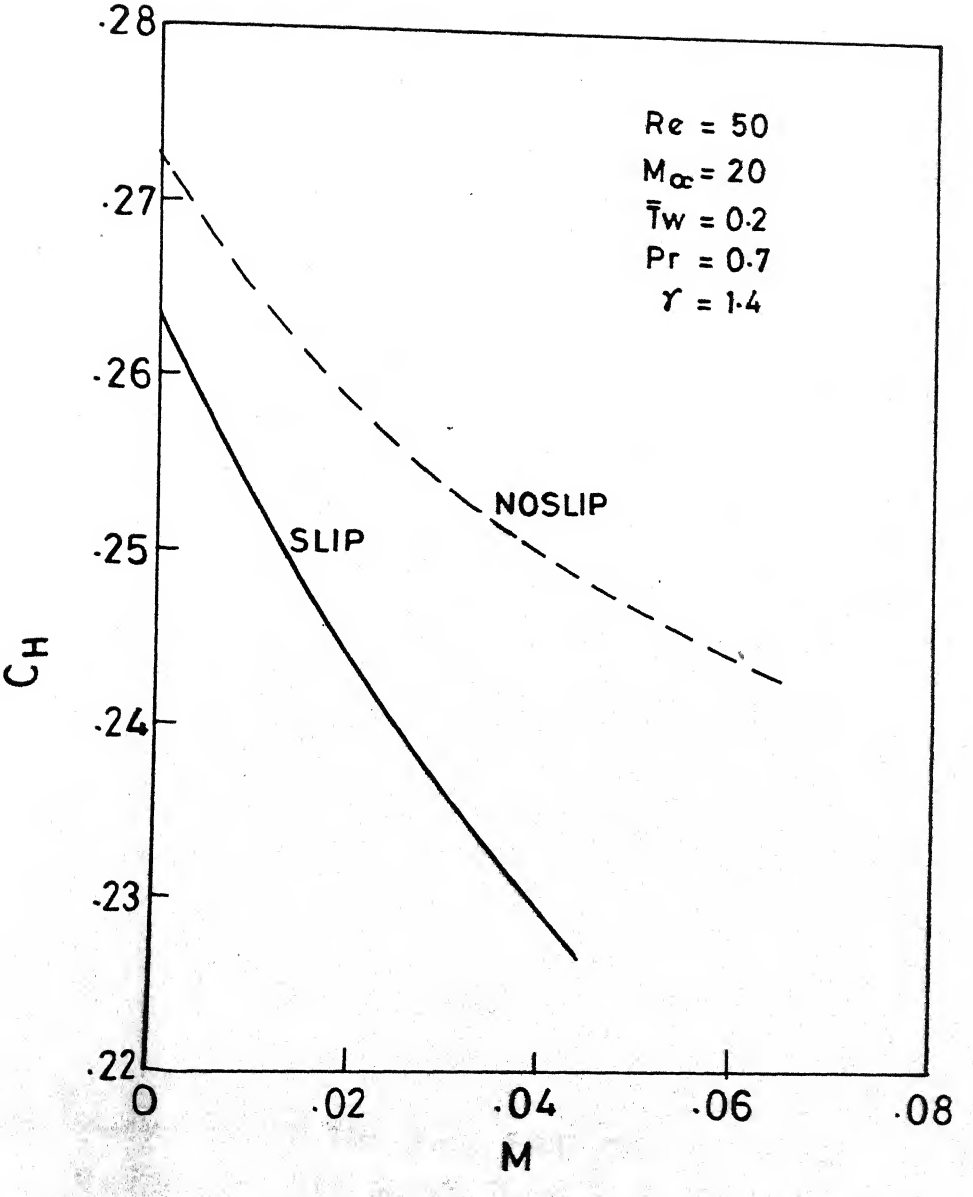

FIG. 39 VARIATION OF HEAT-TRANSFER COEFFICIENT, C_H, WITH MASS TRANSFER PARAMETER, M, FOR SURFACE SLIP AND NOSLIP CONDITIONS

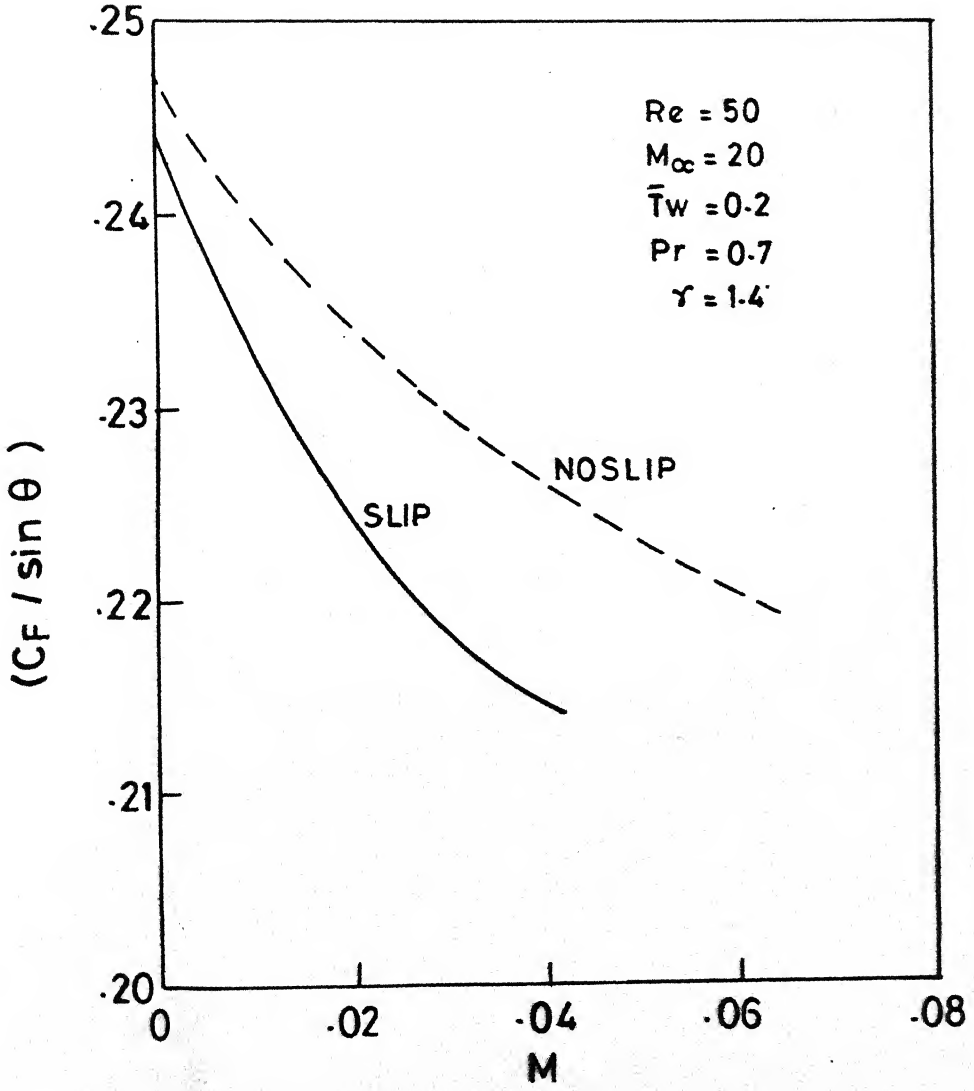

FIG. 40 VARIATION OF THE SKIN-FRICTION COEFFICIENT PARAMETER C_F / sin θ, WITH MASS TRANSFER PARAMETER M, FOR SURFACE SLIP AND NOSLIP CONDITIONS